COMPUTATIONS ON ENDOHEDRAL METALLOFULLERENES: CHARACTERIZATION, PROPERTIES AND GROWTH.

Marc Mulet Gas

Dipòsit Legal: T 1604-2015

Marc Mulet Gas

Computations on Endohedral Metallofullerenes: Characterization, Properties and Growth

PhD Thesis

Supervised by
Dr. Antonio Rodríguez-Fortea and Prof. Josep M. Poblet

Quantum Chemistry Group
Departament de Química Física i Inorgànica

UNIVERSITAT ROVIRA I VIRGILI

Tarragona, January 2015

UNIVERSITAT ROVIRA I VIRGILI
COMPUTATIONS ON ENDOHEDRAL METALLOFULLERENES: CHARACTERIZATION, PROPERTIES AND GROWTH.
Marc Mulet Gas
Dipòsit Legal: T 1604-2015

UNIVERSITAT ROVIRA I VIRGILI

Departament de Química Física i Inorgànica

Antonio Rodríguez Fortea, Professor Agregat del Departament de Química Física i Inorgànica de la Universitat Rovira i Virgili, i Josep M. Poblet Rius, Catedràtic del Departament de Química Física i Inorgànica de la Universitat Rovira i Virgili,

FEM CONSTAR que aquest treball, titulat

"Computations on Endohedral Metallofullerenes: Characterization, Properties and Growth"

que presenta Marc Mulet Gas per a l'obtenció del títol de Doctor, ha estat realitzat sota la nostra direcció al Departament de Química Física i Inorgànica d'aquesta universitat i que acompleix els requeriments per poder optar a Menció Internacional.

Tarragona, 23 de Gener de 2015

Els directors de la tesi doctoral

Dr. Antonio Rodríguez Fortea Prof. Josep M. Poblet Rius

UNIVERSITAT ROVIRA I VIRGILI
COMPUTATIONS ON ENDOHEDRAL METALLOFULLERENES: CHARACTERIZATION, PROPERTIES AND GROWTH.
Marc Mulet Gas
Dipòsit Legal: T 1604-2015

UNIVERSITAT ROVIRA I VIRGILI
COMPUTATIONS ON ENDOHEDRAL METALLOFULLERENES: CHARACTERIZATION, PROPERTIES AND GROWTH.
Marc Mulet Gas
Dipòsit Legal: T 1604-2015

Als meus pares i avis,
als que hi són i als que han marxat...

UNIVERSITAT ROVIRA I VIRGILI
COMPUTATIONS ON ENDOHEDRAL METALLOFULLERENES: CHARACTERIZATION, PROPERTIES AND GROWTH.
Marc Mulet Gas
Dipòsit Legal: T 1604-2015

Contents

UNIVERSITAT ROVIRA I VIRGILI
COMPUTATIONS ON ENDOHEDRAL METALLOFULLERENES: CHARACTERIZATION, PROPERTIES AND GROWTH.
Marc Mulet Gas
Dipòsit Legal: T 1604-2015

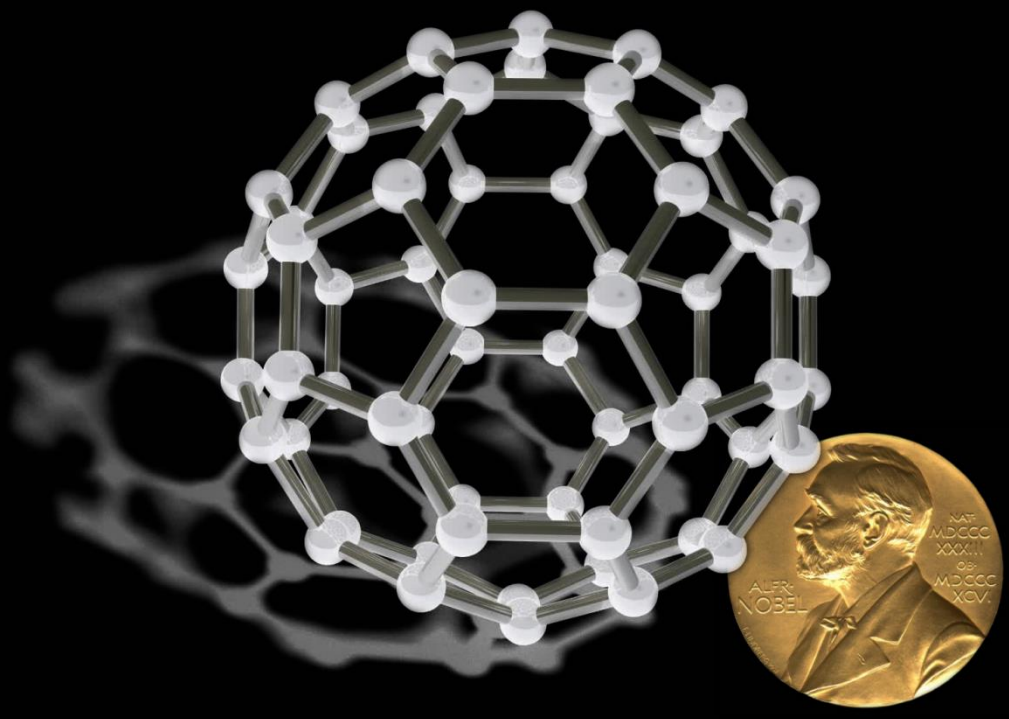

Chapter 1 // *Introduction: Discovery, Nomenclature, Types and Applications*

Chapter 1

Introduction: Discovery, Nomenclature, Types and Applications

In this chapter, the reader will find a brief introduction to the fullerene world, from the discovery of this new family of molecules to the potential applications that they have. This introduction contains a short description of the discovery of the first fullerene, the most interesting properties of these carbon molecules, and some of the interesting aspects that are crucial for their study: the mathematical rules applied to the construction of all possible isomers, nomenclature, properties and different types of fullerenes.

1.1. The discovery of C_{60}, Buckminsterfullerene

Carbon has been extensively studied, and has been considered one of the most versatile elements in chemistry. It was a surprise to find a new allotropic form of carbon, along with graphite and diamond, in 1985 that had gone undetected for many years.[1] Interestingly, the C_{60} carbon cage had been proposed by Osawa two decades before its discovery.[2] It was a fanciful conjecture at that time without any experimental evidence, and the report was published in Japanese. Due to these reasons, the ideas had not a significant impact in the scientific community. Furthermore, it was thought at that time, that any possible larger pure carbon clusters were carbon chains.[3]

Large carbon clusters were first reported by Rohfling *et al.* using a laser vaporization technique.[4] In those experiments, odd and even carbon cluster appeared for lower mass cluster (below C_{30}) but only even numbered clusters were observed for the larger species. C_{60}, was observed as the most abundant cluster in the spectrum. However, no explanation was given for the special abundance of this molecule, and the authors suggested that the detected species were arranged in chain, both for the smaller and the larger species.

Shortly after these experiments, Kroto and co-workers performed a series of experiments aimed to reproduce the conditions of carbon nucleation in the red giant stars. They also found a prominent peak of 720 m/z, corresponding to the C_{60}.[1] In this case, they investigated that 'magic-numbered' 60 carbon atom cluster. The key to their experiments was to probe the clustering conditions, which enabled the team to experimentally demonstrate that the C_{60} possessed a special stability. Inspired by the architect Richard Buckminster Fuller's work on geodesic structures, C_{60} was proposed to possess a closed cage structure in which the carbon atoms bond resembling a geodesic dome (figure 1.1). For this reason, the C_{60} was named Buckminsterfullerene.

The Nobel Prize in Chemistry was awarded to Harold W. Kroto, Robert F. Curl and Richard E. Smalley some years later, in 1996.

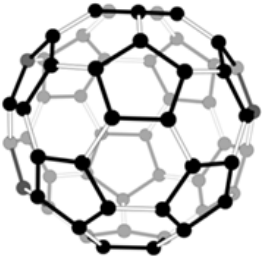

Figure 1.1 (top) The fullerene discovery team in front of the Space Science Building at Rice University. Shown from left to right: Sean O'Brien, Richard E. Smalley, Robert F. Curl, Harold W. Kroto and James Heath. (bottom-left) The geodesic dome designed by Richard Buckminster Fuller for the Universal Expo 1967 in Montreal, (bottom-center) a soccer ball, and (bottom-right) the I_h-C_{60}.

1.2. Fullerene cages: application of Euler's theorem

Fullerenes are closed carbon cages constituted by an even number of atoms. All carbon atoms in the structure are bonded to three adjacent atoms, and are thus sp^2 hybridized to yield a spheroidal, closed cage structure comprised of five and six membered rings. In the resulting bonding framework, a polyhedron is formed in which a carbon atom is located at each vertex, a bond across each edge, and a ring across each face. Because fullerenes are polyhedrons, they follow the Euler's theorem

which states that the number of faces (f), vertices (v), and edges (e) in a spherical polyhedron are related by the equation 1.[5]

$$v + f = e + 2 \qquad \text{(Eq. 1)}$$

For a fullerene C_n, where n equals the total number of carbon atoms, vertices equals n ($v = n$) and, because each carbon atom is bonded to three adjacent atoms, the number of edges is:

$$e = {}^{3n}/_{2} \qquad \text{(Eq. 2)}$$

By combining the equation 1 and the expressions for the vertices and edges, it is found that the number of faces can be related to the number of carbon atoms:

$$f = {}^{n}/_{2} + 2 \qquad \text{(Eq. 3)}$$

Hence, for any typical fullerene, n must be an even number. That explains how even numbered fullerenes are only observed to form spontaneously in the experiments. The number of edges and faces can be determined from equations 2 and 3 for any C_n. Taking C_{60} as an example: n =60 atoms, to give $3 \cdot 60/2 = 90$ edges, and $60/2+2=32$ faces.

Because classical fullerenes are comprised only of pentagons and hexagons, if the number of pentagons is defined as p and the number of hexagons is defined as h, the total number of vertices is then

$$(5p + 6h)/3 = n \qquad \text{(Eq. 4)}$$

and the total number of faces is

$$f = p + h \qquad \text{(Eq. 5)}$$

combining the equations 4 and 5 into equation 3 gives the solution of pentagons and hexagons for any C_n : *p=12* and *h=n/2-10*. Therefore, any classical fullerene must possess exactly 12 pentagons regardless of how many carbon atoms it contains. The smallest possible fullerene that can be constructed is C_{20}, containing only the 12 pentagons, and interestingly, C_{22} is the only even numbered fullerene larger than C_{20} that cannot be formed.[6-8] All the pristine fullerenes that have been isolated and characterized to date possess exactly twelve pentagons, and only hexagons. There are some reports, however, that show it is possible for a fullerene cage to possess square faces and also heptagons.[9, 10] In these cases, the pristine cage is not isolable due to its extremely high reactivity, and therefore, cages that have square bonding and heptagons must be stabilized exohedrally as a fullerene derivative, typically stabilized by chlorination.[11-14] Very recently, Popov and co-workers reported the first endohedral fullerene with a heptagon in the structure.[15]

1.3. Spiral algorithm and nomenclature

The number of isomers that can be constructed for a given number of carbon atoms rapidly increases. Fowler and Manolopoulos proposed the Spiral Algorithm to generate all the possible isomers with pentagonal and hexagonal faces for a given number of C atoms, C_n (table 1.1). Within this algorithm, a spiral code is generated, regarding the position of the pentagons and hexagons in the structure, using this code, all the different isomers can be constructed and labeled.[16]

In order to generate the spiral code, all the faces have to be connected following a single path that joins all the rings giving the lowest possible indexes for the pentagons. This is accomplished drawing a continuous spiral of edge-sharing pentagons and hexagons such that each new face in the spiral after the second shares and edge with both (i) its immediate predecessor and (ii) the first face in the preceding spiral that still has an

open edge. The spiral codes for two different structures, I_h-C_{20} and $T_d(2)$-C_{28}, and an example for the generation spiral path for $T_d(2)$-C_{28} is depicted in figure 1.2.

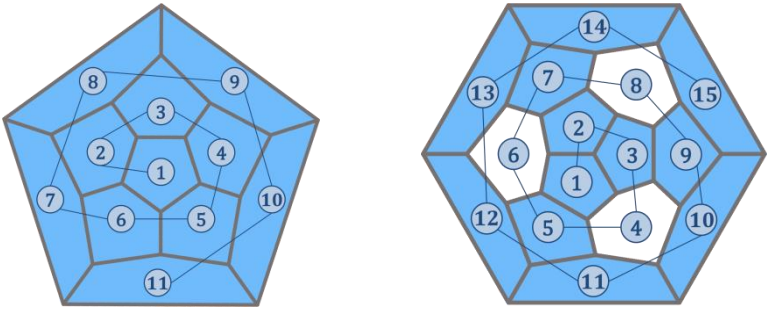

1 2 3 4 5 6 7 8 9 10 11 12 1 2 3 5 7 9 10 11 12 13 14 15

Figure 1.2 Schlegel diagrams for $I_h(1)$-C_{20} (left) and $T_d(2)$-C_{28} (right) and their corresponding spiral codes. All the pentagons are highlighted in blue.

Table 1.1 Fullerene isomers found by the spiral algorithm in the range n= 20 to 60. The entry for each value of *n* is the isomer count obtained when enantiomers are regarded as equivalent, and the left (bracketed) entry is the isomer count obtained when the enantiomers are regarded as distinct.

n	Isomers		n	Isomers	
20	1	(1)	42	45	(80)
24	1	(1)	44	89	(162)
26	1	(1)	46	116	(209)
28	2	(3)	48	199	(374)
30	3	(3)	50	271	(507)
32	6	(10)	52	437	(835)
34	6	(9)	54	580	(1113)
36	15	(23)	56	924	(1778)
38	17	(30)	58	1205	(2344)
40	40	(66)	60	1812	(3532)

Although there is a nomenclature for the fullerene cages proposed by the IUPAC, the most commonly used and widely accepted nomenclature for

fullerenes is the one using the spiral code number and the symmetry of the cage, *i.e.* I_h(1812)-C_{60}, for the Buckminsterfullerene.[17, 18]

The arrangement of the pentagons in a fullerene isomer may be also labeled by a pentagon index. It can be expressed as Ragavachari indices: (p_0, p_1, p_2, p_3, p_4, p_5) where p_k denotes the number of pentagons with k adjacent pentagons.[19] For example, the dodecahedral I_h(1)-C_{20} has the pentagon indices (0,0,0,0,0,12) whereas the T_d(2)-C_{28} has (0,0,0,12,0,0). As it is shown in figure 2, all the pentagons in I_h(1)-C_{20} are surrounded by five pentagons (p_5=12) while in contrast, all the pentagons in T_d(2)-C_{28} are surrounded by three pentagons (p_3=12). Other examples of the Ragavachari indices for other isomers are listed in table 1.2.

Table 1.2 List of several isomers with the corresponding point groups, pentagon indices and N_p values.

n	Isomer	Symmetry	Indices	N_p
20	1	I_h	0 0 0 0 0 12	30
28	2	T_d	0 0 0 12 0 0	18
32	6	D_3	0 0 6 6 0 0	15
36	14	D_{2d}	0 0 12 0 0 0	12
36	15	D_{6h}	0 0 12 0 0 0	12
40	38	D_2	0 4 8 0 0 0	10
40	39	D_{5d}	2 0 10 0 0 0	10
44	75	D_2	0 8 4 0 0 0	8
44	89	D_2	0 8 4 0 0 0	8
50	271	D_{5h}	2 10 0 0 0 0	5

A useful property of the Ragavachari indices is that, using equation (6), the total number of pentagon adjacencies (N_p) can be calculated.

$$N_P = \frac{1}{2}\sum_{k=1}^{5} k\ p_k \qquad \text{(Eq. 6)}$$

1.4. Isolated Pentagon Rule

The connected hexagon configuration in graphite provides the most thermodynamically stable bonding for carbon atoms. However, the carbon frameworks must possess twelve pentagons to form closed fullerenes. The understanding of how the combination of hexagons and pentagons are related to stability may provide insight into why certain fullerenes may preferentially form.

The most important consequence of the strain induced by the presence of the pentagons in the structure is the isolated pentagon rule (IPR), proposed by Kroto in 1987, which states that the most stable fullerenes are those in which all the pentagons are isolated. That means that all the pentagons are surrounded by five hexagons. The presence of fused pentagons in the structure increases significantly the cage tension. The lower the cage tension, *i.e.* the less curved is the structure, the more resembles to graphite, and thus, the more stable it is.[6]

The IPR can be justified easily using the rehybridation ideas. The introduction of a pentagon into a hexagon network, such as graphite, results in carbon atom bonding that is no longer co-planar. As previously described, fullerenes must contain twelve pentagons and thus high deviation from the idealized co-planarity can result. Due to the presence of the pentagons, the π-orbitals no longer overlap in parallel, as happens in the graphite sheets. Therefore, as depicted in figure 1.3, a change in the orbital hybridization occurs.[7, 20]

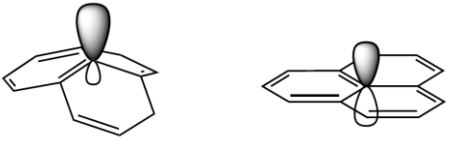

Figure 1.3 Schematic representation of the orbital hybridizations for the (left) curved 665 C atoms and for the (right) planar 666 atoms.

The IPR rule was crucial to explain the larger abundances found in the experiments for C_{60} and C_{70}, which are the first two C_n families that can lead to the construction of IPR isomers. As it is shown in table 1.3, the number of IPR isomers that can be constructed is much lower than the number of non-IPR structures that can be generated for a given number of carbon atoms.

Table 1.3 List of IPR-satisfying and non-IPR fullerene isomers ranging from C_{40} to C_{100}.

n	Non-IPR	IPR	n	Non-IPR	IPR	n	Non-IPR	IPR
42	45	0	62	2385	0	82	39710	9
44	89	0	64	3465	0	84	51568	24
46	116	0	66	4478	0	86	63742	19
48	199	0	68	6332	0	88	81703	35
50	271	0	70	8148	1	90	99872	46
52	437	0	72	11189	1	92	126323	86
54	580	0	74	14245	1	94	153359	134
56	924	0	76	19149	2	96	191652	187
58	1025	0	78	24104	5	98	230758	259
60	1811	1	80	31917	7	100	285463	450

As a consequence of the disposition of the pentagons and the hexagons in the carbon framework, different type of carbon-carbon bonds can be found in a fullerene cage. Thus, as it is shown in figure 1.4, we can distinguish several motifs showing 6-6 bonds (the edge between two hexagons), 6-5 bonds (the edge between a pentagon and a hexagon), and 5-5 bonds (the edge between two pentagons).

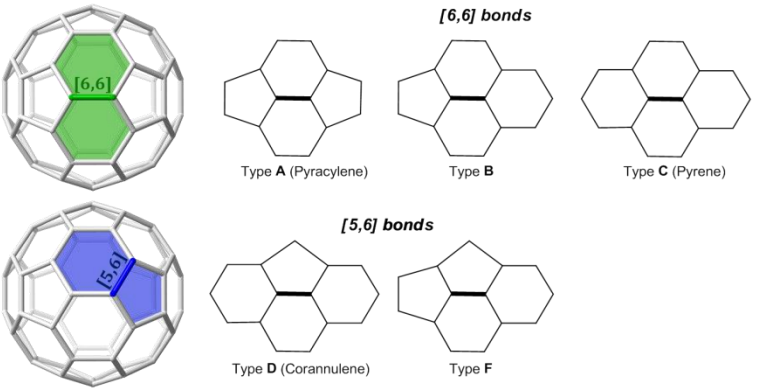

Figure 1.4 Classification of different bond types that might be present in an IPR fullerene cage.

The isomers that present fused pentagon in the structure, *i.e.*, the non-IPR isomers, are usually classified regarding the number of adjacent pentagon pairs (APP) that they present in the carbon framework. Thus, we can found different APPn isomers. Those pentagon adjacencies can be arranged in several ways within the carbon cage as it is shown in figure 1.5.

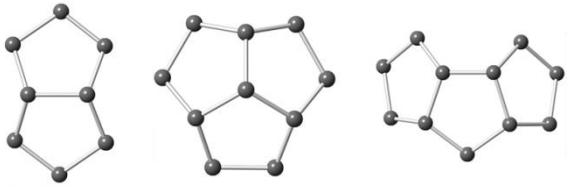

Figure 1.5 Different fused pentagon patterns that can be found in the non-IPR isomers. (left) Adjacent pentagon pair, (middle)triply-fused pentagons with a [5,5,5] central C atom, and (right) sequentially triply-fused pentagons.

The huge number of 'missing' non-IPR fullerenes challenged chemists to bring them into reality. Over the past two decades, significant advances have been achieved in stabilizing and isolating these labile fullerenes by exohedral derivatization, by endohedral encapsulation of electron-donating metal atoms or clusters, or by combinations thereof.

1.5. Types of fullerenes

Different types of fullerenes have been synthesized, isolated and characterized so far. They can be classified according to their special features:

i) *Heterohedral fullerenes*: This kind of systems present carbon atoms replaced by non-carbon atoms, *i.e.* nitrogen, boron, silicon, etc. Azafullerenes, in which one or more carbon atoms are replaced by nitrogen atoms, were the first type of heterohedral fullerenes spectroscopically detected. These systems are the most studied heterohedral fullerenes and they can be obtained in macroscopic quantities. In all the cases they exhibit reduced stability compared to their respective fullerene compounds with only carbon atoms.[21, 22]

ii) *Exohedral fullerenes*: They are formed by the reaction of an atom or a molecule with the fullerene cage, resulting in an external derivatization of the carbon cage. Hawkins and co-workers completely characterized the first exohedral fullerene synthesized which was 1,2-$C_{60}(OsO_4(4\text{-}t\text{-}BuC_5H_4N_2)_2)$.[23]

iii) *Endohedral fullerenes*: These systems are formed when a single atom or a molecule is encapsulated inside the fullerene cage. Soon after the discovery of C_{60}, a peak in the same mass spectra was associated to the endohedral metallofullerene La@C_{60} suggesting that C_{60} could act as a hosting molecule.[24] Apart from the encapsulation of metal-based compounds, diatomic molecules and noble gases have been also trapped inside the cages.[25, 26] This group, has been focused most of the work on this field during the last decades. Their special properties make them very interesting not only because the ability of encapsulating different units, but also for the potential applications they have. This thesis is based on the study of different members of this family of compounds.

1.6. Endohedral Fullerenes

One of the attractive properties of the hollow carbon clusters is the possibility to use them as robust containers for other species. Although there is a specific recommendation by the IUPAC for the nomenclature of this species as 'incar fullerenes', the specification endohedral is the most commonly and widely accepted for fullerenes with trapped atoms or molecules in the carbon cage. This term originates from a combination of Greek words ενδον ("endon" – within), and εδρα ("hedra" – face of a geometrical figure). The endohedral fullerenes are named as M@C_{2n} where the symbol @ is used to define that the left-marked atoms or clusters are encapsulated inside of the right-indicated fullerene cage.[27, 28]

As we have already mentioned previously, the first proposal of an endohedral fullerene was given only a few days after the discovery of C_{60}. However, the large-scale production of endohedral metallofullerenes was not achieved until 1990 by Krätschmer and co-workers.[29] Endohedral metallofullerenes attracted much more attention after the discovery of the macroscopic fullerene production. Many metals were put inside the fullerene cages during this period, many new endohedral metallofullerenes were reported, and therefore, the basis for the further advance in the field were established. Nevertheless, the most important milestone that started the era of the endohedral fullerenes was the discovery and macroscopic production, in 1999, of the first metallic nitride endohedral fullerene, $Sc_3N@I_h$-C_{80}. This endohedral fullerene is, after C_{60} and C_{70}, the third most abundant fullerene among all the fullerenes synthesized up-to-date.[30]

Endohedral metallofullerenes have attracted the attention of the scientific community not only because their unique host-guest behaviors, but also because the properties and, thus, the applications are significantly different from those of the empty cages. The formal electron transfer that has been found to happen between the trapped unit and the carbon cages is determinant for the understanding of these new properties.[31, 32]

Interestingly, another of the important features of the endohedral fullerenes is that, by means of the above-mentioned electron transfer and also due to the interaction between the inner moiety and the carbon cages, it is possible to synthesize and isolate cages that, when empty, are not obtained in the experiments.[33] It is worth mentioning that, depending on the type of metallic atoms or cluster trapped in the cage, it is possible to obtain different cage isomers and even different cage sizes. Therefore, chemists can 'play' with the different experimental settings in order to obtain different cage isomers.[34]

Several types of endohedral fullerenes have been successfully synthesized during the past 15 years. A more detailed description of all the families reported so far is given in the next section.

1.6.1. Classical metallofullerenes: M, M_2 and M_3

Starting from the first proposed metallofullerene La@C_{60} observed in gas phase in 1985, the nature of the metal-fullerene arrangement was under debate for several years. The first strong evidence for the metallic atom trapped inside the cage was given some years later for La@C_{82}, whose endohedral character was confirmed by means of C_2 loss induced by laser photofragmentation. Later on, in 1995, the first monometallic endohedral fullerene structure was solved by means of synchrotron X-ray diffraction experiments for Y@C_{82} by Takata and co-workers.[35, 36]

A large number of different atoms have been found to be trapped inside different sized carbon cages. Among all the different monometallofullerenes isolated and characterized so far, it is worth remarking that the smallest endofullerenes characterized by means of X-ray single crystal diffraction is the Li@I_h-C_{60}.[37, 38] On the other hand, the largest systems characterized, using the same experimental technique, are Sm@C94, Ca@C_{94},and Tm@C_{94}.[39, 40]

All the monometallic species reported so far are listed in table 1.4.

Table 1.4 List of all the monometallic fullerenes reported so far and characterized by means of structural studies. [a]

C_{2n}	Isomer	Metal(s)	C_{2n}	Isomer	Metal(s)
60	I_h (1)	Li	84	C_2 (13)	Yb, Sm
72	C_2 (10612)	La		D_{3d} (19)	Sm
74	D_{3h} (1)	Ca, Yb, Ba, La, Eu, Sr	90	C_2 (40)	Sm
80	C_{2v} (3)	La, Yb, Sm		C_2 (32)	Sm
82	C_2 (5)	Ca, Tm, Sm, Yb, Eu		C_2 (45)	Sm
	C_s (6)	La, Pr, Ca, Tm, Yb, Eu, Sm		C_{2v} (46)	Sm
	C_{3v} (7)	La, Ca, Sm	92	C_s (24)	Sm
	C_{2v} (9)	Ca, Tm, Yb, Eu, Sm, Y, La, Ce, Pr		C_1 (42)	Sm
84	C_2 (11)	Yb, Sm	94	C_{3v} (134)	Ca, Tm, Sm
	C_1 (12)	Yb			

[a] Other species detected by mass spectrometry in gas phase are not included in this table. The techniques used for the elucidation of the structure of each metallofullerene are specified in reference 31.

In addition to the species listed in the table 1.4, new families of small endohedral metallofullerenes, M@C_{2n} (M=Ti, Zr, Hf, U; C_{2n}=28-50) have been recently detected by means of Fourier Transform Ion Cyclotron Resonance (FT-ICR) mass spectrometry. Along with these small families, also a large variety of monometallic fullerenes has been detected using the same technique.[41, 42]

The atoms are trapped both in IPR and non-IPR cages. It is worth mentioning that, when trapped in IPR cages, most of the atoms exhibit free motion inside the cage whereas when the cage possesses adjacent pentagon pairs, the atoms strongly interact with pentalene motifs being more localized in the cage cavity.

Dimetallofullerenes (M_2@C_{2n}) have been obtained in synthesis in parallel to monometallofullerenes, but their yields are usually considerably

lower.[43] Thus, the list of well-characterized dimetallofullerenes is smaller than that of monometallofullerenes (table 1.5).

Table 1.5 List of all the dimetallic fullerenes reported so far and characterized by means of structural studies. [a]

C_{2n}	Isomer	Metal(s)	C_{2n}	Isomer	Metal(s)
66	C_{2v} (4059)	Sc	82	C_{3v} (8)	Er, Y, Sc, Tm
72	D_2 (10611)	La, Ce, Pr		C_{2v} (9)	Er, Tm
76	T_d (1)	Lu	88	D_2 (35)	Sm
78	D_{3h} (5)	La, Ce	90	C_1 (21)	Sm
80	D_{5h} (6)	Ce	92	D_3 (85)	Sm
	I_h (7)	La, Ce, Pr	100	D_5 (450)	La
82	C_s (6)	Er, Tm	104	D_{3d} (822)	Sm

[a] Other species detected by mass spectrometry in gas phase are not included in this table. The techniques used for the elucidation of the structure of each metallofullerene are specified in reference 31.

It is worth mentioning that $Sc_2@C_{66}$ was one of the first non-IPR isomers obtained, in 2000. This molecule was the focus of some controversial studies regarding its structure during the past years. The structural analysis provided by Shinohara and co-workers led them to the assignment of the $C_{2v}(4348)$-C_{66} cage, which possess two pairs of fused pentagons. On the other hand, the computational study reported by Nagase and co-workers pointed to the $C_{2v}(4059)$-C_{66} cage as the most stable when trapping two scandium atoms. This cage dilemma was finally solved very recently, in 2014, when Akasaka, Balch and co-workers reported the single crystal X-Ray structure which confirmed the computational prediction of the cage $C_{2v}(4059)$-C_{66} as the one obtained in the experiments.[44-47]

In addition, the dimetallofullerene family not only contains the smallest non-IPR fullerene characterized by X-Ray so far, but also the largest endohedral metallofullerene characterized by means of structural studies, $Sm_2@D_{3d}(822)$-C_{104}.[48]

Notice that, the cages that are suitable to encapsulate two metals, are in some cases different from that encapsulating one single metal. This is

because the number electrons formally transferred in the dimetallofullerenes is larger and lead to the stabilization of different isomers. Besides the electron transfer, another important feature that governs the stabilization of the dimetallofullerenes is the position of the metals. Since they are formally cations inside the cage, space enough has to be available to allow the separation of the two ions in order to minimize the electrostatic repulsion.

It is also important to comment that, during the last years, it has been recognized that some of the reported $M_2@C_{2n}$ can sometimes correspond to carbide clusterfullerenes $M_2C_2@C_{2n-2}$, and it is not possible to distinguish these two classes of fullerenes based on mass spectrometry data. In the past ten years, some 'dimetallofullerenes' have been reassigned to carbide endohedrals, for example the $Ti_2@C_{80}$ was found to be $Ti_2C_2@C_{78}$ and the $Sc_2@C_{82}$ was found to be $Sc_2C_2@C_{80}$, among many other cases.[49, 50]

Trimetallofullerenes ($M_3@C_{2n}$) are also obtained in the synthesis along with the mono and dimetallofullerenes. Although several trimetallic endohedral fullerenes have been reported ($Er_3@C_{74}$, $Tb_3@C_{80}$, $Y_3@C_{80}$, $Dy_3@C_{98}$), their characterization is limited, for the majority of the cases, to mass spectrometry data and there is no experimental evidences showing whether the detected species are trimetallofullerenes or the corresponding carbide endohedral fullerenes.[51]

1.6.2. Nitride clusterfullerenes, $M_3N@C_{2n}$

This family of compounds was obtained by a synthesis that occurred by chance. Nitride endohedral fullerenes were first reported in 1999 by Dorn and co-workers as a result of accidental leakage of air into the arc discharge chamber.[30] The presence of nitrogen was a key factor for this new type of endohedral fullerenes. Because the internal metallic species invariably have the formula of M_3N, these compounds are also known as the trimetallic nitride template (TNT) family. Numerous features emphasize the importance of this group of endohedral fullerenes. On one

hand, the first nitride EMF reported, $Sc_3N@I_h(7)$-C_{80} is the third most abundant fullerene.[52, 53] On the other hand, the nitride EMFs are generally more stable than the other types of endohedral fullerenes. For these reasons, the $M_3N@I_h(7)$-C_{80} is so far the most extended and most studied group of endohedral metallofullerenes.[54, 55]

The electronic distribution in metallic nitride endohedral fullerenes may be represented by the ionic model $(M_3N)^{6+}@(C_{2n})^{6-}$. Trivalent metal atoms surround a nitride anion, thus, six electrons are formally transferred from the inner cluster to the carbon framework.[56]

As it has been rationalized in several studies, the cluster geometry and the size of the selected cage are highly dependent on the metal cation radius, *i.e.* the size of the encapsulated metal cluster. Thus, with scandium a family of four Sc_3N-containing endohedrals are produced: $Sc_3N@D_3(6140)$-C_{68}, $Sc_3N@D_{3h}(5)$-C_{78}, and two isomers of $Sc_3N@C_{80}$, $D_{5h}(6)$ and $I_h(7)$. When a larger metal, as gadolinium, is forming the TNT unit, six different cage sizes ranging from C_{78} to C_{88} are obtained. With lanthanum, which is even larger, three larger cages from with 88, 92 and 96 carbon atoms respectively. Interestingly, the metal not only influences on the cage size but also on the cage symmetry. Thus, scandium nitride is encapsulation in the IPR $D_{3h}(5)$-C_{78} cage whereas the gadolinium cluster is encapsulated by the non-IPR $C_2(22010)$-C_{78} cage. For these species containing smaller rare-earth elements such as Sc, Y and lanthanides from Gd to Lu, $M_3N@C_{80}$ is always the most abundant while on the contrary, larger M_3N clusters prefer larger cages. However, the production yield of the corresponding endohedral metallofullerenes decreases remarkably with increasing the cage size. Nitride endohedral metallofullerenes containing only divalent metals, such as Sm, Eu and Yb have not been observed. [57-59] In figure 1.6, some of the most representative nitride endohedral metallofullerenes are represented.

In general, the M_3N exhibits a planar geometry inside the cage. The prominent exception is $Gd_3N@I_h(7)$-C_{80}, where the cluster shows an important pyramidalization due to the small hollow space available, the

nitrogen atom is 0.309 Å out of the nitride plane.[60] Furthermore, in most of the nitride clusterfullerenes, the trapped unit can freely rotate inside the cage. However, this motion is hindered in all nitride EMFs that possess cages smaller than C_{80}: IPR $D_{3h}(5)$-C_{78}, and non-IPR $C_2(22010)$-C_{78}, and $D_3(6140)$-C_{68}. Both the topology and size of the fullerene restrict the rotation of the encapsulated guest. For instance, in the case of $Sc_3N@D_3(6140)$-C_{68}, the metal atoms show a strong interaction with the three pentalene motifs present in the carbon cage.[61, 62]

Not only monometallic nitride endohedral fullerenes but also mixed metal nitride endohedral species, showing similar properties to those containing 3 equivalent metals, have been reported in the last few years. Furthermore, a recent work reported the isolation and characterization of the first two metal cyanide endohedral fullerenes, $Sc_3NC@I_h(7)$-C_{80} and $Sc_3NC@C_2(22010)$-C_{78}. The Sc_3NC cluster is planar, with the N atom occupying the center position and the C atom located in one side of the triangle formed by the Sc atoms.[63]

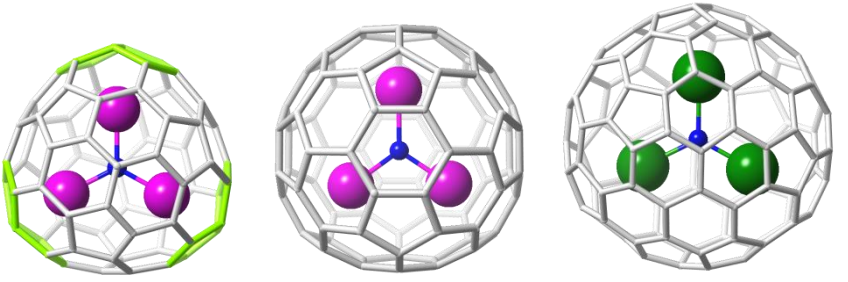

Figure 1.6 Ball and stick representation for $Sc_3N@D_3(6140)$-C_{68}, the smallest nitride EMF (left); $Sc_3N@I_h(7)$-C_{80}, the most abundant EMF (center); and $La_3N@D_2(186)$-C_{92}, the largest nitride EMF (right). Sc atoms are represented in magenta, N atoms in blue and La atoms in green. Pentalene unites are highlighted in lime green.

In table 1.6, all the different nitride endohedral fullerenes well-characterized so far are listed.

Table 1.6 List of all the nitride endohedral fullerenes reported so far and characterized by means of structural studies. [a]

C_{2n}	Isomer	Cluster	C_{2n}	Isomer	Cluster
68	D_3 (6140)	Sc_3N, $DySc_2N$, $LuSc_2N$, Lu_2ScN	82	C_s (39663)	Y_3N, Gd_3N
70	C_{2v} (7854)	Sc_3N	84	C_s (51365)	Tb_3N, Tm_3N, Gd_3N, Y_3N
76	C_s (17490)	$DySc_2N$	86	D_3 (19)	Tb_3N, Gd_3N, Y_3N
78	D_{3h} (5)	Sc_3N	88	D_2 (35)	Tb_3N, Y_3N, Gd_3N, Lu_3N
	C_2 (22010)	Dy_3N, Tm_3N, Y_3N, Gd_3N, Sc_3NC	92	T (86)	La_3N
80	D_{5h} (6)	Sc_3N, $LuSc_2N$, Lu_2ScN	96	D_2 (186)	La_3N
	I_h (7)	Sc_3N, Gd_3N, Tb_3N, Dy_3N, Tm_3M, Lu_3N, $CeSc_2N$, $ErSc_2N$, $GdSc_2N$, $TbSc_2N$, Gd_2ScN, $LaSc_2N$, $NdSc_2N$, Nd_2ScN, $LuSc_2N$, Lu_2ScN, YLu_2N, Y_2LuN, $DySc_2N$, Dy_2ScN, $TiSc_2N$, Sc_3NC			

It is worth remarking that the structural assignment for $La_3N@T(86)$-C_{92} is rather controversial. In a theoretical work reported a few years after the first assignment, the isomer $La_3N@C_2(36)$-C_{92} was found to be lower in energy but its small HOMO-LUMO gap does not match with the experimental electrochemical data.[64, 65] Besides of that, while encapsulation of La_3N cluster inside the carbon cages smaller than C_{86} was not observed, metallic nitride azafullerene $La_3N@C_{79}N$ was detected by mass spectrometry and its extended DFT study was reported. The extra electron occupying a bonding orbital between the three La atoms might be the reason for the extra stabilization of this system.[66]

1.6.3. Carbide clusterfullerenes

Interestingly, this family of endohedral fullerenes is obtained without the addition of any heterogeneous additive to the reactor, only the graphite rod and the metal source.

The first carbide clusterfullerene reported was the $Sc_2C_2@D_{2d}(23)$-C_{84}. Assumed as $Sc_2@C_{86}$ when firstly detected, it was after some discrepancies between the experimental data and the computations when it was suggested to be $Sc_2C_2@C_{84}$.[49] A few years after the first proposal, the carbide suggestion was confirmed by the structural analysis. Very soon after this finding, all the $M_2@C_{2n}$ family was checked in order to find more cases like the present one. Surprisingly, several endohedral metallofullerenes that were originally proposed to be $M_2@C_{2n}$ have recently been identified as carbides. Such examples include $Sc_2C_2@C_{80}$ (in place of $Sc_2@C_{82}$), $Sc_2C_2@C_{82}$ and $Dy_2C_2@C_{82}$ (instead of $Sc_2@C_{84}$ and $Dy_2@C_{84}$), $Ti_2C_2@C_{78}$ (rather than $Ti_2@C_{80}$), $Gd_2C_2@C_{88}$ and $Gd_2C_2@C_{90}$ (in lieu of $Gd_2@C_{90}$ and $Gd_2@C_{92}$).[67, 68] Consequently, it is expected that some other carbide endohedral fullerenes will be discovered in the near future.

The family of carbide clusterfullerenes is not limited to those with two metal atoms inside the cage. Similar events than those of dimetallic carbides led to the discovery of trimetallic carbide endohedral fullerenes. What was thought to be a trimetallic endohedral, $Sc_3@C_{82}$, was later on reported to be $Sc_3C_2@C_{80}$. Its structure was elucidated by means of singe crystal X-ray diffraction analysis by Akasaka and co-workers.[69] Very recently, a carbide clusterfullerene containing four metal atoms has been reported, $Sc_4C_2@C_{80}$.[70] All the metal carbides that have been detected and characterized are listed in table 1.7.

The cluster can adopt several geometries inside the cages, depending on the number of metal atoms in the carbide and the size of the cage. Structural and computational studies showed that the geometry of the M_2C_2 cluster strongly depends on the carbon cage and can vary from almost linear in the case of $Ti_2C_2@C_{78}$ and $Y_2C_2@C_{100}$, to butterfly-like in

$Sc_2C_2@C_{82}$. Furthermore, progressive variations in the Y_2C_2 cluster shape with the cage size were described by Dorn as a consequence of what they called 'nanoscale fullerene compression' (see figure 1.7).[71, 72]

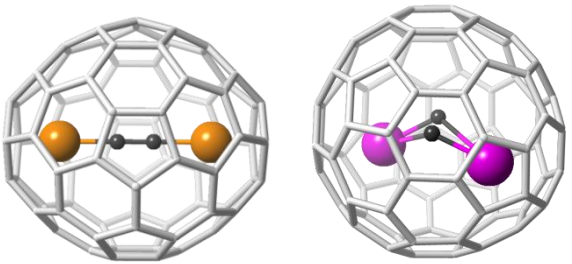

Figure 1.7 Ball and stick representation of $Ti_2C_2@D_{5h}(5)$-C_{78}, in which the carbide has an almost linear disposition (left), and $Sc_2C_2@C_{2v}(5)$-C_{80}, showing the butterfly-like geometry of the cluster (right). Ti atoms are represented in orange, Sc atoms in magenta, and C atoms in the cluster are represented in dark grey.

Notice that, in the particular case of the M_2C_2, the cages that have been reported are different from those found to encapsulate the nitride clusters. In this case, the carbide transfers four electrons to the carbon cage leading to the stabilization of the cages that have a more suitable electronic structure to accommodate the number of transferred electrons.

Table 1.7 List of all the carbide clusterfullerenes reported so far and characterized by means of structural studies.

C_{2n}	Isomer	Cluster	C_{2n}	Isomer	Cluster
68	C_{2v} (6073)	Sc_2C_2	82	C_{3v} (8)	Sc_2C_2
78	D_{3h} (5)	Ti_2C_2	84	D_{2d} (23)	Sc_2C_2
80	C_{2v} (5)	Sc_2C_2		C_1 (51383)	Y_2C_2
	I_h (7)	Sc_3C_2, Sc_4C_2	88	D_2 (35)	Gd_2C_2, Lu_3C_2
82	C_s (6)	Sc_2C_2, Y_2C_2, Er_2C_2, $ErYC_2$, Dy_2C_2	90	C_1 (21)	Gd_2C_2
	C_3 (8)	Sc_2C_2, Y_2C_2, Er_2C_2, $ErYC_2$, Dy_2C_2	92	D_3 (85)	Y_2C_2, Gd_2C_2
	C_{2v} (9)	Sc_2C_2, Y_2C_2, Er_2C_2, Dy_2C_2	100	D_5 (450)	Y_2C_2

1.6.4. Oxide clusterfullerenes

The oxide clusterfullerenes are a rather small family of endohedrals, which was discovered by Stevenson and co-workers in 2008. Only three different systems have been reported so far, $Sc_4O_2@I_h(7)$-C_{80} which is the most abundant, $Sc_4O_3@I_h(7)$-C_{80} and $Sc_2O@C_s(6)$-C_{82}. All three member of this family were characterized by single crystal X-ray diffraction. In $Sc_4O_2@I_h(7)$-C_{80} and $Sc_4O_3@I_h(7)$-C_{80}, the Sc atoms form a distorted tetrahedron in which the O atom are located above its faces.[73-75]

It is worth remarking that computational studies showed that the $Sc_2O@C_s(6)$-C_{82} is not the lowest-energy isomer at 0 K, but it becomes the most favored above 1200 K. This is the first example in which the relevance of the thermal and entropic contributions to the stability of the fullerene isomer has been confirmed through crystallographic structural characterization.

1.6.5. Sulfide clusterfullerenes

Sulfide clusterfullerenes appeared in 2010. Two different methods of synthesis were reported. The main difference between them was the sulfur source in the reactor. Dunsch and co-workers reported the formation of one isomer of $M_2S@C_{82}$ by introducing a solid sulfur source in the reactor, in this particular case, CH_5N_3·HSCN. In this experiment, three different metals were found to be part of the metallic sulfide cluster in the C_{82} cage, Sc, Lu, and Dy.[76] At the same time, Echegoyen and co-workers, reported that an extensive family of sulfide cluster fullerenes was obtained in macroscopic quantities with cages ranging from C_{80} to C_{100} using SO_2 instead of a solid sulfur source.[77] Later on, the same group reported the detection of a large number of scandium sulfide cluster fullerenes with cages ranging from C_{68} to C_{80}.[78]

Two isomers of $Sc_2S@C_{82}$, $Sc_2S@C_s(6)$-C_{82} and $Sc_2S@C_{3v}(8)C_{82}$, were the first two sulfide clusterfullerenes fully characterized by means of single crystal X-ray diffraction. These isomers, both with IPR-satisfying cages,

were found to be the two most abundant species in the sulfide clusterfullerene family.[79]

Shortly after the report of the first IPR sulfide endohedral fullerenes, the first two Sc_2S endohedrals with non-IPR cages were found. As a result of an extensive collaboration between our group and Prof. Echegoyen's group, the structure and properties of these first two non-IPR sulfide clusterfullerenes were elucidated. This work is an important part of the present thesis and it will be further discussed in chapter 4.[78, 80]

Apart from the scandium sulfide endohedral fullerenes, also a endohedral fullerene containing only transition metals was isolated and characterized, $Ti_2S@D_{5h}(5)$-C_{78}, whose structural study and features are also detailed in chapter 5.[81]

Very recently, some theoretical studies have been reported focusing on the study of $Sc_2S@C_{68}$, $Sc_2S@C_{74}$, $Sc_2S@C_{76}$ and $Sc_2S@C_{80}$. The different cages that encapsulate the Sc_2S were proposed but further experimental work will be necessary in order to confirm or discard these assignments.[82-85]

1.7. Synthesis of endohedral metallofullerenes

Different strategies have been developed up to date for preparing macroscopic amounts of endohedral fullerenes. This includes vaporization of graphite, implantation of the atoms through the walls of already existing carbon cages, and chemical routes via opening and closing the fullerene cages. Among these different methodologies, the vaporization of graphite, in particular the laser ablation and the arc-discharge are the two most popular synthetic procedures.[24, 86, 87]

Laser ablation was the first method which indicated that endohedral metallofullerenes may exist. In these experiments, a target rod composed

of graphite and the metal source is place in a furnace at high temperature and under high pressure. A laser shot impacts the target and the fullerenes and endohedral fullerenes generated are carried by a gas flow to be finally trapped on a quartz tube wall near the end of the furnace. The laser ablation method is the most commonly used to the study of the growth mechanism of fullerenes and endohedral metallofullerenes but it is not used for the macroscopic production of EMFs due to the high cost and the low synthesis rate.[88]

It was the arc-discharge method proposed by Krätschmer and Huffman that made high yield of EMFs available for the first time in 1991. The Krätschmer-Huffman generator is the most popular apparatus for the large-scale synthesis of EMFs.[29] The rods typically contain the metal (or metal oxide) and graphite. The soot produced after the arcing of the corresponding rods contains fullerenes, endohedral fullerenes and a large amount of other carbon structures. For this reason, the obtained soot has to be extracted and purified in order to obtain the desired endohedral fullerenes. The arc-discharge method is simple and cost-effective. However, the uncontrolled process that occurs in the arc does not allow the use of this technique to study the formation mechanism of endohedral fullerenes. But on the other hand, it is the most extensively utilized for the synthesis of endohedral fullerenes.[43, 89]

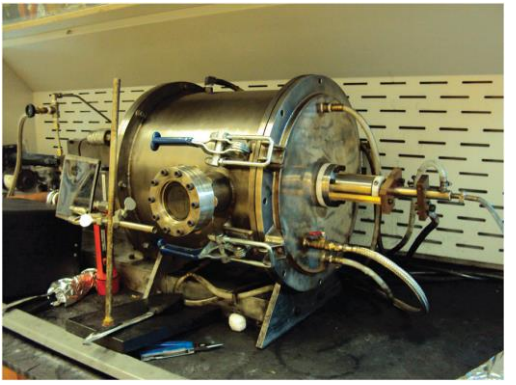

Figure 1.8 A Krätschmer-Huffman arc-discharge reactor for the generation of endohedral fullerenes (courtesy of Prof. Echegoyen's group).

Nevertheless, for some of the endohedral metallofullerene families, the growth of crystal suitable for X-ray analysis is difficult and often not successful. It is at this point when the computational contributions to this field become critical. As it can be seen from most of the new endohedral fullerenes reported in the past few years, the combination of experiments and computations are the perfect synergy to elucidate which are the isomers formed in the reactors and what is the structure and properties of each of those new obtained isomers.

1.8. Potential applications of endohedral fullerenes

The discovery of this new family of compounds attracted the attention of the scientific community very rapidly. High expectations on their promising potential applications were created due to their novel properties. During the past decades, most of the efforts have been devoted to the study of those applications in different fields such as medicine and photovoltaics, among many others.

Biomedical applications are a field under constant development that holds special promise for fullerene-based materials. The nontoxicity of the carbon cages makes endohedral fullerene-containing drugs doable for medical applications. Related to this field, the most important studies and developments are focused on the use of EMFs as MRI contrast agents, X-ray contrast agents, radiotracers and radiopharmaceuticals, and antitumor and antimicrobial drugs.[90-92]

The applications of endohedral fullerenes in organic photovoltaics are another of the very promising fields. Endohedral fullerenes as new acceptors in polymeric solar cells, endohedrals fullerene-based donor-acceptor dyads and photoelectrochemistry cells based on endohedral fullerenes have attracted most of the research in this field during the past few years.[93-95]

Other potential applications were also predicted on the basis of their peculiar electronic, chemical and physical properties, including superconductors, metallofullerene lasers, nanomemory devices, etc.[96-100]

New endohedral fullerenes are synthesized every year providing to the field new molecules with different features that keep pushing toward the discovery of new applications. Therefore, a lot of work has been done, but even more work is coming on the endohedral fullerene world.

1.9. References

1. H. W. Kroto, J. R. Heath, S. C. Obrien, R. F. Curl and R. E. Smalley, *Nature*, 1985, **318**, 162-163.
2. H. W. Kroto, A. W. Allaf and S. P. Balm, *Chem. Rev.* , 1991, **91**, 1213-1235.
3. E. A. Rohlfing, D. M. Cox and A. Kaldor, *J. Chem. Phys.*, 1984, **81**, 3322-3330.
4. D. M. Cox, D. J. Trevor, K. C. Reichmann and A. Kaldor, *J. Am. Chem. Soc.*, 1986, **108**, 2457-2458.
5. I. Lakatos, *Proofs and refutations*, Cambridge University Press, Cambridge, 1976.
6. H. W. Kroto, *Nature*, 1987, **329**, 529-531.
7. T. G. Schmalz, W. A. Seitz, D. J. Klein and G. E. Hite, *J. Am. Chem. Soc.*, 1988, **110**, 1113-1127.
8. P. W. Fowler, D. E. Manolopoulos, D. B. Redmond and R. P. Ryan, *Chem. Phys. Lett.*, 1993, **202**, 371-378.
9. P. W. Fowler, T. Heine, D. E. Manolopoulos, D. Mitchell, G. Orlandi, R. Schmidt, G. Seifert and F. Zerbetto, *The Journal of Physical Chemistry*, 1996, **100**, 6984-6991.
10. P. W. Fowler, T. Heine, D. Mitchell, G. Orlandi, R. Schmidt, G. Seifert and F. Zerbetto, *J. Chem. Soc., Faraday Trans.*, 1996, **92**, 2203-2210.
11. W. Qian, M. D. Bartberger, S. J. Pastor, K. N. Houk, C. L. Wilkins and Y. Rubin, *J. Am. Chem. Soc.*, 2000, **122**, 8333-8334.
12. P. A. Troshin, A. G. Avent, A. D. Darwish, N. Martsinovich, A. a. K. Abdul-Sada, J. M. Street and R. Taylor, *Science*, 2005, **309**, 278-281.
13. Y.-Z. Tan, R.-T. Chen, Z.-J. Liao, J. Li, F. Zhu, X. Lu, S.-Y. Xie, J. Li, R.-B. Huang and L.-S. Zheng, *Nat. Commun.*, 2011, **2**, 420.
14. Y.-Z. Tan, Z.-J. Liao, Z.-Z. Qian, R.-T. Chen, X. Wu, H. Liang, X. Han, F. Zhu, S.-J. Zhou, Z. Zheng, X. Lu, S.-Y. Xie, R.-B. Huang and L.-S. Zheng, *Nat. Mater.*, 2008, **7**, 790-794.
15. Y. Zhang, K. B. Ghiassi, Q. Deng, N. A. Samoylova, M. M. Olmstead, A. L. Balch and A. A. Popov, *Angew. Chem. Int. Ed*, 2014.
16. P. W. Fowler and D. E. Manolopoulos, *An Atlas of Fullerenes*, Oxford University Press, Oxford, 1995.
17. F. Cozzi, W. H. Powell and C. Thilgen, *Pure Appl. Chem.*, 2005, **77**, 843-923.
18. W. H. Powell, F. Cozzi, C. Moss, C. Thilgen, R. J. R. Hwu and A. Yerin, *Pure Appl. Chem.*, 2002, **74**, 629-695.
19. R. C. Haddon, L. E. Brus and K. Raghavachari, *Chem. Phys. Lett.*, 1986, **125**, 459-464.

20. R. C. Haddon, L. E. Brus and K. Raghavachari, *Chem. Phys. Lett.*, 1986, **131**, 165-169.
21. T. Pradeep, V. Vijayakrishnan, A. K. Santra and C. N. R. Rao, *J. Phys. Chem.*, 1991, **95**, 10564-10565.
22. W. Branz, I. M. L. Billas, N. Malinowski, F. Tast, M. Heinebrodt and T. P. Martin, *J. Chem. Phys.*, 1998, **109**, 3425-3430.
23. J. M. Hawkins, A. Meyer, T. A. Lewis, S. Loren and F. J. Hollander, *Science*, 1991, **252**, 312.
24. J. R. Heath, S. C. O'Brien, Q. Zhang, Y. Liu, R. F. Curl, F. K. Tittel and R. E. Smalley, *J. Am. Chem. Soc.*, 1985, **107**, 7779-7780.
25. M. Saunders, R. J. Cross, H. A. Jiménez-Vázquez, R. Shimshi and A. Khong, *Science*, 1996, **271**, 1693-1697.
26. J. Cioslowski, *J. Am. Chem. Soc.*, 1991, **113**, 4139-4141.
27. J. Cioslowski and E. D. Fleischmann, *J. Chem. Phys.*, 1991, **94**, 3730.
28. T. Weiske, D. K. Bohme, J. Hrusak, W. Kratschmer and H. Schwarz, *Angew. Chem., Int. Ed. Engl.*, 1991, **30**, 884-886.
29. W. Kratschmer, L. D. Lamb, K. Fostiropoulos and D. R. Huffman, *Nature*, 1990, **347**, 354-358.
30. S. Stevenson, G. Rice, T. Glass, K. Harich, F. Cromer, M. R. Jordan, J. Craft, E. Hadju, R. Bible, M. M. Olmstead, K. Maitra, A. J. Fisher, A. L. Balch and H. C. Dorn, *Nature*, 1999, **401**, 55-57.
31. M. Chaur, F. Melin, A. Ortiz and L. Echegoyen, *Angew. Chem., Int. Ed.*, 2009, **48**, 7514-7538.
32. A. Rodríguez-Fortea, A. Balch and J. Poblet, *Chem. Soc. Rev.*, 2011, **40**, 3551-3563.
33. Y.-Z. Tan, S.-Y. Xie, R.-B. Huang and L.-S. Zheng, *Nat Chem*, 2009, **1**, 450-460.
34. A. A. Popov, S. Yang and L. Dunsch, *Chem. Rev.* , 2013, **113**, 5989-6113.
35. D. C. Lorents, D. H. Yu, C. Brink, N. Jensen and P. Hvelplund, *Chem. Phys. Lett.*, 1995, **236**, 141-149.
36. M. Takata, B. Umeda, E. Nishibori, M. Sakata, Y. Saitot, M. Ohno and H. Shinohara, *Nature*, 1995, **377**, 46-49.
37. S. Aoyagi, E. Nishibori, H. Sawa, K. Sugimoto, M. Takata, Y. Miyata, R. Kitaura, H. Shinohara, H. Okada, T. Sakai, Y. Ono, K. Kawachi, K. Yokoo, S. Ono, K. Omote, Y. Kasama, S. Ishikawa, T. Komuro and H. Tobita, *Nat Chem*, 2010, **2**, 678-683.
38. S. Fukuzumi, K. Ohkubo, Y. Kawashima, D. S. Kim, J. S. Park, A. Jana, V. M. Lynch, D. Kim and J. L. Sessler, *J. Am. Chem. Soc.*, 2011, **133**, 15938-15941.
39. H. Jin, H. Yang, M. Yu, Z. Liu, C. M. Beavers, M. M. Olmstead and A. L. Balch, *J. Am. Chem. Soc.*, 2012, **134**, 10933-10941.

40. Y. Che, H. Yang, Z. Wang, H. Jin, Z. Liu, C. Lu, T. Zuo, H. C. Dorn, C. M. Beavers, M. M. Olmstead and A. L. Balch, *Inorg. Chem.*, 2009, **48**, 6004-6010.
41. P. Dunk, N. Kaiser, M. Mulet-Gas, A. Rodríguez-Fortea, J. Poblet, H. Shinohara, C. Hendrickson, A. Marshall and H. Kroto, *J. Am. Chem. Soc.*, 2012, **134**, 9380-9389.
42. P. W. Dunk, M. Mulet-Gas, Y. Nakanishi, N. K. Kaiser, A. Rodríguez-Fortea, H. Shinohara, J. M. Poblet, A. G. Marshall and H. W. Kroto, *Nat. Commun.*, 2014, (Accepted).
43. H. Shinohara, *Rep. Prog. Phys.*, 2000, **63**, 843.
44. C. Wang, T. Kai, T. Tomiyama, T. Yoshida, Y. Kobayashi, E. Nishibori, M. Takata, M. Sakata and H. Shinohara, *Nature*, 2000, **408**, 426-427.
45. K. Kobayashi and S. Nagase, *Chem. Phys. Lett.*, 2002, **362**, 373-379.
46. Y. H. Cui, W. Q. Tian, J. K. Feng and D. L. Chen, *J. Nanopart. Res.*, 2009, **12**, 429.
47. M. Yamada, H. Kurihara, M. Suzuki, J. D. Guo, M. Waelchli, M. M. Olmstead, A. L. Balch, S. Nagase, Y. Maeda, T. Hasegawa, X. Lu and T. Akasaka, *J. Am. Chem. Soc.*, 2014, **136**, 7611-7614.
48. B. Q. Mercado, A. Jiang, H. Yang, Z. Wang, H. Jin, Z. Liu, M. M. Olmstead and A. L. Balch, *Angew. Chem. Int. Ed*, 2009, **48**, 9114-9116.
49. Y. Yamazaki, K. Nakajima, T. Wakahara, T. Tsuchiya, M. Ishitsuka, Y. Maeda, T. Akasaka, M. Waelchli, N. Mizorogi and S. Nagase, *Angew. Chem. Int. Ed*, 2008, **47**, 7905-7908.
50. Z.-Q. Shi, X. Wu, C.-R. Wang, X. Lu and H. Shinohara, *Angew. Chem. Int. Ed*, 2006, **45**, 2107-2111.
51. A. A. Popov, L. Zhang and L. Dunsch, *ACS Nano*, 2010, **4**, 795-802.
52. B. Elliott, L. Yu and L. Echegoyen, *J. Am. Chem. Soc.*, 2005, **127**, 10885-10888.
53. S. Stevenson, M. A. Mackey, M. C. Thompson, H. L. Coumbe, P. K. Madasu, C. E. Coumbe and J. P. Phillips, *Chem. Commun.* , 2007, 4263-4265.
54. Y. Iiduka, O. Ikenaga, A. Sakuraba, T. Wakahara, T. Tsuchiya, Y. Maeda, T. Nakahodo, T. Akasaka, M. Kako, N. Mizorogi and S. Nagase, *J. Am. Chem. Soc.*, 2005, **127**, 9956-9957.
55. F.-F. Li, A. Rodríguez-Fortea, J. M. Poblet and L. Echegoyen, *J. Am. Chem. Soc.*, 2011, **133**, 2760-2765.
56. A. A. Popov and L. Dunsch, *J. Am. Chem. Soc.*, 2007, **129**, 11835-11849.
57. F. Melin, M. N. Chaur, S. Engmann, B. Elliott, A. Kumbhar, A. J. Athans and L. Echegoyen, *Angew. Chem. Int. Ed*, 2007, **46**, 9032-9035.

58. M. N. Chaur, F. Melin, J. Ashby, B. Elliott, A. Kumbhar, A. M. Rao and L. Echegoyen, *Chem. Eur. J.*, 2008, **14**, 8213-8219.
59. C. M. Beavers, M. N. Chaur, M. M. Olmstead, L. Echegoyen and A. L. Balch, *J. Am. Chem. Soc.*, 2009, **131**, 11519-11524.
60. T. M. Zuo, M. M. Olmstead, C. M. Beavers, A. L. Balch, G. B. Wang, G. T. Yee, C. Y. Shu, L. S. Xu, B. Elliott, L. Echegoyen, J. C. Duchamp and H. C. Dorn, *Inorg. Chem.*, 2008, **47**, 5234-5244.
61. M. M. Olmstead, A. de Bettencourt-Dias, J. C. Duchamp, S. Stevenson, D. Marciu, H. C. Dorn and A. L. Balch, *Angew. Chem. Int. Ed*, 2001, **40**, 1223-1225.
62. J. M. Campanera, C. Bo, M. M. Olmstead, A. L. Balch and J. M. Poblet, *J. Phys. Chem. A*, 2002, **106**, 12356-12364.
63. T.-S. Wang, L. Feng, J.-Y. Wu, W. Xu, J.-F. Xiang, K. Tan, Y.-H. Ma, J.-P. Zheng, L. Jiang, X. Lu, C.-Y. Shu and C.-R. Wang, *J. Am. Chem. Soc.*, 2010, **132**, 16362-16364.
64. M. Chaur, R. Valencia, A. Rodríguez-Fortea, J. Poblet and L. Echegoyen, *Angew. Chem. Int. Ed*, 2009, **48**, 1425-1428.
65. J. Zheng, X. Zhao, J. Dang, Y. Chen, Q. Xu and W. Wang, *Chem. Phys. Lett.*, 2011, **514**, 104-108.
66. S. Stevenson, Y. Ling, C. E. Coumbe, M. A. Mackey, B. S. Confait, J. P. Phillips, H. C. Dorn and Y. Zhang, *J. Am. Chem. Soc.*, 2009, **131**, 17780-17782.
67. X. Lu, K. Nakajima, Y. Iiduka, H. Nikawa, T. Tsuchiya, N. Mizorogi, Z. Slanina, S. Nagase and T. Akasaka, *Angew. Chem., Int. Ed.*, 2012, **51**, 5889-5892.
68. H. Yang, C. Lu, Z. Liu, H. Jin, Y. Che, M. M. Olmstead and A. L. Balch, *J. Am. Chem. Soc.*, 2008, **130**, 17296-17300.
69. Y. Iiduka, T. Wakahara, T. Nakahodo, T. Tsuchiya, A. Sakuraba, Y. Maeda, T. Akasaka, K. Yoza, E. Horn, T. Kato, M. T. H. Liu, N. Mizorogi, K. Kobayashi and S. Nagase, *J. Am. Chem. Soc.*, 2005, **127**, 12500-12501.
70. T.-S. Wang, N. Chen, J.-F. Xiang, B. Li, J.-Y. Wu, W. Xu, L. Jiang, K. Tan, C.-Y. Shu, X. Lu and C.-R. Wang, *J. Am. Chem. Soc.*, 2009, **131**, 16646-16647.
71. K. Tan and X. Lu, *Chem. Commun.* , 2005, 4444-4446.
72. J. Zhang, T. Fuhrer, W. Fu, J. Ge, D. W. Bearden, J. Dallas, J. Duchamp, K. Walker, H. Champion, H. Azurmendi, K. Harich and H. C. Dorn, *J. Am. Chem. Soc.*, 2012, **134**, 8487-8493.
73. S. Stevenson, M. A. Mackey, M. A. Stuart, J. P. Phillips, M. L. Easterling, C. J. Chancellor, M. M. Olmstead and A. L. Balch, *J. Am. Chem. Soc.*, 2008, **130**, 11844-11845.

74. B. Q. Mercado, M. M. Olmstead, C. M. Beavers, M. L. Easterling, S. Stevenson, M. A. Mackey, C. E. Coumbe, J. D. Phillips, J. P. Phillips, J. M. Poblet and A. L. Balch, *Chem. Commun.* , 2010, **46**, 279-281.
75. B. Q. Mercado, M. A. Stuart, M. A. Mackey, J. E. Pickens, B. S. Confait, S. Stevenson, M. L. Easterling, R. Valencia, A. Rodríguez-Fortea, J. M. Poblet, M. M. Olmstead and A. L. Balch, *J. Am. Chem. Soc.*, 2010, **132**, 12098-12105.
76. L. Dunsch, S. Yang, L. Zhang, A. Svitova, S. Oswald and A. A. Popov, *J. Am. Chem. Soc.*, 2010, **132**, 5413-5421.
77. N. Chen, M. N. Chaur, C. Moore, J. R. Pinzon, R. Valencia, A. Rodriguez-Fortea, J. M. Poblet and L. Echegoyen, *Chem. Commun.* , 2010, **46**, 4818-4820.
78. N. Chen, C. Beavers, M. Mulet-Gas, A. Rodr√≠guez-Fortea, E. Munoz, Y.-Y. Li, M. Olmstead, A. Balch, J. Poblet and L. Echegoyen, *J. Am. Chem. Soc.*, 2012, **134**, 7851-7860.
79. B. Q. Mercado, N. Chen, A. Rodríguez-Fortea, M. A. Mackey, S. Stevenson, L. Echegoyen, J. M. Poblet, M. M. Olmstead and A. L. Balch, *J. Am. Chem. Soc.*, 2011, **133**, 6752-6760.
80. N. Chen, M. Mulet-Gas, Y.-Y. Li, R. E. Stene, C. W. Atherton, A. Rodriguez-Fortea, J. M. Poblet and L. Echegoyen, *Chem. Sci.*, 2013, **4**, 180-186.
81. F.-F. Li, N. Chen, M. Mulet-Gas, V. Triana, J. Murillo, A. Rodriguez-Fortea, J. M. Poblet and L. Echegoyen, *Chemical Science*, 2013, **4**, 3404-3410.
82. Y.-J. Guo, B.-C. Gao, T. Yang, S. Nagase and X. Zhao, *Phys. Chem. Chem. Phys.*, 2014, **16**, 15994-16002.
83. L.-H. Gan, Q. Chang, C. Zhao and C.-R. Wang, *Chem. Phys. Lett.*, 2013, **570**, 121-124.
84. P. Zhao, T. Yang, Y.-J. Guo, J.-S. Dang, X. Zhao and S. Nagase, *J. Comput. Chem.*, 2014, **35**, 1657-1663.
85. L.-H. Gan, D. Lei, C. Zhao and X. Guo, *Chem. Phys. Lett.*, 2014, **604**, 101-104.
86. Y. Chai, T. Guo, C. Jin, R. E. Haufler, L. P. F. Chibante, J. Fure, L. Wang, J. M. Alford and R. E. Smalley, *J. Phys. Chem.*, 1991, **95**, 7564-7568.
87. R. D. Johnson, M. S. de Vries and et al., *Nature*, 1992, **355**, 239.
88. P. W. Dunk, N. K. Kaiser, C. L. Hendrickson, J. P. Quinn, C. P. Ewels, Y. Nakanishi, Y. Sasaki, H. Shinohara, A. G. Marshall and H. W. Kroto, *Nat. Commun.*, 2012, **3**, 855-863.
89. S. Bandow, H. Kitagawa, T. Mitani, H. Inokuchi, Y. Saito, H. Yamaguchi, N. Hayashi, H. Sato and H. Shinohara, *The Journal of Physical Chemistry*, 1992, **96**, 9609-9612.
90. E. B. Iezzi, J. C. Duchamp, K. R. Fletcher, T. E. Glass and H. C. Dorn, *Nano Lett.*, 2002, **2**, 1187-1190.

91. R. B. Lauffer, *Chem. Rev.* , 1987, **87**, 901-927.
92. H. Yukichi, K. Shinpei and N. Yukio, *Sci. Technol. Adv. Mater.*, 2011, **12**, 044607.
93. R. B. Ross, C. M. Cardona, D. M. Guldi, S. G. Sankaranarayanan, M. O. Reese, N. Kopidakis, J. Peet, B. Walker, G. C. Bazan, E. Van Keuren, B. C. Holloway and M. Drees, *Nat. Mater.*, 2009, **8**, 208-212.
94. S. Licht, *Semiconductor Electrodes and Photoelectrochemistry*, Wiley, Weinheim, 2002.
95. J. R. Pinzón, M. E. Plonska-Brzezinska, C. M. Cardona, A. J. Athans, S. S. Gayathri, D. M. Guldi, M. Á. Herranz, N. Martín, T. Torres and L. Echegoyen, *Angew. Chem. Int. Ed*, 2008, **47**, 4173-4176.
96. A. Enyashin, S. Gemming, T. Heine, G. Seifert and L. Zhechkov, *Phys. Chem. Chem. Phys.*, 2006, **8**, 3320-3325.
97. G. Seifert, A. N. Enyashin and T. Heine, *Phys. Rev. B*, 2005, **72**.
98. D. S. Bethune, R. D. Johnson, J. R. Salem, M. S. de Vries and C. S. Yannoni, *Nature*, 1993, **366**, 123-128.
99. M. Feng and J. Twamley, *Phys. Rev. A*, 2004, **70**, 030303.
100. K. Yakigaya, A. Takeda, Y. Yokoyama, S. Ito and T. Miyazaki, *New J. Chem.*, 2007, **31**, 973-979.

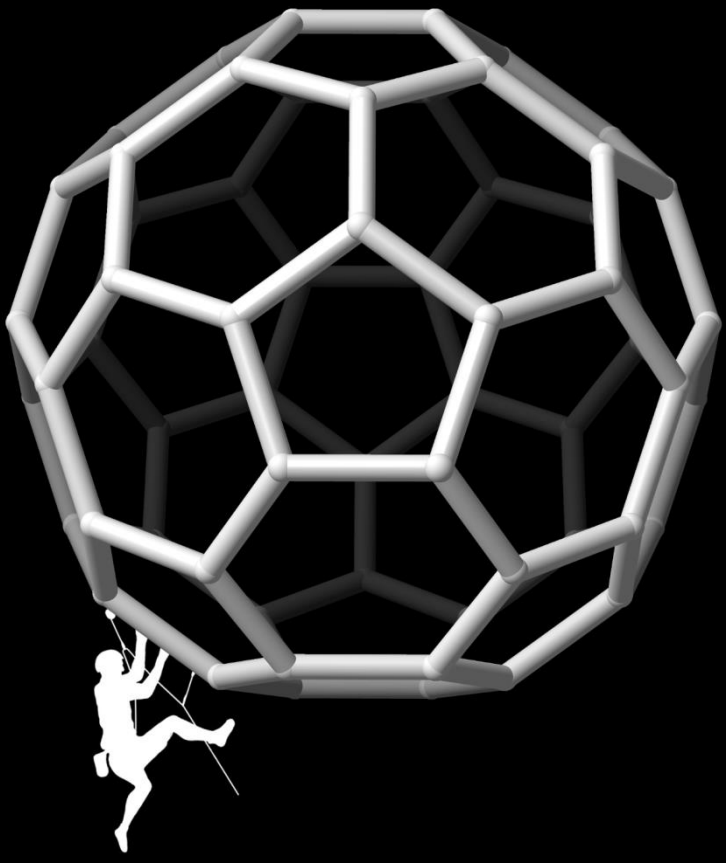

Chapter 2 // *Goals of the Thesis*

Chapter 2

Goals of this thesis

Several goals were expected to be reached during the development of this thesis. Sometimes, things do not go as expected and/or not all the objectives can be achieved. Contrarily, other times things are easier (or go better) than expected and all the milestones can be reached as foreseen.

In this chapter the main goals for each part of this thesis are listed in order to clarify what were our thoughts and requirements at the beginning of every project.

Chapter 3 | *Computational Methods and Modeling*

A good computational strategy is crucial in order to fully characterize the new isolated EMF and to do so; several aspects have to be taken into account:

- Understand the most important factors that govern the stabilization of EMFs.
- Design a computational strategy taking into account all this factors in order to be able to characterize the new EMFs families.
- Accurate modeling of the different data available from the experiments. The comparison of the predicted and experimental data is crucial in the cage assignment.

Chapter 4 | *Identifying the First Two Scandium Sulfide Endohedral Fullerenes with non-IPR Cages*

These were the first two projects in collaboration with Prof. Echegoyen group at the University of Texas at El Paso. They were able to synthesize and isolate these two new EMFs and we designed the corresponding computational study in order to solve the structure of both systems. The main objectives were:

- Compute and analyze the results for the anionic cages and the endohedral systems in order to find a suitable candidate for each family.
- Confirm the formal electron transfer from the cluster to the cage.
- Compute the electrochemical and spectroscopic data.
- Assign the cage symmetries and solve the cluster position.
- Analyze the cage structure to find any connection that could suggest a growth through the Closed Network Growth mechanism.

Chapter 5 | *$Ti_2S@D_{3h}(24109)$-C_{78}: a Sulfide Cluster Fullerene Containing Only Transition Metal Atoms*

This work also arises after the detection and isolation of this new EMF at UTEP laboratories by Echegoyen and co-workers. In this case, the study has the same scheme as in the previous chapter with the additional challenge of being the first Ti_2S ever trapped in a carbon cage. The main goals at the beginning of this work were:

- Confirm the titanium oxidation state and the formal transfer from the cluster to the cage.
- Find the lowest-energy isomer of $Ti_2S@C_{78}$.
- Determine the importance of the cluster geometry and position in the case of a IPR cage.
- Simulate the absorption spectrum and the electrochemical data for the isomer assignment.
- Compare the present system with possible similar systems like $Ti_2C_2@C_{78}$.

Chapter 6 | *Small Endohedral Metallofullerenes: Exploration of the Structure, Growth and Abundances*

The experimental detection of a new family of metallofullerenes achieved by means of the state-of-the-art Fourier Transform Ion Cyclotron Resonance (FT-ICR) mass spectrometry was the starting point of this project. The main goals in order to rationalize and characterize the species detected were:

- Validate the ionic model for these small families of metallofullerenes.
- Explore all the structures in order to find the lowest-energy isomers for $Ti@C_{2n}$ (2n=26-50).
- Identify the charge formally transferred from the metal atoms to the cage.

- Rationalize the special abundance of the experimental peaks.
- Look for connections between cages in order to confirm the possible Closed Network Growth.
- Extend the study to other metals: Ca@C_{2n} family.
- Understand the importance of the charge transfer and ionic radii on the experimental distributions of the detected species in the mass spectra.
- Study of two new Ga and In EMFs and the uncommon oxidation state of these metals inside the carbon cages.
- Explain the abundances and its independence of the ionization potentials.

Chapter 7 | *Relevance of Thermal Effects in the Formation of Metallofullerenes: the Case of $Gd_3N@C_s(39663)$-C_{82} and Other Related Systems*

The computational predictions at 0 K usually explain the experimental results, but in some cases, the effects of the high temperatures reached in the reactors are determinant to understand which isomers are formed. This study wanted to give more insight into these thermal effects by:

- Evaluate the effect of the temperature in the case of the lowest-energy isomers for $Gd_3N@C_{82}$.
- See the influence of computing the energies using different functionals.
- Find and structural relation between different cages.
- Study the importance of the different contribution of the partition function when computing the molar fractions using the approximations proposed by Slanina and co-workers.

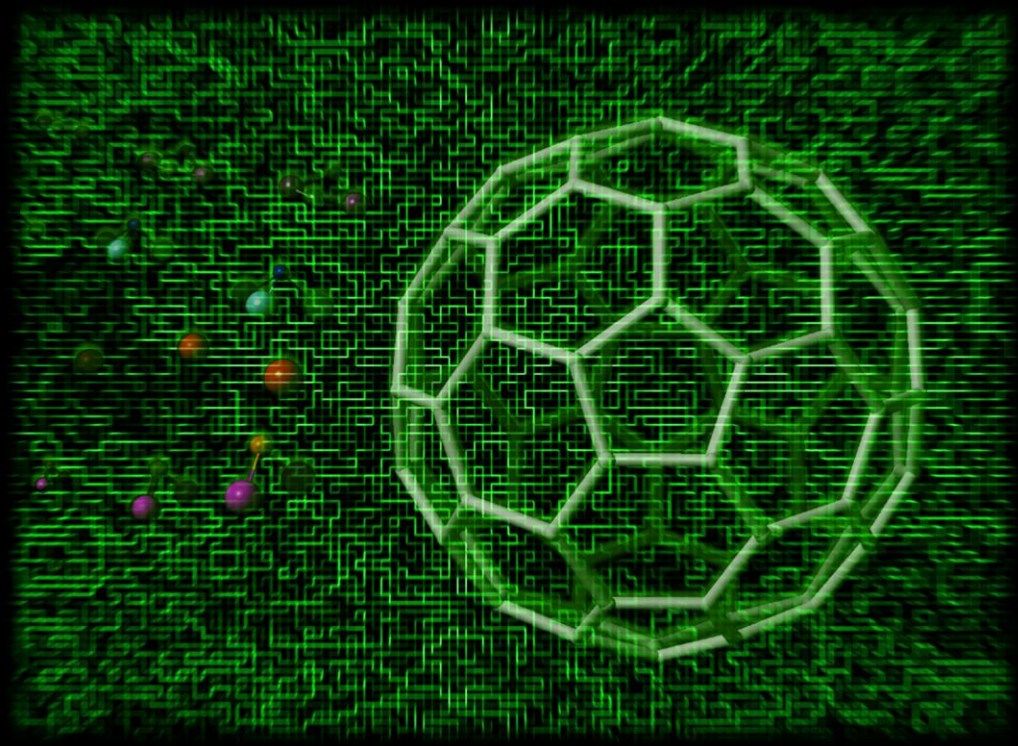

Chapter 3 // *Computational Methods and Modeling*

Related Publications:

Electronic Structure of IPR and non-IPR Endohedral Metallofullerenes: Connecting Orbital and Topological Rules

N. Alegret, M. Mulet-Gas, X. Aparicio-Anglès, A. Rodríguez-Fortea and J. M. Poblet. *Comptes Rendus Chimie*, **2012**, 15, 152-158.

Chapter 3

Computational Methods and Modeling

Herein, we have included a detailed explanation of the key factors that govern the stabilization of endohedral metallofullerenes. It is important to take them into account in order to follow an efficient computational strategy. On the other hand, the computational methods used to compute all the structures and the properties are also described. The computations of these properties are crucial for the comparison with the experimental data available when new endohedral metallofullerenes are synthesized.

3.1. Introduction

One of the most interesting features of endohedral metallofullerenes is their capacity to stabilize carbon cages that are not formed when empty.[1] Among the hundreds, or even thousands, of different isomers that can be generated for a given number of carbon atoms, only one (sometimes two or three) is usually found to encapsulate a cluster forming a new endohedral metallofullerene. Therefore, structural elucidation by X-ray diffraction is the final and conclusive step for the precise determination of the isomeric structure of the carbon cages. It is necessary to clarify that for a complete elucidation of the structure, the determination of the carbon cage isomer as well as the geometry and position of the inner cluster must be achieved. However, there is a major obstacle that causes difficulties in the experimental structural assignments: the low yield obtained for most of the new species. For this reason the combination of extensive theoretical studies along with the experimental data that can be obtained is of major importance to obtain a correct assignment.[2]

In order to design an effective computational strategy to solve the structural problems that arose when a new endofullerene is formed, the most important factors that govern the stabilization of the EMFs have to be taken into account.

Hence, we consider that the three most important factors that control the selection of a specific cage over all the different isomer are related to (i) the electron transfer from the trapped unit to the carbon cage; (ii) the disposition of the pentagon rings in the carbon framework; and (iii) the size and geometry of the endocluster and the cage, and the interaction between them. It is important to understand the effect of each factor and how to properly consider them in order to unambiguously assign the cage symmetry and the structure of the new EMFs.

3.2. Ionic model and orbital rules

The electronic properties of the endohedral metallofullerenes can be rationalized taking into account a simple ionic model, which considers that there is a formal transfer of electrons from the encapsulated atoms or cluster to the carbon cage. The number of transferred electrons depends on the internal guest as it is shown in table 3.1. Thus, the endohedral fullerenes can be described as $(cluster)^{m+}@(C_{2n})^{m-}$.

Table 3.1 List of different charge transfer depending on the internal guest.

Inner moiety	Charge transfer	Inner moiety	Charge transfer
M	1, 2, 3	M_2O	4
M_2	4,6	M_4O_2, M_4O_3	6
M_3N	6	M_2C_2	4
M_2S [a]	4	M_3C_2, M_4C_2	6

[a] Four electrons are formally transferred in all the metallic sulfides reported except for the $Ti_2S@C_{78}$ in which six electrons are transferred.

Considering this electron transfer and the corresponding ionic description of the endohedral systems, in 2005, Poblet and co-workers proposed an orbital rule in order to predict the suitable carbon cage to encapsulate metallic clusters and to predict the relative stabilities of EMFs (based on the $M_3N@C_{2n}$ species where six electrons are transferred). The rule states that 'a suitable host must have three low-lying unoccupied molecular orbitals and sizeable energy gap between the LUMO+2 and the LUMO+3', taking into account that the charge is transferred from the highest-occupied molecular orbitals (HOMOs) of the internal guest to the lowest-unoccupied molecular orbitals (LUMOs) of the carbon cage.[3] As it is shown in figure 3.1, nitride endohedral metallofullerenes that have been fully characterized by single crystal X-ray diffraction satisfy this rule so far. Later on, the same trend was observed for the endohedral fullerenes with an electron transfer of four electrons from the cluster to the carbon cage, such as $M_2C_2@C_{2n}$.[4]

In addition, this orbital rule helped to rationalize why different clusters are found to be encapsulated by different isomers with the same cage size,

or why different cages (despite being topologically very similar) prefer clusters that transfer a certain amount of charge. In particular, in figure 3.2, we show the case of C_{80} and C_{82}.

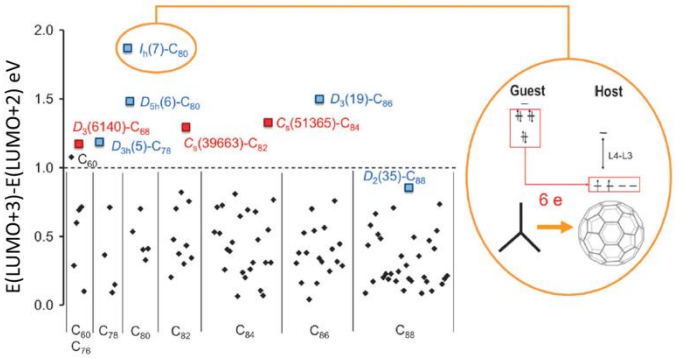

Figure 3.1 Gaps between the energies of the LUMO+2 and the LUMO+3 in eV for empty fullerenes between C_{60} and C_{88}. Fullerenes that have been characterized encapsulating a metallic nitride are highlighted in blue (IPR) and in red (non-IPR). The figure also show schematically the formal transfer of six electrons from the HOMOs of the M_3N to the LUMOs (partially occupied) of the $I_h(7)$-C_{80}.

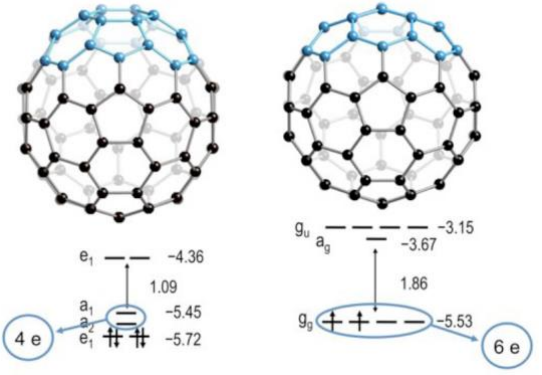

Figure 3.2 Comparison of the geometry and the electronic structure of C_3v(8)-C_{82} and $I_h(7)$-C_{80}. The different motifs in the cage structures are highlighted in blue.

Because of this different charge transfer, it has been found that whereas nitrides have as the major product the $I_h(7)$ isomer of C_{80}, carbides prefer isomer C_3v(8) of C_{82}.

Soon after this orbital rule was published, Popov and Dunsch reported an exhaustive computational study showing that the lowest-energy hexaanionic isomers always match the lowest-energy nitride endohedral fullerenes, and thus, the species obtained in the experiments.[5] This work was also based on the metallic nitride species. Further on time, we have shown that this trend is also reproduced in the case of species that transfer four electrons, such as carbides and sulfides, and in the case of species that transfer two electrons, such as divalent atoms in classical $M@C_{2n}$ fullerenes.[6]

According to this, the anionic empty cages can reproduce the relative energies of the endohedral systems. This is a valuable tool for the selection of the suitable isomer that can form endohedral fullerenes. Therefore, the computation of the anions is going to be the first step in our computational strategy, not only because they have been found to reproduce the energy of the endohedrals, but also because the computation of the empty anions is much cheaper in terms of computational cost.

3.3. The importance of pentagon distribution

The stability of charged fullerene isomers was already interpreted according to a favorable disposition of the pentagons in the structure in order to minimize the steric strain.[7] Recently, in a work reported by our group, it has been shown that the stability of a particular isomer is related to the separation among pentagons.[8] The separation can be measured by the inverse pentagon separation index (IPSI) computed by the formula shown in figure 3.3, where R_{ij} is the distance between the centroids of pentagons *i* and *j*. Charge has been shown to be located in the pentagons, consequently, the isomers with largest separation among pentagons (smallest IPSI values) reduce the coulombic repulsion and thus become the most stable.

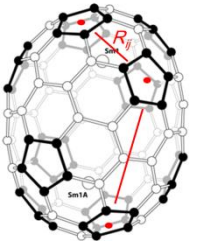

$$IPSI = \sum_{i=1}^{12} \sum_{j>i}^{12} 1/R_{ij}$$

Figure 3.3 Equation for the computation of the IPSI value and a schematic representation showing two examples of distances between pentagon centroids.

It has been shown that IPSI values correlate with the relative stability of charged cages for a given C_{2n} family, especially for tetra- and hexaanions due to the larger ability of the pentagons to attract negative charge.[9]

Very recently, another prediction tool for endohedral fullerenes has been reported. The so-called maximum aromaticity criterion (MARC), based on the additive local aromaticity (ALA), shows that the stability of anionic cages correlates with their aromatic character.[10] Recently, it has been also observed that ALA, computed with the HOMA index, is correlated with the IPSI value and the number of pyracylenes.[11] The most important improvement with respect to the IPSI is that the MARC allows the comparison of isomers with different number of pentagon adjacencies.

An example that perfectly illustrates the importance of the pentagon disposition in the carbon structure is depicted in figure 3.4. The different isomers of C_{80} are represented. All of them, like all the fullerenes, contain twelve pentagons, but they are occupying different positions. The arrangement of the pentagons is crucial to understand that isomer $D_{5d}(1)$ is the most favored when the cage is empty, whereas isomers $D_{5h}(6)$ and $I_h(7)$ are the most stable ones when the cage is charged. The disposition of the pentagons allows a better distribution of the charge reducing the repulsion.

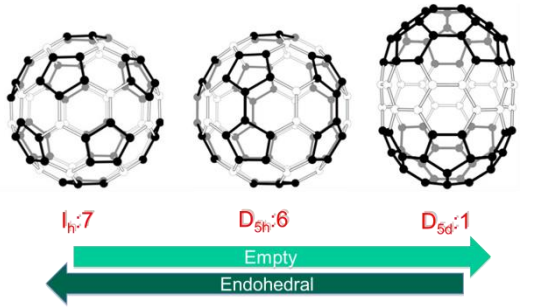

Figure 3.4 Representation of three isomers of C_{80}. Pentagons are highlighted in black. Different isomers are favored when cages are empty or encapsulating a cluster.

The charge distribution over the carbon cages is also important when the structures show adjacent pentagon pairs. In the case of the non-IPR isomers, more charge is localized at the pentalene bonds. This is also an important feature to take into account for the non-IPR isomers stabilization. As it is shown in figure 3.5 (left) for C_{84}, most of the 24 neutral IPR present lower energies than the 110 non-IPR isomers with a pair of adjacent pentagons (APP1), as already predicted by the isolated pentagon rule. However, when the cages are computed as hexaanions, the energy differences of the two sets of isomers are rather decreased to the point that one of the APP1 isomers becomes competitive to the IPR cages.

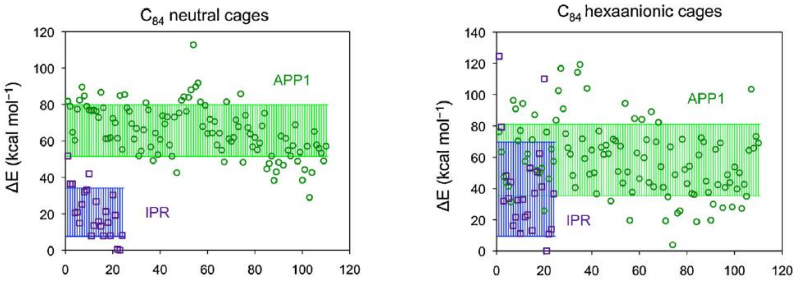

Figure 3.5 Relative energies for IPR and non-IPR with one adjacent pentagon pair (APP1) isomers of C_{84}.

3.4. Cluster cage matching: hollow space and cluster size and shape

This is, along with the charge transfer and the pentagon distribution, a key factor to understand the cage selection given a certain endocluster.

If we take into account the effect of the charge transfer, considering the orbital rules, and the different parameters that explain the charge distribution on the cages with respect to their stability, we can select a set of isomers suitable to encapsulate a given cluster, even sometimes a single isomer. However, further aspects have to be taken into consideration. These aspects are: (i) the available space in the fullerene cage; (ii) the interaction between the trapped cluster and the fullerene cage; and (iii) the geometry of the cluster itself.

It is very intuitive to understand that there is a physical limitation in the encapsulation of certain species for a given size of carbon cages. It has been shown that the larger the cluster, the larger the most favored cages. Moreover, for a particular type of cluster, the size of the metallic atoms is also critical for the selection of the most favored cage. Figure 3.5 shows the preferred cages for different types of nitride clusters. As the metallic radii increase the size of the preferred cages also increases.[12, 13]

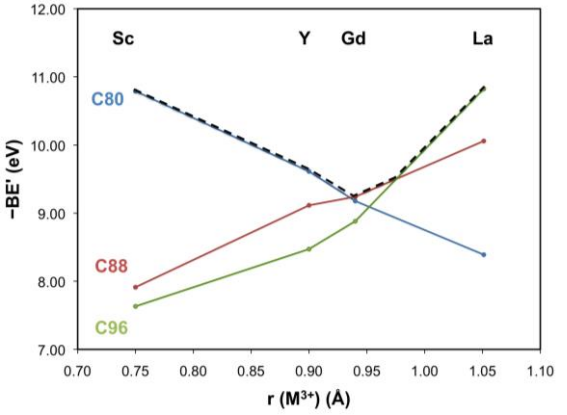

Figure 3.5 Binding energies with respect to the most stable neutral cage as a function of the metal radii. The larger the BE the more favored the cage size.

However, some cases are not as intuitive. For instance, although Sc_3N cluster fits better in a C_{80} cage, it has been detected in a C_{68} cage. Also the larger Gd_3N, which prefer the C_{80} cage, has been found encapsulated in both a C_{78} and a C_{88} cage. Interestingly, all this smaller cages that surprisingly can encapsulate large cluster possess adjacent pentagon pairs. Therefore, in addition to the stabilization provided by the charge transfer, there is an important effect due to the interaction of the cluster and the cage. This effect is critical when the cages show fused pentagons in the carbon framework. If we think about the charge distribution over the cage, the pentagons and pentagon junctions are nucleophilic regions, the trapped metals are formally cations (since they have transferred charge to the cage) resulting in a favorable interaction between the two moieties.

As a consequence of this rather strong interaction, metal atoms are always pointing toward the pentalene bonds when trapped in non-IPR cages. This leads us to the third important factor: the cluster geometry, or cluster distortion. If we analyze the different disposition that a cluster can adopt inside a carbon cage, we found that clusters usually tend to get a configuration where the metal atoms are maximally separated in order to minimize the electrostatic repulsion. A very recent study by Popov and co-workers showed that each cluster has an ideal geometry (distances and angles).[14] Some energy penalty appears when the cluster is distorted in order to fit in carbon cages. Therefore, there is an optimal combination regarding the cluster geometry and the cage structure. Those combinations that allow the clusters to have geometries close to the ideal ones and, at the same time, allows a strong interaction between cluster and cage will lead to the most stable endohedral fullerenes.

3.5. Computational strategy for structure selection

Computational studies have become determinant for the complete characterization of new endohedral metallofullerenes. For this reason it is very important to make sure that the path followed in order to elucidate the structure will lead us to a correct assignment. In order to design an efficient computational strategy we have to take into account all the previously-described key factors that govern the stabilization of endohedral metallofullerenes. Figure 3.6 shows schematically the computational strategy that we followed through the whole thesis to propose a cage candidate and help in the structure characterization of the synthesized metallofullerenes.[15]

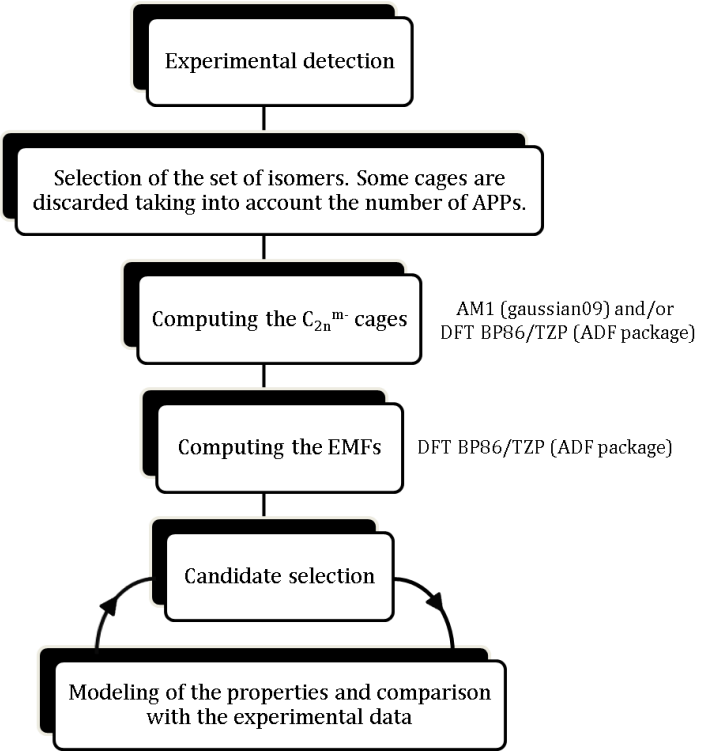

Figure 3.6 Computational strategy designed in order to elucidate the structure of new endohedral fullerenes. When there is more than one candidate, the last step is a kind of iterative process to discard some of them by comparison of computed and experimental properties.

In the next section the computational details and the most important aspects that have to be taken into account are detailed.

3.5.1. Selection of a set of isomers

This is the first step in our computational protocol. From the experiments, usually from the mass spectrometry data, we know how many carbon atoms the synthesized fullerene has. Therefore, we know how many isomers can be possible and which of them are IPR and non-IPR. In order to select the desired set of isomers, we use a code developed in our group that allows us to obtain the number and geometries of the IPR, and APPn (n=1, 2, 3, 4, 5, 6) isomers from the spiral algorithm.

This first selection is based on the energy penalty induced by the presence of adjacent pentagon pairs in the structure and the number of metal atoms that can strongly interact with those pentalenes in order to stabilize the system.[16, 17]

3.5.2. Computing the C_{2n}^{m-} cages

At this point, we have a set of isomers to work with. We have already shown that the energies of the anionic cages have been found to correlate with the endohedral metallofullerenes, in accordance with the ionic model. Therefore, we compute the anionic cages to keep narrowing down the set of suitable isomers. Depending on the size of the set of isomers we proceed in two different ways. If the set of isomers is relatively small, we compute all the isomers at DFT BP86/TZP level.[18-20] Contrarily, if the set of isomers is too large and thus not affordable at DFT level, we compute the whole set at the semiempirical Austin Model (AM1) level, which is really cheap and gives reasonably good results, and then we refine the lowest-energy isomers at DFT level.[21] It has been shown in many works that the energies of the cages computed at AM1 and DFT level show a very good correlation which indicates the validity of this approximation.[6]

Reached this point, we select the lowest-energy cages (from the anionic calculations) in a range of ~20/30 kcal mol^{-1}. The next step will be the computation of the endohedral fullerenes. It is important to follow these previous steps before the computations of the endohedrals in order to reduce the set of isomers as much as possible because the number of different conformations that the cluster can take inside the cage is enormous, and this increases the amount of computational resources and time that we are going to need. Obviously, we follow this strategy trying to be effective but aimed to not endanger the quality of the results.

3.5.3. Computing the endohedrals: the candidate selection

It is important to keep in mind that for a complete structural characterization, we not only need to elucidate the cage isomer but also the position and geometry that the internal guest has inside the cage. For this reason, and once we have a relatively reduced set of isomers, we have to compute all the different orientations and geometries that the cluster can adopt inside the carbon cages. It is worth noting that this has a certain different degree of complexity depending on the type of cage. For IPR cages, in which the interaction between the cluster and the cage is not determinant, the geometry of the cluster is rather more important than its position. On the other hand, when the cage is a non-IPR isomer, along with the cluster geometry, the position of the cluster is determinant in order to maximize the (strong) interaction between the metal atoms and the pentalene motifs. In all the computational works reported so far involving non-IPR cages, the metal atoms have been found to be pointing to the adjacent pentagon pairs. For this reason, the number of different orientations that we can construct is reduced compared to the number of different orientations that we have to check for IPR isomers.

After carrying out all the computations for the EMF candidates, all the minima structures are characterized as absolute minimum points in the potential energy surface by means of analytical frequency calculations. Harmonic frequencies can be computed in ADF either numerically or analytically. The analytical frequencies are, in the last releases of ADF, as

accurate as the numerical frequencies but can be up to 3 to 5 times quicker to compute, depending on the molecule, integration and basis set parameters.

At this point, the analysis of the results obtained from all this set of calculations lead us to the selection of the candidate. This candidate is the structure that we propose as the one obtained in the experiments. At that time, we will compute the properties of this structure in order to compare them with the experimental data available for the obtained product.

3.5.4. Modeling of properties: comparison of experimental and computed data

The comparison of the data that can be obtained by experimental measurements with the data that can be computed is a very valuable tool in order to confirm or discard the selected candidate(s).

Among all the possible experimental measurement that can be done to a fullerene sample, we will focus our attention to the electrochemistry, the absorption spectroscopy and the single crystal X-ray diffraction. It has been shown that reliable theoretical prediction can be made on this properties and thus the comparison with the experiments will be determinant. Moreover, since the fullerenes are synthesized at very high temperatures, the effect of the temperature on the cluster formation has to be taken into account.

Electrochemistry

Cyclic voltammetry is among the most useful techniques to characterize the oxidation/reduction properties of endohedral metallofullerenes and to determine their electrochemical gap. The large sensitivity of this method facilitates the analysis of the very small quantities in which most of these materials are usually available.[2, 22]

Anodic and cathodic potentials as well as electrochemical gaps have been predicted at DFT level for several compounds of the $M_3N@C_{2n}$ family and

for sulfide and oxide clusterfullerenes.[23] To predict the experimental cathodic and anodic potentials, (i) we compute the absolute reduction and oxidation potentials and then made them relative to the normal hydrogen electrode, which has an estimated absolute reduction potential of +4.28 eV, as determined by Cramer and co-workers; and (ii) we have to take into account that ferrocene is added in the experiments as internal standard, thus the Fc/Fc^+ of +0.40 V has to be included.[24, 25]

Since the cyclic voltammetry is performed in solution, usually *o*-dichlorobenzene, solvation effects must be taken into account in the computations. The conductor like screening model (COSMO) implemented in ADF is the method used to include the solvent effect in the calculations.[26] COSMO is a dielectric model in which the solute is embedded in a molecule-shaped cavity surrounded by a dielectric medium with given dielectric constant (ε). As depicted in figure 3.7, starting from van der Waals spheres centered on the solute atoms, three different models for the molecule surface can be generated: (i) the proper van der Waals (vdW) surface, which consist on the union of the all atomic spheres; (ii) the solvent accessible surface (SAS), which is similar to the vdW but consists on the path traced by the center of a spherical molecule rolling over the vdW surface, or equivalently, a vdW surface created by atomic spheres to which the solvent radius has been added; and (iii) the solvent excluding surface (SES), which consist on the path traced by the surface of a spherical solvent molecule rolling over the vdW surface. This also consists of the vdW surface but in the regions where spheres would intersect, the concave part if the solvent sphere replaces the cusp. The latter is the model used in this work. The list of atomic radii and the solvent dielectric constant for the solvent used (*o*-dichlorobenzene) are listed in table 3.2.

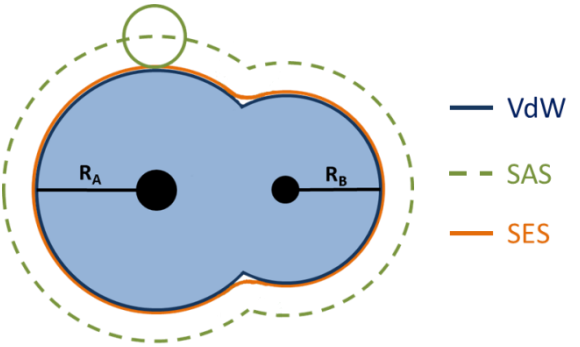

Figure 3.7 Schematic representation of the cavity construction method for COSMO.

Table 3.2 Dielectric constant (ε) and VdW radii used for the computation of the electrochemistry within the COSMO approximation.

dielectric constant	(ε)
o-DCB	9.8

VdW radii (Å)	
C	1.70
S	1.80
Sc	2.00
Ti	2.00

Using this computational set up, several studies have shown the validity of the theoretical predictions versus the experimental electrochemical data.[1, 23, 27] Very good correlations have been found for the anodic potentials and for the electrochemical gaps for a large group of different endohedral metallofullerenes. Considering this, and despite of the approximations used, the results from the computations are reliable and thus very helpful for our main objective of confirming and discarding possible candidate isomers.

UV-vis-NIR absorption spectroscopy

UV-vis-NIR absorption spectroscopy remains one of the most important characterization techniques of endohedral metallofullerenes. The main reasons are the relatively inexpensive instrumentation and simple sample

preparation. Thus, absorption spectra are reported almost for all isolated fullerenes.

The most important advantage of this technique is its high structural sensitivity. Absorption spectra of fullerenes are dominated by the $\pi \rightarrow \pi^*$ excitations of their carbon cages. As a result, it has been recognized that the spectra of EMFs with the same carbon cage isomer in the same formal charge state are almost identical, independently of the encapsulated metal or cluster. For instance, absorption spectra of all $M^{III}@C_{2v}(9)$-C_{82} monometallofullerenes (M=Y, La, Ce, Pr, Nd, Gd, Tb, Dy, Ho, Er, Lu) are very similar and, simultaneously, very different from the spectra of $M^{II}@C_{2v}(9)$-C_{82}, which has the same cage isomer but different charge state for M= Ca, Sm, Tm, Eu, Yb; or $M^{III}@C_s(6)$-C_{82}, which has same charged state but different cage symmetry. It is necessary to mention that this similarity on the UV-vis-NIR spectra is no longer maintained when the metal atoms have significant contributions to the frontier orbitals. This happens for example for Sc_3N, La_2 and Ti_2C_2 trapped in the $D_{3h}(5)$-C_{78} cage. Although the three structures have the same cage isomer and the three internal guests transfer six electrons to the cage, their absorption spectra are impressively different. The reason for this fact is that the metal-cage interactions are considerably different which changes the energy distribution of the frontier molecular orbitals and thus the absorption spectra.[28]

An important parameter available from the absorption spectra that helps in the isomer assignment (or rejection) is the optical gap. In principle, this parameter should be determined as the energy of the lowest-energy excitation. However, sometimes the assignment of the lowest-energy excitations is difficult for EMFs due to the overlapping of broad bands in the spectra. Therefore, the optical gap is often estimated from the absorption onset. The importance of the optical gap emanates from the fact that it intimately related to the HOMO-LUMO gap and according to this, it is very helpful to discard possible isomers.

The time-dependent density functional theory (TDDFT) has become the predominant single-reference theory for modeling the exited states of medium-sized and large molecules. Endohedral metallofullerenes are still too large for the post-Hartree-Fock methods. Despite the underestimation of the excitation energies, and the dependence on the exchange-correlation functional, it has been shown that the prediction of absorption spectra using at the PB86/TZP level gives reasonably good agreement with the experiments, helping us to assign or discard possible cage symmetries for the new EMFs synthesized.[29]

Thermochemistry: the effect of the temperature

The stability of fullerenes has been traditionally considered in terms of differences of potential energies. Although this approach gives a good result on the structural characterization of most of the systems, in some cases, the electronic energies at 0 K cannot justify the experimental results and the thermal effects have to be taken into account. Slanina and co-workers demonstrated that the Gibbs energy should be taken into account in order to incorporate the effect of the high temperatures reached during the fullerene formations. To do so, the relative concentrations of a set of *m* isomers can be obtained from the partition functions q_i according to the classical expression (Eq. 1)

$$x_i = \frac{q_i \exp\left[-\Delta H^0_{0,i} \Big/ RT\right]}{\sum_j^m q_j \exp\left[-\Delta H^0_{0,j} \Big/ RT\right]} \qquad \text{Eq. 1}$$

Where x_i is the mole fraction and $\Delta H^0_{0,i}$ is the enthalpy at the absolute zero temperature (the relative potential energy corrected for the vibrational zero-point energies of isomer *i*). Two different approximations are used in order to compute the mole fraction for the endohedral metallofullerenes: (i) the conventional rigid rotor harmonic oscillator (RRHO),[30, 31] a method that has been systematically employed to analyze the effect of the

temperature on the isomer population for many empty fullerenes, where rotational and vibrational partition functions are computed using rigid rotor and the harmonic oscillator approximation; and (ii) the free encapsulation model (FEM) in which, considering that the atoms or clusters trapped in the carbon cages can exhibit large amplitude motions, up to the six lowest vibrational frequencies, which belong to the metal clusters are removed and the symmetry of the cage is taken as the highest topologically possible.[32]

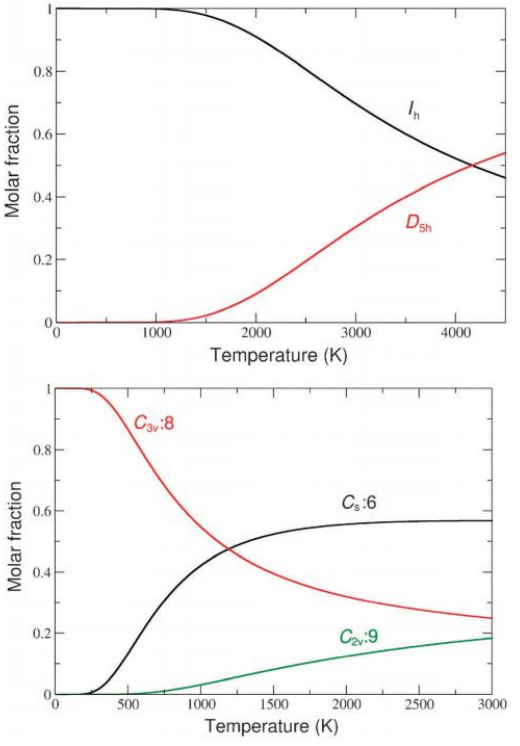

Figure 3.8 Relative concentrations determined for $I_h(7)$ and $D_{5h}(6)$ IPR isomers of $Sc_3N@C_{80}$ (to) and for the three lowest-energy isomers of $Sc_2O@C_{82}$ (bottom).

It is worth remarking two of the most important examples where these approximations are crucial to explain the experimental results. On one hand, this model predicts the achieving of the $Sc_3N@D_{5h}(6)$-C_{80} isomer which cannot be explained by the electronic energies at 0 K.[33, 34] On the

other hand, it has been found very recently that the X-ray structure of the endohedral $Sc_2O@C_{82}$ does not correspond to the lowest-energy isomer at 0 K. Only when the thermal effects are considered, the most favored isomer is found to be the $Sc_2O@C_s(6)$-C_{82}, in good agreement with the structural data from the experiments.[35] (figure 3.8).

3.6. Conclusions

Principally determined by the low yield obtained in the synthesis of EMFs, the combination of computational studies and experimental analysis has become the most powerful tool to characterize the structure of the new isolated species. In order to design an effective computational strategy, all the key factors that govern and affect the stabilization of the cluster fullerenes have to be taken into account.

To this end, aspects as the electron transfer, topology of the carbon cages, and the geometry and interaction of the internal guests and the carbon framework have to be considered to accomplish the structural assignment properly, and lead us to adopt a specific computational strategy that has been shown to give very good results in all the cases that we have studied so far.

On the other hand, it is very important to take into account the available data from the experiments, and the computational modeling of the related properties. Particularly, the electrochemical data and the absorption spectroscopy are very useful to discard candidates for a proper cage assignment.

It is work remarking that we never use a single property to assign the cage symmetry or to characterize the isomers. It is the combination of all those parameters that allow us to make a reliable assignment of the cage isomer.

3.7. References

1. A. Rodríguez-Fortea, A. Balch and J. Poblet, *Chem. Soc. Rev.*, 2011, **40**, 3551-3563.
2. A. A. Popov, S. Yang and L. Dunsch, *Chem. Rev.* , 2013, **113**, 5989-6113.
3. J. M. Campanera, C. Bo and J. M. Poblet, *Angew. Chem. Int. Ed*, 2005, **44**, 7230-7233.
4. R. Valencia, A. Rodriguez-Fortea and J. M. Poblet, *J. Phys. Chem. A*, 2008, **112**, 4550-4555.
5. A. A. Popov and L. Dunsch, *J. Am. Chem. Soc.*, 2007, **129**, 11835-11849.
6. M. Mulet-Gas, L. Abella, P. W. Dunk, A. Rodríguez-Fortea, H. W. Kroto and J. M. Poblet, *Chem. Sci.*, 2014, (Accepted).
7. H. W. Kroto, *Nature*, 1987, **329**, 529-531.
8. A. Rodriguez-Fortea, N. Alegret, A. L. Balch and J. M. Poblet, *Nature Chem.*, 2010, **2**, 955-961.
9. N. Alegret, M. Mulet-Gas, X. Aparicio-Anglès, A. Rodríguez-Fortea and J. M. Poblet, *C. R. Chim.*, 2012, **15**, 152-158.
10. M. Garcia-Borràs, S. Osuna, M. Swart, J. M. Luis and M. Solà, *Angew. Chem. Int. Ed*, 2013, **52**, 9275-9278.
11. A. Rodriguez-Fortea and J. M. Poblet, *Faraday Discuss.*, 2014, **173**, 201-213.
12. M. N. Chaur, X. Aparicio-Anglès, B. Q. Mercado, B. Elliott, A. Rodríguez-Fortea, A. Clotet, M. M. Olmstead, A. L. Balch, J. M. Poblet and L. Echegoyen, *The Journal of Physical Chemistry C*, 2010, **114**, 13003-13009.
13. X. Aparicio-Anglès, N. Alegret, A. Clotet, A. Rodríguez-Fortea and J. M. Poblet, *The Journal of Physical Chemistry C*, 2013, **117**, 12916-12921.
14. Q. Deng and A. A. Popov, *J. Am. Chem. Soc.*, 2014, **136**, 4257-4264.
15. M. J. Frisch, G. W. Trucks, H. B. Schlegel, G. E. Scuseria, M. A. Robb, J. R. Cheeseman, G. Scalmani, V. Barone, B. Mennucci, G. A. Petersson, H. Nakatsuji, M. Caricato, X. Li, H. P. Hratchian, A. F. Izmaylov, J. Bloino, G. Zheng, J. L. Sonnenberg, M. Hada, M. Ehara, K. Toyota, R. Fukuda, J. Hasegawa, M. Ishida, T. Nakajima, Y. Honda, O. Kitao, H. Nakai, T. Vreven, J. J. A. Montgomery, J. E. Peralta, F. Ogliaro, M. Bearpark, J. J. Heyd, E. Brothers, K. N. Kudin, V. N. Staroverov, R. Kobayashi, J. Normand, K. Raghavachari, A. Rendell, J. C. Burant, S. S. Iyengar, J. Tomasi, M. Cossi, N. Rega, J. M. Millam, M. Klene, J. E. Knox, J. B. Cross, V. Bakken, C. Adamo, J. Jaramillo, R. Gomperts, R. E. Stratmann, O. Yazyev, A. J. Austin, R. Cammi, C. Pomelli, J. W. Ochterski, R. L. Martin, K. Morokuma, V. G.

Zakrzewski, G. A. Voth, P. Salvador, J. J. Dannenberg, S. Dapprich, A. D. Daniels, Ö. Farkas, J. B. Foresman, J. V. Ortiz, J. Cioslowski and D. J. Fox, Gaussian, Inc, Wallingford CT, 2009.

16. B. L. Zhang, C. Z. Wang, K. M. Ho, C. H. Xu and C. T. Chan, *J. Chem. Phys.*, 1992, **97**, 5007-5011.
17. E. Albertazzi, C. Domene, P. W. Fowler, T. Heine and G. Seifert, *Phys. Chem. Chem. Phys.*, 1999, **1**, 2913-2918.
18. A. D. Becke, *J. Chem. Phys.*, 1986, **84**, 4524.
19. J. P. Perdew, *Phys. Rev. B*, 1986, **33**, 8822-8824.
20. S. H. Vosko, L. Wilk and M. Nusair, *Can. J. Phys.*, 1980, **58**, 1200.
21. M. J. S. Dewar, E. G. Zoebisch, E. F. Healy and J. J. P. Stewart, *J. Am. Chem. Soc.*, 1985, **107**, 3902-3909.
22. M. Chaur, F. Melin, A. Ortiz and L. Echegoyen, *Angew. Chem., Int. Ed.*, 2009, **48**, 7514-7538.
23. M. Chaur, R. Valencia, A. Rodríguez-Fortea, J. Poblet and L. Echegoyen, *Angew. Chem. Int. Ed*, 2009, **48**, 1425-1428.
24. D. G. Truhlar, C. J. Cramer, A. Lewis and J. A. Bumpus, *J. Chem. Educ.*, 2004, **81**, 596.
25. R. R. Gagne, C. A. Koval and G. C. Lisensky, *Inorg. Chem.*, 1980, **19**, 2854-2855.
26. C. C. Pye and T. Ziegler, *Theor. Chem. Acc.*, 1999, **101**, 396-408.
27. N. Chen, M. Mulet-Gas, Y.-Y. Li, R. E. Stene, C. W. Atherton, A. Rodriguez-Fortea, J. M. Poblet and L. Echegoyen, *Chem. Sci.*, 2013, **4**, 180-186.
28. H. Shinohara, *Rep. Prog. Phys.*, 2000, **63**, 843.
29. M. E. Casida, *Journal of Molecular Structure: THEOCHEM*, 2009, **914**, 3-18.
30. X. Zhao, Z. Slanina and H. Goto, *J. Phys. Chem. A*, 2004, **108**, 4479-4484.
31. X. Zhao, Z. Slanina, H. Goto and E. Osawa, *J. Chem. Phys.*, 2003, **118**, 10534.
32. Z. Slanina and S. Nagase, *ChemPhysChem*, 2005, **6**, 2060-2063.
33. J. C. Duchamp, A. Demortier, K. R. Fletcher, D. Dorn, E. B. Iezzi, T. Glass and H. C. Dorn, *Chem. Phys. Lett.*, 2003, **375**, 655-659.
34. M. Krause and L. Dunsch, *ChemPhysChem*, 2004, **5**, 1445-1449.
35. B. Q. Mercado, M. A. Stuart, M. A. Mackey, J. E. Pickens, B. S. Confait, S. Stevenson, M. L. Easterling, R. Valencia, A. Rodríguez-Fortea, J. M. Poblet, M. M. Olmstead and A. L. Balch, *J. Am. Chem. Soc.*, 2010, **132**, 12098-12105.

UNIVERSITAT ROVIRA I VIRGILI
COMPUTATIONS ON ENDOHEDRAL METALLOFULLERENES: CHARACTERIZATION, PROPERTIES AND GROWTH.
Marc Mulet Gas
Dipòsit Legal: T 1604-2015

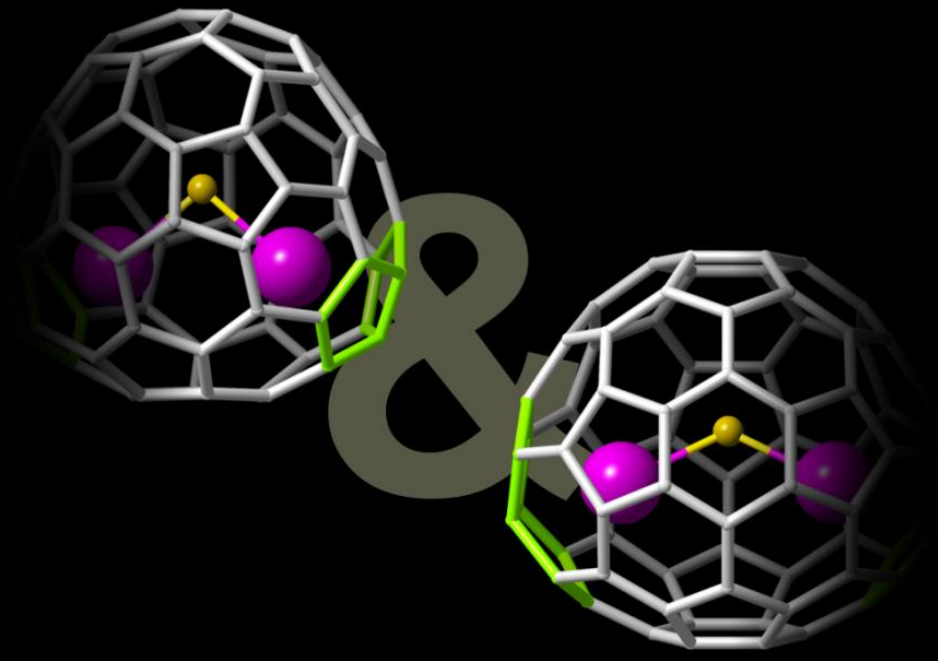

Chapter 4 // ***Identifying the First Two Scandium Sulfide EMFs with non-IPR Cages***

Related Publications:

$Sc_2S@C_2(7892)$-C_{70}: a Metallic Sulfide Cluster Inside a non-IPR C_{70} Cage
N. Chen, M. Mulet-Gas, Y.-Y. Li, R. E. Stene, C. W. Atherton, A. Rodríguez-Fortea, J. M. Poblet and L. Echegoyen. *Chemical Science*, **2013**, 4, 180-186.

$Sc_2S@C_s(10528)$-C_{72}: a Dimetallic Endohedral Fullerene with a non-IPR Cage
N. Chen, M. Mulet-Gas, C. M. Beavers, A. Rodríguez-Fortea, E. J. Muñoz, Y.-Y. Li, M. M. Olmstead, A. L. Balch, J. M. Poblet and L. Echegoyen. *Journal of the American Chemical Society*, **2012**, 134, 7851-7860.

Chapter 4

Identifying the First Two Scandium Sulfide Endohedral Fullerenes with non-IPR Cages

Two new metallic sulfide clusterfullerenes have been isolated from a raw mixture obtained by arc-discharging graphite rods packed with Sc_2O_3 and graphite powder under an atmosphere of SO_2 and helium. Multistage HPLC methods were utilized to isolate and purify the mixture. These first two non-IPR cage sulfide clusterfullerenes, $Sc_2S@C_{70}$ and $Sc_2S@C_{72}$, have been characterized by mass spectrometry, UV-vis-NIR absorption spectroscopy, cyclic voltammetry and DFT calculations (and single crystal X-ray diffraction in the case of the $Sc_2S@C_{72}$). The combined experimental and computational studies lead to the unambiguous assignment of the cage symmetries to C_2(7892)-C_{70} and C_s(10528)-C_{72}, respectively. A close structural resemblance between these two cages suggests that the conversion between them may be the result of a simple insertion/extrusion of a C_2 unit. This is part of the work in collaboration with the group of Prof. Echegoyen at the University of Texas at El Paso.

4.1. Introduction

Among the numerous studies devoted to endohedral fullerenes, the study of clusterfullerenes that do not obey the isolated pentagon rule (IPR) is particularly interesting. The number of IPR isomers is limited, but the number of the possible non-IPR isomers can often be in the thousands as the cage sizes increase. Interestingly, with certain endohedral clusters and cage sizes, out of thousands of possibilities, there is frequently only one match between a particular cage isomer and the cluster. Medium size cages, such as $Gd_3N@C_s(39663)$-C_{82} and $M_3N@C_s(51365)$-C_{84} (M = Gd, Tb, Tm) were found to have a single pair of fused pentagons.[1, 2] Smaller cages, such as $Gd_3N@C_2(22010)$-C_{78}, and $Sc_2C_2@C_{2v}(6073)$-C_{68} possess two pairs of fused pentagons.[3, 4] Endohedral fullerenes that have three pairs of fused pentagons were also found for cages no larger than C_{70}, *i.e.* $Sc_3N@C_{2v}(7854)$-C_{70}, and $Sc_3N@D_3(6140)$-C_{68}.[5, 6] These cages are not stable when empty and are stabilized by charge transfer from the encaged cluster. All these non-IPR endohedrals have the common feature that the internal metal ions are positioned in close proximity to the adjacent pentagon pairs.

Sulfide clusterfullerenes (SCFs) are the newest member in the clusterfullerene families. Different methods have been utilized to synthesize these compounds. Dunsch and coworkers reported the formation of one isomer of $M_2S@C_{82}$ (M= Sc, Lu, Dy) by introducing CH_5N_3·HSCN as a solid sulfur source.[7] Recently, in a work reported by Echegoyen and co-workers, an extensive family of novel scandium sulfide clusterfullerenes, with cages ranging from C_{68} to C_{100}, were obtained in macroscopic quantities by introducing SO_2 into the arc reactor.[8] Further isolation and characterization of some of these new species revealed novel structures and properties which are unique to this family. Two isomers of $Sc_2S@C_{82}$, $Sc_2S@C_s(6)$-C_{82} and $Sc_2S@C_{3v}(8)$-C_{82}, were identified as the most abundant products in this family and were characterized by single crystal X-ray crystallography. $Sc_2S@C_s(6)$-C_{82}, in particular, was found to possess

completely ordered cage and cluster in its single crystal structure, becoming the first one in the clusterfullerene series.[9]

A combined computational and experimental study revealed that the unique geometry of the Sc_2S cluster together with a formal charge transfer of four electrons between the cluster and the cage play an important role in the stabilization of this new cages which had never been detected experimentally before in any of the endohedral fullerene families. These results indicate that more novel endohedral structures are likely to be found in the SCF family and systematic studies of these structures might provide a better understanding of the fundamental aspects of SCFs, and useful design principles to guide the preparation of high yielding endohedral compounds.

In this chapter, we report the combined experimental and computational work developed in order to study and identify these two new scandium sulfide cluster fullerenes, $Sc_2S@C_{70}$ and $Sc_2S@C_{72}$, which possess non-IPR cages.[10, 11]

4.2. Experimental detection and isolation

The experimental work was done by members of the research group of Prof. Echegoyen at UTEP. The scandium sulfide clusterfullerenes were synthesized in a conventional Krätschmer-Huffman reactor using a mixture of helium and SO_2 atmosphere. The as-produced soot was Soxhlet-extracted with CS_2, and a multistage high-performance-liquid chromatography (HPLC) was utilized to isolate and purify the two species, $Sc_2S@C_{70}$ and $Sc_2S@C_{72}$.

Two different synthetic methods have been employed for the production of dimetallic sulfide endohedral metallofullerenes. Using the method proposed by Dunsch and co-workers, who introduced solid guanidium thiocyanate (CH_5N_3·HSCN) as the sulfur source and added it to the

metal/graphite powder, a single isomer $Sc_2S@C_{3v}$-(6)-C_{82} was obtained as minor along with $Sc_3N@C_{80}$ and $Sc_3N@C_{78}$ as major products. The method used in this work gives SCFs as major products along with some oxide clusterfullerenes (OCFs) as minor products. In a previous study, recently reported by Prof. Echegoyen and co-workers, it was shown that an extensive family of $Sc_2S@C_{2n}$ (n=40-50) could be obtained by this method.

In the present work, as is shown in figure 4.1, SCFs with cages ranging from C_{68} to C_{80} were also obtained. This family, $Sc_2S@C_{2n}$ (n=34-50), is unique in cage variety among all the clusterfullerene families. $Sc_2S@C_{70}$ and $Sc_2S@C_{72}$ are the second and the third smallest fullerenes in the SCFs family, respectively.

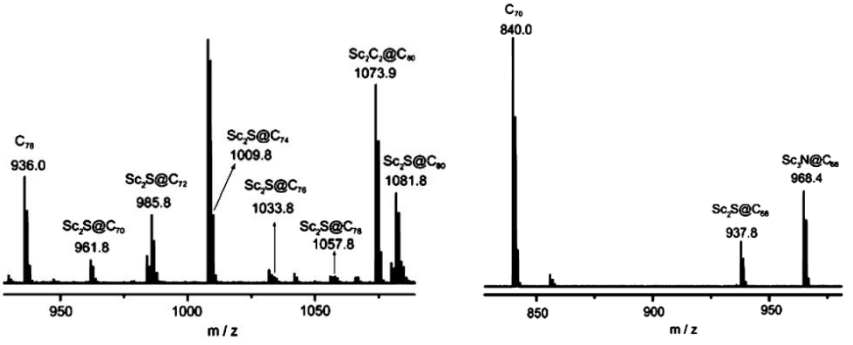

Figure 4.1 (left) Mass spectra of the raw extract of $Sc_2S@C_{2n}$ (n=35-40) and (right) the isolated fraction containing the $Sc_2S@C_{68}$, the smallest system detected for this family.

The HPLC-MALDI TOF (MALDI TOF = matrix assisted laser desorption ionization time-of-flight) analysis show that on a 5PYE column, the $Sc_2S@C_{70}$ and the $Sc_2S@C_{72}$ fractions overlap with each other and with those of C_{76}, and C_{78}. The retention time of $Sc_2S@C_{70}$ is shorter than that of $Sc_2S@C_{72}$, which agrees with the relatively smaller size of this compound. Both fractions were further separated by a two-stage recycling HPLC procedure running with a Buckyprep column and resulted in the isolation of pure $Sc_2S@C_{70}$ and $Sc_2S@C_{72}$. The MALDI TOF spectrum of the $Sc_2S@C_{70}$ isolated fraction shows a single peak at 961.904 m/z. The isotopic distribution of the experimental MALDI spectrum shows excellent

agreement with the corresponding theoretical spectrum (see figure 4.2). The purity of this sample was further checked by HPLC as shown in the inset of figure 4.2. The MALDI TOF spectrum of the purified fraction $Sc_2S@C_{72}$ shows a single peak at 985.973 m/z. Also in this case, the isotopic distribution of the experimental MALDI TOF spectrum shows a very good agreement (see figure 4.2). Following the same experimental procedure, the purity of this fraction was also checked by HPLC analysis as it is shown in figure 4.2.

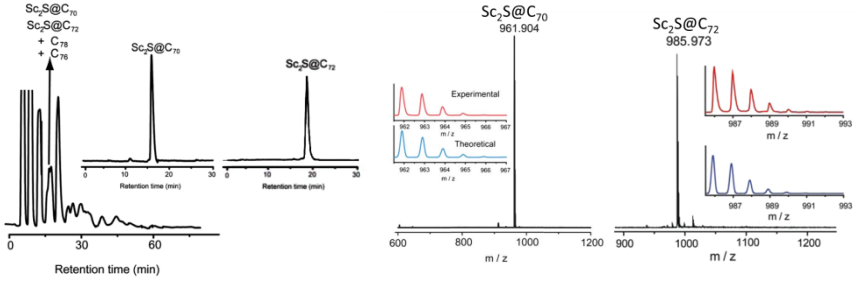

Figure 4.2 (left) HPLC chromatograms of the fullerene extract obtained on a 10 mm x 250 mm 5PYE column using λ= 320 nm, a flow rate of 4mL min^{-1}, and toluene as the eluent at 25 ˚C. Insets: HPLC of the purified $Sc_2S@C_{70}$ and $Sc_2S@C_{72}$ fractions obtained using the same conditions. (right) Mass spectra of the purified $Sc_2S@C_{70}$ and $Sc_2S@C_{72}$. The insets show the experimental (red) and theoretical (blue) isotopic distribution.

The yield of the obtained fraction of $Sc_2S@C_{70}$ compared to the isolated fraction of $Sc_2S@C_{72}$ is much lower. Out of the arching process of 60 packed graphite rods, along with 2.0 mg of $Sc_2S@C_{72}$, only 0.4mg of $Sc_2S@C_{70}$ mg were obtained. This yield difference was crucial when attempting to obtain suitable crystals for X-ray diffraction analysis. Multiple attempts to obtain the above-mentioned crystal for $Sc_2S@C_{70}$ were unsuccessful whereas a $Sc_2S@C_{72}$ single crystal was successfully obtained.

4.3. Combining computations and experiments to elucidate the $Sc_2S@C_{70}$ structure

When a new endohedral metallofullerene is detected and isolated, one of the most important and challenging steps is to elucidate which one of the thousands of possible isomers is the one detected in the experiments. To do so, an extensive study combining computations and experiments has to be carried out. In order to solve this problem, we followed a computational strategy designed taking into account all the key factors that govern the stabilization of the endohedral metallofullerenes (see chapter 3).

4.3.1. Looking for the best C_{70} candidates to encapsulate Sc_2S

A relatively large number of isomers, 8149, can be obtained following the spiral algorithm for a C_{70} structure. From a previous work recently published by our group, we know that for the larger $Sc_2S@C_{82}$ systems, there is a formal transfer of four electrons from the trapped cluster to the carbon cage.[9] Therefore, the first step in the computational study is to compute the tetraanions, C_{70}^{4-}.

We computed the energies of the tetraanions at DFT BP86/TZP level for all C_{70} cages with three or less adjacent pentagon pairs (APPs): 1 IPR structure, 1 APP1 structure, 18 APP2 structures and 91 APP2 structures. This selection is based on the energy penalty induced by the presence of each pentalene unit on the carbon framework. The more pentalenes in the structure the less stable the structure is. Thus, those structures with more than 3 APPs are too high in energy. Furthermore, a very important stabilization factor for the non-IPR cages is the interaction between the metal ions in the cage and the pentalene units. In this case, only two Sc atoms are trapped inside the cage and strongly interact with the carbon cage. For this reason, cages with more than 3 pentagon pairs would not be stabilized enough and would remain too high in energy. After the calculations on tetraanionic species, the endohedral fullerenes for the

lowest-energy tetraanionic cages, in a range of 15-20 kcal mol^{-1}, were computed (see table 4.1).

Table 4.1 List of the relative energies, in kcal mol^{-1}, for several isomers of C_{70} in the tetraanion and endohedral forms. Isomers are labeled according to the spiral algorithm by Fowler and Manolopoulos, and APP is the number of adjacent pentagon pairs in the carbon framework.

Isomer	APP	C_{72}^{4-}	$Sc_2S@C_{74}$
8149	0	0.0	20.6
7892	2	3.9	0.0
7957	2	4.7	19.1
7851	3	6.2	20.3
7852	3	6.3	23.5
7887	3	7.0	21.6
7854	3	8.5	26.3
7893	3	9.4	19.7
7886	3	10.8	21.5
7924	2	11.6	18.6
7846	3	13.2	29.3
7960	2	14.1	21.9
7922	3	14.2	27.7
7921	3	14.7	29.1
7850	3	14.7	33.2
7847	3	15.6	28.8
8094	1	16.7	26.5

Interestingly, the IPR cage, D_{5h}(8149)-C_{70}, was found to be the lowest-energy tetraanion. Other cage isomers with two and three adjacent pentagon pairs show relative energies within 10 kcal mol^{-1}. In particular, cage C_2(7892)-C_{70} exhibits the second most-stable tetraanion and is only 4 kcal mol^{-1} higher in energy than the IPR cage tetraanion. Among the 18 isomers with two pairs of fused pentagons, cage C_2(7892)-C_{70} shows the lowest number of pyracylene motifs and maxim separation between the pentagons in the structure, which is in agreement with the Maximum Pentagon Separation Rule (MSPR) proposed by Poblet and co-workers to explain the stability of the carbon cages taking into account the charge

distribution over the pentagons and the position of them in order to minimize the electrostatic energy.[12]

To predict the stability of a given clusterfullerene, it is necessary to consider the formal electron transfer from the inner moiety to the cage but also the stability provided by the interaction between the metal ions of the cluster and the carbon framework. These interactions are not very critical for IPR cages; however, these cluster-cage interactions are crucial for those clusterfullerenes that have one or more pentalene units in the structure. The systems with non-IPR cages are stabilized by the proximity of the metal cations of the cluster to the pentalene motifs. Thus, an appropriate location of the fused pentagons on the fullerene cage that provide an optimal interaction between the Sc atoms and the carbon cage is a key factor in the stabilization of non-IPR cluster fullerenes. In the present case, it is only after the encapsulation of the Sc_2S unit that the C_2(7892)-C_{70} cage becomes by far, ~20 kcal mol^{-1}, the most stable endohedral isomer (see table 4.1). It is worth mentioning that, due to the previously mentioned rather strong interaction between the metal atoms and the pentalenes, in all the endohedral structures with fused pentagons the metal atoms are pointing towards the fused pentagons (see figure 4.3).

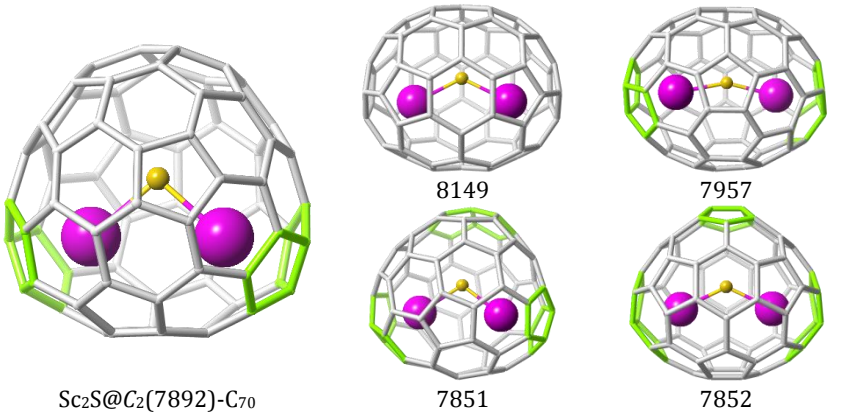

Figure 4.3 DFT-optimized structures for some of the lowest-energy $Sc_2S@C_{70}$ isomers. Pentalene units are highlighted in lime green. Sc atoms are represented in magenta and sulfur atoms in yellow. Isomers labeled according to the spiral algorithm.

The IPR structure, which is the lowest-energy as tetraanion, is found to be destabilized due to the lack of interaction between the metal atoms and the carbon cage when the Sc_2S cluster is encapsulated. The other non-IPR cages do not possess the optimal positioning of the APPs to maximize the metal-pentalene interactions as observed for the $Sc_2S@C_2(7892)$-C_{70}, and for this reason, are also found to have higher relative energies when the cluster is inside than when computed as tetraanions.

The computation and analysis of all the different isomers of $Sc_2S@C_{72}$ lead us to the selection of $Sc_2S@C_2(7892)$-C_{70} as the candidate isomer. This means that our calculations suggest that this is the isomer detected and isolated in the experiments. At this point, we have to compare all the available experimental data with the computed properties in order to confirm or discard this selection.

4.3.2. Formal Electron Transfer

It is important to confirm that, as previously described for the $Sc_2S@C_{82}$, the formal electron transfer is of four electrons. In order to check the electron transfer, we analyzed the orbital interaction diagram for the endohedral fullerene from the corresponding C_{70} and Sc_2S fragments.

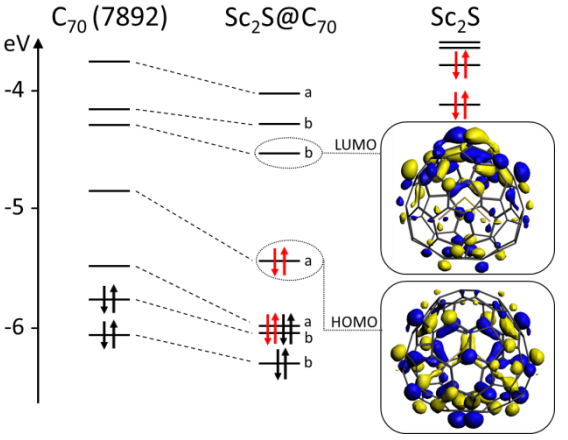

Figure 4.4 Orbital interaction diagram for $Sc_2S@C_2(7892)$-C_{70}. The fragments were computed with the same geometry they have in the clusterfullerene. The four electrons formally transferred from the cluster to the cage are highlighted in red.

This type of analysis allows us to see the molecular orbitals of the clusterfullerene as a result of the interaction between the orbitals of each fragment, C_{70} and Sc_2S.

As it is shown in figure 4.4, four electrons are formally transferred form the two highest-occupied molecular orbitals (HOMO) of the cluster to the two lowest-unoccupied molecular orbitals (LUMO) of the carbon cage. Both, the HOMO and the LUMO of the clusterfullerene are mainly localized in the carbon framework, as it can be seen in the orbital representation. Thus, a four electron transfer is confirmed, verifying that the system can be formally described as $(Sc_2S)^{4+}@(C_{70})^{4-}$.

4.3.4. Thermal and entropic effects

It is important to take into account the possible effects of the high temperatures reached in the reactor during the fullerene synthesis. For this reason, the molar fractions of the lowest-energy $Sc_2S@C_{70}$ isomers as a function of the temperature were also computed using the rigid rotor harmonic approximation (RRHO) and the free-encapsulating model (FEM) proposed by Slanina (see figure 4.5).[13, 14] Somewhat different results were obtained for the FEM and RRHO approximations. For the FEM, The SCF with the $C_2(7892)$ cage is the most abundant isomer in the whole temperature range (to 4000 K). Within the RRHO approximation, there is an isomer preference crossing at around 1700 K, with the IPR $D_{5h}(8149)$ isomer predominating at higher temperatures. So far, in most of the reported studies, the predictions derived from the FEM model are in better agreement than the predictions derived from the RRHO approximation. In the present case, the Sc_2S would probably rotate freely inside the spherical IPR cage at sufficiently high temperatures, due to the lack of strong interaction between the metal atoms and the carbon cage (no metal-pentalene interactions). Contrarily, it is not so clear the behavior of the Sc_2S inside the non-IPR cage. Probably, the cluster would not freely rotate inside the $C_2(7892)$ cage due to the strong interaction of the metal ions and the pentalene units. Therefore, the FEM approximation would be the most suitable in the case of the IPR cage but not for the non-

IPR isomer. So, the important increase of the molar fraction for $Sc_2S@D_{5h}(8149)$-C_{70} at T>1000 K predicted within the RRHO approximation is somewhat overestimated.

Consequently, we predict the $Sc_2S@C_2(7892)$-C_{70} to be the most abundant isomer at the whole range of temperatures. However, we will consider the IPR isomer in the comparison of experimental and computational data to clearly discard this possibility.

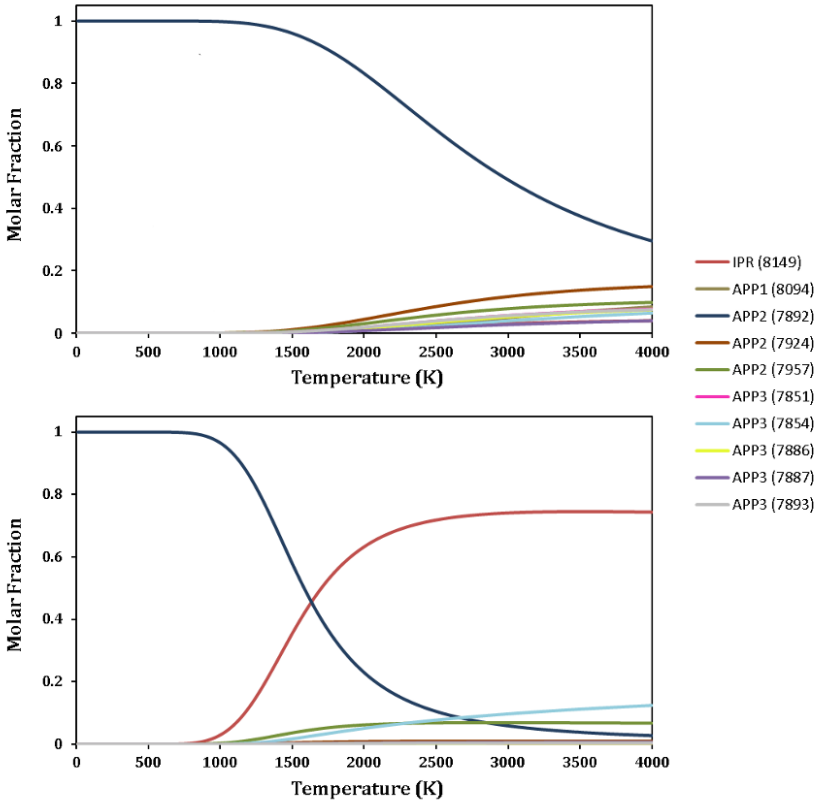

Figure 4.5 Predicted molar fraction as a function of the temperature for the lowest-energy isomers of $Sc_2S@C_{70}$ within the FEM (top) and RRHO (bottom) approximations.

4.3.5. Electrochemical Studies

The cyclic voltammogram (CV) of $Sc_2S@C_{70}$ was recorded in *o*-dichlorobenzene (*o*-DCB) containing 0.05 M tetra(*n*-butyl)ammonium-hexafluorophosphate (*n*-Bu_4NPF_6) as the supporting electrolyte using a scan rate of 100 mV s^{-1} (figure 4.6).

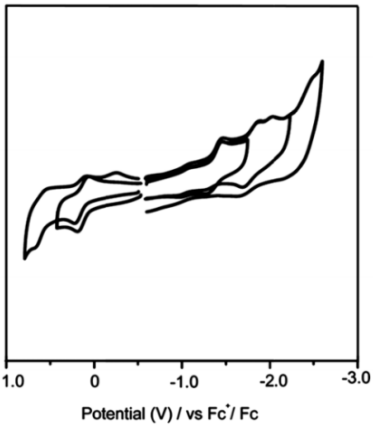

Figure 4.6 Cyclic voltammogram of $Sc_2S@C_{70}$ recorded in a 0.05M *o*-DCB/*n*-Bu_4NPF_6 solution at a scan rate of 100 mVs^{-1}. Ferrocene was added as the internal standard.

The CV shows some similarities and differences when compared to those of other reported Sc_2S endohedral fullerenes. In this particular case, the CV shows a reversible first oxidation followed by an irreversible second oxidation step, which is very similar to the oxidative behavior of $Sc_2S@C_{72}$ but different from those of the two isomers of $Sc_2S@C_{82}$, which exhibit two reversible oxidative steps. On the other hand, while $Sc_2S@C_{72}$ shows all-reversible reductive processes, the reductive behavior of $Sc_2S@C_2(7892)$-C_{70} shows similarities to those of the two isomers of $Sc_2S@C_{82}$ as well as to the most of the clusterfullerenes, which typically show irreversible reductive processes.[10, 15]

The redox potentials of $Sc_2S@C_2(7892)$-C_{70} also show major differences from those of other reported SCFs. The electrochemical gap is found to be 1.57 eV, which is smaller than that of $Sc_2S@C_{72}$ (1.78 eV) and somewhat

larger than those of the corresponding $Sc_2S@C_{82}$ isomers (1.56 eV for $Sc_2S@C_{3v}(8)$-C_{82} and 1.47 eV for $Sc_2S@C_s(6)$-C_{82}).

Good agreement of the computed first and second oxidation and reduction potentials of $Sc_2S@C_2(7892)$-C_{70} with the peaks measured experimentally by CV was found (see table 4.2). The first anodic potential, corresponding to the first oxidative process, is predicted to appear at +0.04 V, in good agreement with the experimental half-wave potential (+0.14 V). The predicted first cathodic potential, due to the first reductive process, is also close to the experimental value with a difference around 100 mV (see table 4.2). The computed electrochemical (EC) gap, 1.37 V, compares reasonably well with the experimental value, 1.58 V, although the error (210 mV) is somewhat larger than the error found for the nitride cluster fullerenes.[16, 17]

Table 4.2 Experimental oxidation and reduction potentials (in V versus Fc+/Fc) and computed oxidation and reduction potentials (in V) for $Sc_2S@C_2(7892)$-C_{70}.

	$E^{+/2+}$	$E^{0/+}$	$E^{0/-}$	$E^{-/2-}$	$E^{2-/3-}$	$E^{3-/4-}$	$\Delta E_{gap,ec}$
Exp.	+0.65[b]	+0.14[a]	-1.44[b]	-1.87[b]	-1.99[b]	-2.45[b]	1.58
Comp.	+0.60	+0.04	-1.33	-1.82			1.37

[a] Half-wave potential (reversible process). [b] Peak potential (irreversible process).

The inclusion of thermal and entropic effects does not improve the computed gap as it has been shown before for the family of nitrides. It is worth noting that, for irreversible processes, the comparison between experimental and theoretical EC gaps is difficult, because computations predict standard potentials, and not experimental peak potentials. The predictions for the second anodic and cathodic potentials are in excellent agreement with the experimental data (with an error of only 50 mV). The HOMO-LUMO gap of the IPR cluster fullerene, 0.56 eV, is much smaller than for the $Sc_2S@C_2(7892)$-C_{70}, 0.95 eV. We also computed the first oxidation potential for the IPR $Sc_2S@D_{5h}(8149)$-C_{70} (-0.016 V versus +0.04V respectively). Thus, the IPR is much easily oxidized. We had problems computing the first reduction potential for $Sc_2S@D_{5h}(8149)$-C_{70} because the LUMO and the LUMO+1 orbitals are almost degenerate and

the DFT monodeterminantal approach is not suitable to describe such a reduced state (multi-determinant wavefunctions would be needed, but the computational cost is too high for such a large systems). According to the energy of the LUMOs ($Sc_2S@D_{5h}(8149)$-C_{70} : -4.04 eV; $Sc_2S@C_2(7892)$-C_{70}: -3.82 eV) the first reduction potential for $Sc_2S@D_{5h}(8149)$-C_{70} should be lower (around 200 mV) than for $Sc_2S@C_2(7892)$-C_{70}, leading to a much smaller EC gap (around 1 eV or even smaller). According to all these results, the comparison between the computed and experimental electrochemical properties clearly discards the $Sc_2S@D_{5h}(8149)$-C_{70} and suggests the $Sc_2S@C_2(7892)$-C_{70} as the isomer formed in the arc.

4.3.6. UV-vis-NIR absorption spectroscopy

The definitive experiment that confirms isomer 7892 as the carbon cage that encapsulates the scandium sulfide cluster is the UV-vis-NIR spectrum.

The purified $Sc_2S@C_{70}$ has a yellow-brown color in toluene solution. The experimental UV-vis-NIR absorption spectrum is shown in figure 4.7. A relatively strong absorption occurs at 1102 nm along with other absorptions at 461, 634, and 952 nm. The characteristic features of this spectrum are also substantially different from those of empty C_{70} and the previously reported $Sc_3N@C_{2v}(7854)$-C_{70}, which presents the strongest absorptions at 696 nm along with several shoulder peaks at 468, 558, 807 and 894 nm. Since the absorption spectra of fullerenes in the visible and NIR region are dominated by the π- π* transitions of the carbon cages and the spectra are very sensitive to the cage symmetries, these differences clearly indicate that $Sc_2S@C_{70}$ has a non-IPR cage and the cage symmetry is different from that of $Sc_3N@C_{2v}(7854)$-C_{70}.

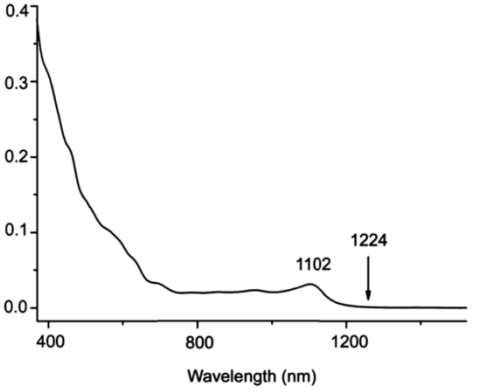

Figure 4.7 UV-vis-NIR absorption spectra in CS_2 solution.

We computed the spectra using time-dependent (TD) DFT for the two possible isomers, $Sc_2S@C_2(7892)$-C_{70} and $Sc_2S@D_{5h}(8149)$-C_{70}. Despite the systematic underestimation of the excitation energies by TDDFT, this methodology provides a reasonable agreement with experiments, as it has been already shown in previous studies.

Table 4.3 TDDFT predictions for the most intense lowest-energy excitations in the absorption spectrum of $Sc_2S@C_2(7892)$-C_{70} and $Sc_2S@D_{5h}(8149)$-C_{70}.

E (eV)	λ (nm)	[a] f	[b] Leading configurations (%)
$Sc_2S@C_2(7892)$-C_{70}			
1.071	1158	0.00650	HOMO → LUMO (98)
1.212	1023	0.00356	HOMO → LUMO+1 (98)
1.664	745	0.00104	HOMO → LUMO+3 (99)
1.681	738	0.00519	HOMO → LUMO+4 (96)
1.853	669	0.00721	HOMO-1 → LUMO (89)
$Sc_2S@D_{5h}(8149)$-C_{70}			
0.688	1802	0.00365	HOMO → LUMO (63); HOMO → LUMO+1 (98)
0.763	1625	0.00103	HOMO-1 → LUMO+1 (63); HOMO-1 → LUMO (26)
0.802	1546	0.00715	HOMO-1 → LUMO (71); HOMO-1 → LUMO+1 (28)
0.980	1265	0.00138	HOMO → LUMO+2 (50); HOMO-1 → LUMO+3 (47)
1.295	958	0.05558	HOMO-1 → LUMO+3 (46); HOMO → LUMO+2 (35)

[a] Only excitations with f (oscillator strength) > 0.001 are listed. [b] Contributions less than 10% are omitted.

From the computations, we can clearly discard the $Sc_2S@D_{5h}(8149)$-C_{70} because its spectrum shows transitions at large wavelengths (around 1800 and 1600 nm) as it is shown in table 4.3, in total contrast with the experimental observations. The spectral onset appears at 1224 nm, see figure 4.7. In addition, the spectrum predicted for $Sc_2S@C_2(7892)$-C_{70} agrees rather well with the experimental one, with the first transition, corresponding to the HOMO-LUMO transition, at 1158 nm (to be compared with the experimental 1102 nm).

4.3.7. The crucial role of the cluster: $Sc_2S@C_2(7892)$-C_{70} versus $Sc_3N@C_{2v}(7854)$-C_{70}

Besides the $Sc_2S@C_2(7892)$-C_{70}, only one non-IPR C_{70} endohedral fullerene, $Sc_3N@C_{2v}(7854)$-C_{70}, has been reported so far. Although, very recently Nagase, Zhao and co-workers proposed, using functional density theory calculations, that $Sc_2@C_{2v}(7854)$-C_{70} and not the corresponding carbide, $Sc_2C_2@C_{2v}(6073)$-C_{68}, is the metallofullerene detected as Sc_2C_{70}, there are no experimental evidences confirming this suggestion.

These two isomers, $C_2(7892)$-C_{70} and $C_{2v}(7854)$-C_{70}, are rather close in energy when computed as tetraanions. On the other hand, the hexaanionic state is much more favored for $C_{2v}(7854)$-C_{70}. If the trapped cluster is Sc_3N, a six electron transfer combined with the optimal interaction between the three Sc atoms and the three pentalenes on cage $C_{2v}(7854)$-C_{70} (figure 4.8) lead to the preferential stabilization of $Sc_3N@C_{2v}(7854)$-C_{70}. However, with the Sc_2S cluster inside the Sc-pentalene interactions are optimal for $Sc_2S@C_2(7892)$-C_{70}, which has, by far, the lowest energy (tables 4.1 and 4.4). Although sharing the same cage size, the number and the position of the fused pentagons are significantly different in these two isomers. This shows that the nature and geometry of the encaged cluster plays an important role on the selection of the cage isomer, along with the electronic stabilization resulting from the cluster-cage electron transfer.

Table 4.4 Relative energies, in kcal mol^{-1}, for cages C_2(7892)-C_{70} and C_{2v}(7854)-C_{70} in different anionic states and encapsulating different clusters.

	C_2(7892)-C_{70}	C_{2v}(7854)-C_{70}
C_{70}^{4-}	0.0	4.6
C_{70}^{6-}	16.2	0.0
$Sc_2S@C_{70}$	0.0	26.3
$Sc_3N@C_{70}$	10.5	0.0

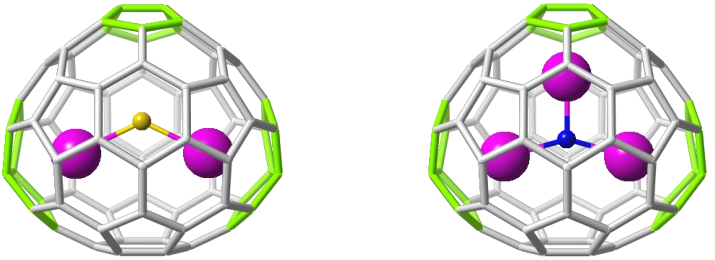

Figure 4.8 DFT-optimized structures for $Sc_2S@C_{2v}$(7854)-C_{70} (left) and $Sc_3N@C_{2v}$(7854)-C_{70} (right). The pentalene motifs are highlighted in lime green. Sc atoms are represented in magenta, S atom in yellow and N atom in blue.

4.4. Experiments and computations for the identification of $Sc_2S@C_{72}$

In this section, all the work done in order to elucidate the structure of $Sc_2S@C_{72}$ is detailed. We essentially followed the same scheme we utilized for the $Sc_2S@C_{70}$, explained in the previous section. However, due to the difference of yields obtained for these two systems, $Sc_2S@C_2$(7892)-C_{70} and $Sc_2S@C_s$(10528)-C_{72}, there is an important difference on the experimental data obtained reflected on the successful formation of a crystal. Therefore, the single crystal X-ray diffraction data was obtained for $Sc_2S@C_{72}$ which is a decisive experiment to confirm the cage assignment.

4.4.1. Which are the C_{72} candidates to encapsulate Sc_2S?

A large number of isomers can be constructed for cages with 72 vertices, a total of 11190, following the spiral algorithm. The first selection is based, once again, in the penalty induced by the presence of fused pentagons in the structure, and the number of metal atoms that the trapped cluster has. Thus, the isomers with three and more adjacent pentagon pairs were discarded. Accordingly to this first selection, the different isomers that were computed are a total of 41: 1 IPR structure, 3 APP1 structures and 37 APP2 structures. In this case, the APP3 isomers were also excluded of the selection. As we have shown previously in this chapter for $Sc_2C@C_{70}$, they have much higher relative energies.

Considering that, as shown in previous works, for the $Sc_2S@C_{82}$ and $Sc_2S@C_{70}$, there is a formal transfer of four electrons from the trapped Sc_2S to the carbon cage, we first computed the tetraanionic states of the above-mentioned isomers. The lowest-energy tetraanions, in a range of 15 kcal·mol^{-1}, were computed as endohedrals. The energies of all the most stable isomers are listed in table 4.5.

Table 4.5 Relative energies, in kcal mol^{-1}, for the lowest-energy isomers of C_{72}^{4-} and $Sc_2S@C_{72}$, along with their number of APP, pyracylenes and IPSI values, in Å^{-1}, for the tetraanionic cages.

Isomer	APP	C_{72}^{4-}	$Sc_2S@C_{74}$	Pyracylenes	IPSI
10528	2	0.0	0.0	8	13.4996
10611	2	1.7	20.7	6	13.4986
10616	2	4.5	13.1	8	13.5041
11188	1	6.5	21.2	14	13.3922
10610	2	8.8	22.4	9	13.5034
10538	2	14.8	17.8	11	13.5078
10626	2	15.2	28.3	10	13.5097
10612	1	15.2	28.3	15	13.3926

As shown before, to predict the stability of a given clusterfullerene one has to take into account, not only the formal electronic transfer, but also

the significant interactions between the metal atoms of the cluster and the specific structural motifs on the carbon cage. For IPR fullerenes with sufficiently large cages, for example, $M_3N@C_{2n}$ (2n > 78), $Sc_4O_k@I_h$-C_{80} (k=2, 3), $Sc_2X@C_{82}$ (X=S, O) and $M_2C_2@C_{2n}$ (2n=82, 84), where the metal cluster has enough space to rotate, the M-cage interactions are not as critical as in the cluster fullerenes that show one or more adjacent pentagon pairs. It is seen that endohedral fullerenes with non-IPR cages are stabilized when the metal atoms of the cluster point towards the APP, as in $Sc_3N@D_3(6140)$-C_{68}, $Gd_3N@C_s(39663)$-C_{82}, or the previously described $Sc_2S@C_2(7892)$-C_{70}. Therefore, proper positioning of the pentalene motifs within the non-IPR carbon framework is crucial for the stabilization of non-IPR endohedral fullerenes.

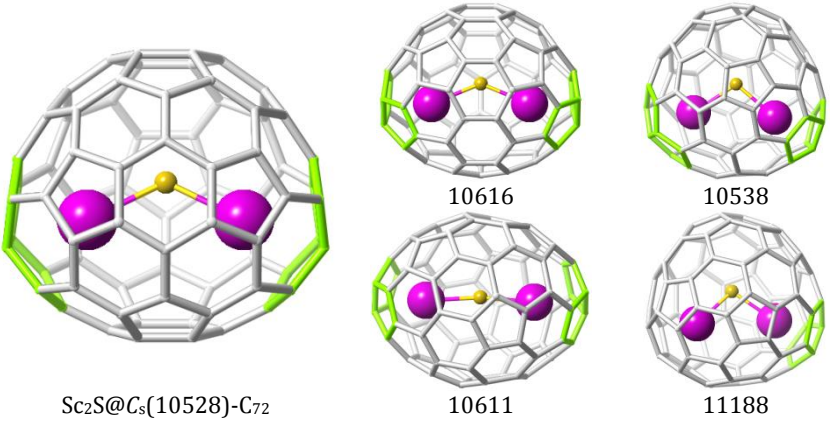

Figure 4.9 DFT-optimized $Sc_2S@C_s(10528)$-C_{72} structure (left) and different cage isomers with one and two fused pentagons in the carbon cage (right). Pentalene units are highlighted in lime green. Sc atoms are represented in magenta and sulfur atoms in yellow. Isomers labeled according to the spiral algorithm.

For the present case, the cage $C_s(10528)$-C_{72} is not only the most favored tetraanion cage, but also the cage with the most convenient disposition of the two pentalene units to interact with the two Sc atoms of the internal cluster (see figure 4.9).[12, 18] Cage $D_2(10611)$-C_{72}, which also has a low number of pyracylene motifs and a small value of IPSI (Inverse Pentagon Separation Index), similar to cage $C_s(10528)$-C_{72}, is energetically comparable to the latter in the tetraanionic state, only 1.7 kcal mol^{-1}

higher in energy. It is important to note that cage D_2(10611)-C_{72} leads to a much more destabilized clusterfullerene (around 20 kcal mol^{-1}) because the Sc_2S is forced in an almost linear arrangement (Sc-S-Sc angle is 171.4˚) due to the location of the two pentalene motifs n the carbon cage (see figure 4.9).

The second lowest-energy endohedral metallofullerene is found to be $Sc_2S@C_s$(10616)-C_{72} with a relative energy of 13 kcal mol^{-1}, and which has the cluster slightly distorted (Sc-S-Sc angle is 134.1˚) compared to that of $Sc_2S@C_s$(10528)-C_{72}. The importance of the optimal angles and distances for the inner cluster has been recently reported by Popov and co-workers. They show how each cluster has an optimal distances and angles which can vary, within a given range, depending on the size of the cage. The destabilization of the other isomers compared to the $Sc_2S@C_s$(10528)-C_{72} is easily rationalized if we observe the ideal value of the angle proposed by Popov (110.3˚) and the angles of the $Sc_2S@C_s$(10528)-C_{72} (124.4˚), $Sc_2S@C_s$(10616)-C_{72} (134.1˚) and $Sc_2S@D_2$(10611)-C_{72} (171.4˚).[19] It is also worth mentioning that the $Sc_2S@C_{72}$ isomers with only one fused pentagon in the carbon framework are also destabilized by more than 20 kcal mol^{-1} due to the fact that only one favorable Sc-pentalene interaction exists.

In summary, isomer C_s(10528)-C_{72} is the most favorable cage to encapsulate the Sc_2S cluster because (i) it is the most favored tetraanion and (ii) it has the proper location of the pentalene motifs to optimize the interaction with the metal cluster. For this reason, we suggest the $Sc_2S@C_s$(10528)-C_{72} isomer as the one obtained in the arc. At this point, we have to compare the experimental available data with the properties that can be computed in order to confirm or discard this selection.

4.4.2. Checking the formal electron transfer

We assumed that for this family four electrons are formally transferred from the trapped Sc_2S unit to the carbon cage, as previously reported and described for the $Sc_2S@C_{82}$ and $Sc_2S@C_2$(7892)-C_{70}. In order to confirm

the charge transferred, we computed the molecular orbital interaction diagram (figure 4.10).

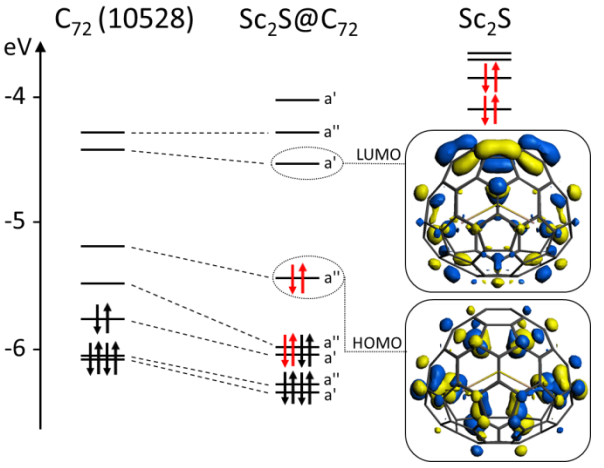

Figure 4.10 Orbital interaction diagram for $Sc_2S@C_s(10528)\text{-}C_{72}$. The fragments Sc_2S and $C_s(10528)\text{-}C_{72}$ were computed with the same geometry they have in the endohedral fullerene.

As it is shown in the interaction diagram, four electrons (highlighted in red) from the two highest-occupied molecular orbitals of the Sc_2S are formally transferred to the two lowest-unoccupied molecular orbitals of the carbon cage. The HOMO and the LUMO of the endohedral fullerene are found to be mainly localized on the carbon framework as it is been also observed for the $Sc_2S@C_2(7892)\text{-}C_{70}$. Therefore, the electronic structure of this family of compounds can be easily explained taking into consideration an ionic model with a formal transfer from the cluster to the cage, as we have verified once again using this molecular orbital diagram. This system can be formally described as $(Sc_2S)^{4+}@(C_{72})^{4-}$.

4.4.3. Thermal effects on the synthesis of the endohedral $Sc_2S@C_{72}$

Although the $Sc_2S@C_s(10528)\text{-}C_{72}$ is by far the lowest-energy isomer, we have to take into account the possible effects of the high temperatures reached during the synthesis. To evaluate how the temperature could

influence on this process favoring or not other isomers, we computed the molar fractions of the considered set of isomers using the approximations proposed by Slanina (figure 4.11).

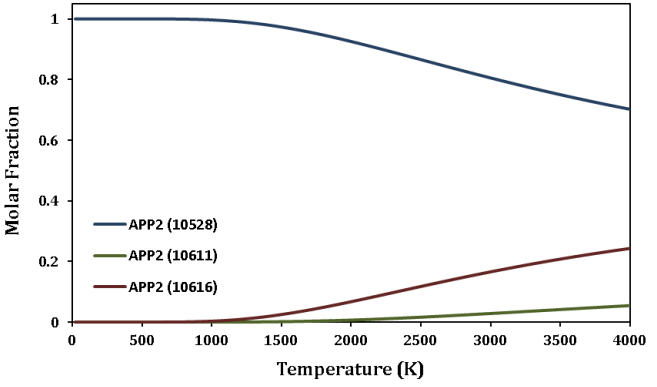

Figure 4.11 Predicted molar fractions within the FEM approximation, as a function of the temperature, for the three lowest-energy isomers of $Sc_2S@C_{72}$.

The two approximations provide, in this case, the same prediction. The lowest energy isomer, $Sc_2S@C_s(10528)$-C_{72}, is the most abundant isomer in for the temperature range up to 4000 K.

4.4.5. UV-vis-NIR absorption spectroscopy

The purified $Sc_2S@C_{72}$ has a yellow-green color in toluene solution. The UV-vis-NIR absorption of $Sc_2S@C_{72}$ is shown in figure 4.12. A strong absorption occurs at 1076 nm with other absorptions at 432, 535, 678 and 939 nm. The characteristic features of this spectrum are substantially different from those of $La@C_2(10612)$-C_{72}, $La_2@D_2(10611)$-C_{72}, and $C_{2v}(11188)$-$C_{72}Cl_4$. However, these main feature are rather similar from those of $Sc_2S@C_2(7892)$-C_{70}.

As it has been already mentioned, the absorption spectra of fullerenes in the visible and NIR regions are dominated by the π-π* transitions of the carbon cages, and the spectra are very sensitive to the carbon cage symmetries. For this reason, the comparison of the UV-vis-NIR spectra is a convenient way to assign the cage symmetry of unknown endohedral

fullerenes, or at least, to discard some of the possibilities. The differences between the UV-vis-NIR spectrum of $Sc_2S@C_{72}$ and those of the other C_{72} endohedral fullerenes reported suggest that Sc_2S is trapped in a different cage isomer.

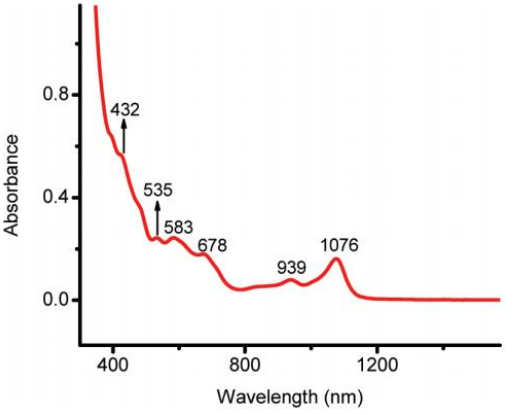

Figure 4.12 UV-vis-NIR absorption experimental spectrum for $Sc_2S@C_{72}$ in CS_2 solution.

The computational study of the UV-vis-NIR absorption spectrum of $Sc_2S@C_{72}$ has also been performed by means of time-dependent (TD) DFT calculations. Despite the already mentioned underestimation of the excitation energies by TDDFT, this methodology provides a good agreement with experiments and allows the assignment of the absorption bands to electronic transitions within the molecule. The strong NIR absorption at 1076 nm (1.15 eV) is assigned to the HOMO → LUMO excitation with a predicted energy if 1.14 eV. The much weaker peak at 939 nm (1.32 eV) is assigned to the HOMO → LUMO+1 transition, predicted at 1.34 eV. The assignment of other highlighted peaks of the absorption spectra is shown in table 4.6. All those predicted transitions show a very good agreement with the experimental data.

Table 4.6 Experimental and TDDFT predictions for the most intense low-energy excitations in the absorption spectrum of $Sc_2S@C_s(10528)$-C_{72}.

Exp. λ (nm)	Exp. E (eV)	Comp. E (eV)	[a] f	[b] Leading configurations (%)
1076	1.15	1.14	0.00994	HOMO → LUMO (98)
939	1.32	1.34	0.00261	HOMO → LUMO+1 (96)
678	1.83	1.83	0.00987	HOMO-1 → LUMO+1 (91)
583	2.13	2.12	0.00484	HOMO-2 → LUMO+2 (90)
				HOMO-1 → LUMO+3 (61)
535	2.32	2.29	0.00306	HOMO → LUMO+7 (14)
				HOMO-7 → LUMO (12)

[a] Only excitations with f (oscillator strength) > 0.001 are listed. [b] Contributions less than 10% are omitted.

The comparison of the experimental and the predicted UV-vis-NIR absorption signals, strongly supports the selection of $Sc_2S@C_s(10528)$-C_{72} as the isomer obtained in the experiments.

4.4.6. Crystallographic study

Contrarily to what happened in the case of $Sc_2S@C_2(7892)$-C_{70}, the crystal of $Sc_2S@C_{72}$ was successfully grown and single crystal X-ray diffraction analysis was performed. The crystal of $Sc_2S@C_{72}{\cdot}Ni^{II}(OEP){\cdot}1.5CH_3C_6H_5$ (OEP= octaethylporphyrin) was obtained by slow diffusion of a toluene solution of $Ni^{II}(OEP)$ into a toluene solution of the purified endohedral fullerene, followed by gradual evaporation of the solvent until the sample was nearly dry. The major site of the endohedral fullerene site and its orientation relative to the porphyrin is shown in figure 4.13. It is seen in the crystallographic data that the cage has C_s symmetry and two pentalene junctions (highlighted in blue in figure 4.13). The scandium atom positions are nestled into the folds of the fused pentagons displaying the characteristic orientation of non-IPR endohedral fullerenes. At the major site, the Sc_2S unit has Sc-S bond distances that are nearly equivalent, 2.325 and 2.347 Å. These distances are slightly shorter than the Sc-S bond distances in the two other X-ray solved structures of Sc_2S endohedral fullerenes: 2.335 and 2.416 Å in $Sc_2S@C_{3v}(8)$-C_{82} and 2.353 and 2.390 Å in $Sc_2S@C_s(6)$-C_{82} which agrees with the smaller size of the inner cavity in

the present system. However, the angle in $Sc_2S@C_s(10528)$-C_{72} (125.36˚) is more obtuse than the corresponding angles in $Sc_2S@C_{3v}(8)$-C_{82} (97.34) and $Sc_2S@C_s(6)$-C_{82} (113.84). The larger angle in the C_{72} isomer might be rationalized by the stronger interaction between the scandium atoms and the pentalene units and the location of these motifs in the cage. The structural parameters obtained after the DFT study of this structure are very similar to those obtained in the experiments

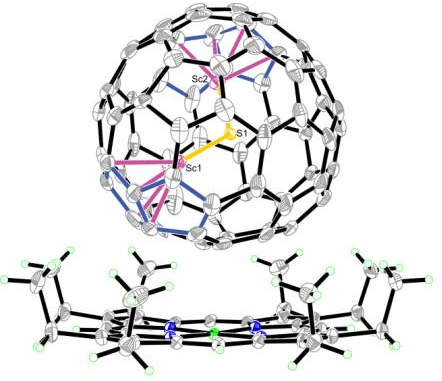

Figure 4.13 Thermal ellipsoid diagram, drawn at 40% probability, of the endohedral fullerene and the cocrystallized nickel octaethylporphyrin in $Sc_2S@C_{72}\cdot Ni^{II}(OEP)\cdot 1.5CH_3C_6H_5$. Only the major cage orientation and Sc_2S unit are shown. Solvate molecules have been omitted for clarity.

Therefore, we clearly have another strong confirmation for the selection of $Sc_2S@C_s(10528)$-C_{72} as the endohedral fullerenes detected and isolated in the experiments.

4.4.7 Structural relation between $Sc_2S@C_2(7892)$-C_{70} and $Sc_2S@C_s(10528)$-C_{72}

At this point, when we have already unambiguously identified the structures of $Sc_2S@C_2(7892)$-C_{70} and $Sc_2S@C_s(10528)$-C_{72}, it is worth remarking that these structures are intimately related as the two dimensional representation shows in figure 4.14.

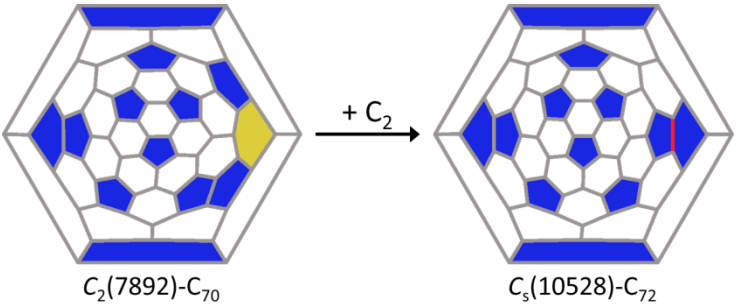

Figure 4.14 Schlegel diagrams showing the C_2(7892)-C_{70} conversion to C_s(10528)-C_{72} by means of singe C_2 insertion. The hexagon where the addition takes place is highlighted in yellow, the bond formed is highlighted in red, and all the pentagons present in the structures are highlighted in blue. The larger distance between the two APPs in cage C_s(10528)-C_{72} compared to that of C_2(7892)-C_{70} makes the Sc-S-Sc angle in $Sc_2S@C_s$(10528)-C_{72} (124˚) larger than that found for $Sc_2S@C_2$(7892)-C_{70} (98˚).

The cage C_s(10528)-C_{72} can be obtained by a single C_2 addition to a hexagon of the C_2(7892)-C_{70} isomer. Therefore, the conversion between these two sulfide clusterfullerenes may happen by single addition/extrusion of a C_2 molecule without further atomic rearrangements. This single insertion growth would be in good agreement with the recently reported closed network growth (CNG) proposed by Kroto, Dunk and co-workers.[20]

It is also worth mentioning that, very recently, the structures of $Sc_2S@C_{74}$ and $Sc_2S@C_{76}$ have been proposed by means of DFT calculations.[21, 22] However, no experimental data is available for these systems and, for this reason, the comparison between experiments and computations in order to confirm the structures is not possible.

Nevertheless, we have studied the structural characteristics of these cages with the aim of finding structural similarities and possible connections. As it is shown in figure 4.15, all these structures, from C_2(7892)-C_{70} to C_1(17459)-C_{76} are connected by a single addition/extrusion of a C_2 unit. Only in the case of the C_{74}, a Stone-Wales rearrangement is needed. That suggests once again that this family of molecules could growth following the proposed CNG mechanism.

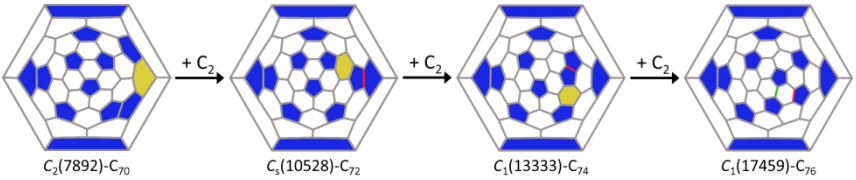

Figure 4.15 Schlegel diagrams showing the connectivity between C_2(7892)-C_{70}, C_s(105228)-C_{72}, C_1(13333)-C_{74}, and C_1(17459)-C_{76}. The bonds formed by the C_2 insertion are highlighted in red, the bond where the Stone-Wales rearrangement takes place is highlighted in green, and all the pentagons are highlighted in blue.

4.5. Conclusions

In summary, a new isomer of C_{70}, $Sc_2S@C_2$(7892)-C_{70}, and a new isomer of C_{72}, $Sc_2S@C_s$(10528)-C_{72}, have been successfully synthesized, isolated and characterized by mass spectrometry, UV-vis-NIR absorption spectrometry, cyclic voltammetry and DFT calculations.

For the $Sc_2S@C_{70}$, the combined experimental and computational studies led to the unambiguous assignment of the cage symmetry to C_2(7892)-C_{70}, the second non-IPR isomer of C_{70} to be detected experimentally. $Sc_2S@C_2$(7892)-C_{70} is by far the lowest-energy isomer and the major candidate to be the experimentally detected species. At high temperatures, isomer $Sc_2S@D_{5h}$(8149)-C_{70} could also be formed, but comparison of the experimental and computational electrochemical properties and UV-vis-NIR spectra clearly discards the IPR $Sc_2S@D_{5h}$(8149)-C_{70}. The four electron formal transfer from the inner cluster to the cages was also verified. The important role of the electron transfer, the geometry of the cluster, and the interaction between the metal ions and carbon cages has been detailed.

In the case of $Sc_2S@C_{72}$, the combination of the computed and experimental data led us to the unambiguous assignment of the C_s(10528)-C_{72} cage symmetry. Computational studies show that also for this system the formal transfer is of 4 electrons. The C_s(10528)-C_{72} cage is

the lowest-energy isomer both in the tetraanion and endohedral forms. Also in this case, the role of the electron transfer along with the geometry of the cluster and the metal-cage interaction was found to be crucial. Moreover, the growth of a crystal was successful and the single crystal X-ray diffraction analysis clearly confirmed the symmetry of the cage and the orientation of the cluster.

Finally, both systems, $Sc_2S@C_2(7892)$-C_{70} and, $Sc_2S@C_s(10528)$-C_{72}, along with two larger non-IPR scandium sulfide endohedral fullerenes, $Sc_2S@C_1(13333)$-C_{74} and $Sc_2S@C_1(17459)$-C_{76} were found to be connected by single addition/extrusion of a C_2 molecule without further atomic rearrangements (except in the case of C_{76} in which a Stone-Wales isomerization is needed). This suggests that this family could grow following the recently proposed Closed Network Growth mechanism.

4.6. References

1. B. Q. Mercado, C. M. Beavers, M. M. Olmstead, M. N. Chaur, K. Walker, B. C. Holloway, L. Echegoyen and A. L. Balch, *J. Am. Chem. Soc.*, 2008, **130**, 7854-7855.
2. C. M. Beavers, T. Zuo, J. C. Duchamp, K. Harich, H. C. Dorn, M. M. Olmstead and A. L. Balch, *J. Am. Chem. Soc.*, 2006, **128**, 11352-11353.
3. M. M. Olmstead, A. de Bettencourt-Dias, J. C. Duchamp, S. Stevenson, D. Marciu, H. C. Dorn and A. L. Balch, *Angew. Chem. Int. Ed*, 2001, **40**, 1223-1225.
4. Z.-Q. Shi, X. Wu, C.-R. Wang, X. Lu and H. Shinohara, *Angew. Chem. Int. Ed*, 2006, **45**, 2107-2111.
5. S. Yang, A. Popov and L. Dunsch, *Angew. Chem. Int. Ed*, 2007, **46**, 1256-1259.
6. M. M. Olmstead, H. M. Lee, J. C. Duchamp, S. Stevenson, D. Marciu, H. C. Dorn and A. L. Balch, *Angew. Chem. Int. Ed*, 2003, **42**, 900-903.
7. L. Dunsch, S. Yang, L. Zhang, A. Svitova, S. Oswald and A. A. Popov, *J. Am. Chem. Soc.*, 2010, **132**, 5413-5421.
8. N. Chen, M. N. Chaur, C. Moore, J. R. Pinzon, R. Valencia, A. Rodriguez-Fortea, J. M. Poblet and L. Echegoyen, *Chem. Commun.* , 2010, **46**, 4818-4820.
9. B. Q. Mercado, N. Chen, A. Rodríguez-Fortea, M. A. Mackey, S. Stevenson, L. Echegoyen, J. M. Poblet, M. M. Olmstead and A. L. Balch, *J. Am. Chem. Soc.*, 2011, **133**, 6752-6760.
10. N. Chen, C. M. Beavers, M. Mulet-Gas, A. Rodríguez-Fortea, E. J. Munoz, Y.-Y. Li, M. M. Olmstead, A. L. Balch, J. M. Poblet and L. Echegoyen, *J. Am. Chem. Soc.*, 2012, **134**, 7851-7860.
11. N. Chen, M. Mulet-Gas, Y.-Y. Li, R. E. Stene, C. W. Atherton, A. Rodriguez-Fortea, J. M. Poblet and L. Echegoyen, *Chem. Sci.*, 2013, **4**, 180-186.
12. A. Rodriguez-Fortea, N. Alegret, A. L. Balch and J. M. Poblet, *Nature Chem.*, 2010, **2**, 955-961.
13. Z. Slanina and S. Nagase, *ChemPhysChem*, 2005, **6**, 2060-2063.
14. Z. Slanina, S.-L. Lee, F. Uhlík, L. Adamowicz and S. Nagase, *Theor. Chem. Acc.*, 2007, **117**, 315-322.
15. B. Q. Mercado, M. A. Stuart, M. A. Mackey, J. E. Pickens, B. S. Confait, S. Stevenson, M. L. Easterling, R. Valencia, A. Rodríguez-Fortea, J. M. Poblet, M. M. Olmstead and A. L. Balch, *J. Am. Chem. Soc.*, 2010, **132**, 12098-12105.

16. R. Valencia, A. Rodríguez-Fortea, A. Clotet, C. de Graaf, M. Chaur, L. Echegoyen and J. M. Poblet, *Chemistry – A European Journal*, 2009, **15**, 10997-11009.
17. M. Chaur, R. Valencia, A. Rodríguez-Fortea, J. Poblet and L. Echegoyen, *Angew. Chem. Int. Ed*, 2009, **48**, 1425-1428.
18. N. Alegret, M. Mulet-Gas, X. Aparicio-Anglès, A. Rodríguez-Fortea and J. M. Poblet, *C. R. Chim.*, 2012, **15**, 152-158.
19. Q. Deng and A. A. Popov, *J. Am. Chem. Soc.*, 2014, **136**, 4257-4264.
20. P. W. Dunk, N. K. Kaiser, C. L. Hendrickson, J. P. Quinn, C. P. Ewels, Y. Nakanishi, Y. Sasaki, H. Shinohara, A. G. Marshall and H. W. Kroto, *Nat. Commun.*, 2012, **3**, 855-863.
21. P. Zhao, T. Yang, Y.-J. Guo, J.-S. Dang, X. Zhao and S. Nagase, *J. Comput. Chem.*, 2014, **35**, 1657-1663.
22. L.-H. Gan, Q. Chang, C. Zhao and C.-R. Wang, *Chem. Phys. Lett.*, 2013, **570**, 121-124.

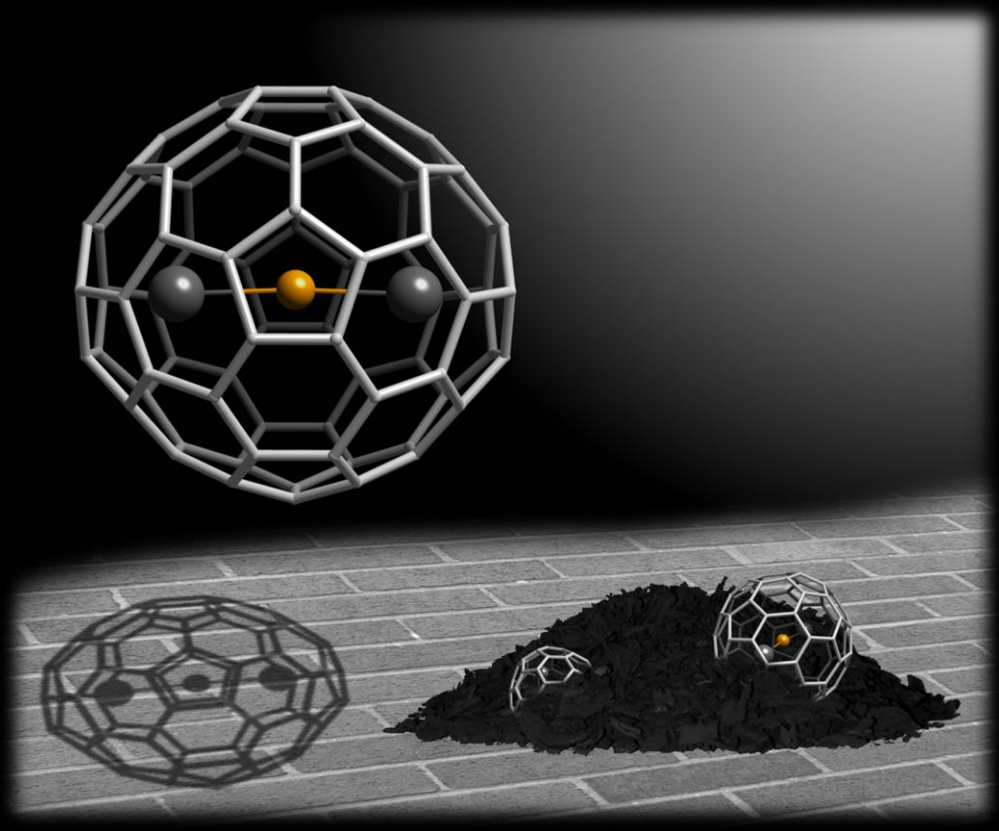

Chapter 5 // ***$Ti_2S@D_{3h}(24109)$-C_{78}: A Sulfide Clusterfullerene Containing Only Transition Metal Atoms***

Related Publications:

$Ti_2S@D_{3h}(24109)$-C_{78}: a Sulfide Cluster Metallofullerene Containing Only Transition Metals Inside the Cage

F-F. Li, M. Mulet-Gas, N. Chen, V. Triana, J. Murillo, A. Rodríguez-Fortea, J. M. Poblet and L. Echegoyen. *Chemical Science*, **2013**, 4, 3404-3410.

Chapter 5

$Ti_2S@D_{3h}(24109)$-C_{78}: A Sulfide Clusterfullerene Containing Only Transition Metal Atoms

This chapter is built on the detection of a new titanium-based sulfide endohedral fullerene, $Ti_2S@D_{3h}(24109)$-C_{78}, which has been successfully synthesized by arc-discharging graphite rods packed with pure TiO_2 and graphite powder under an atmosphere of $S0_2$ and helium. Multistage HPLC methods were utilized to isolate and purify the $Ti_2S@C_{78}$, and mass spectrometric characterization confirmed the composition of a Ti_2S cluster within a C_{78} cage. The combination of an extensive DFT study with the data obtained from experimental analysis such as UV-Vis-NIR absorption spectroscopy and electrochemical characterization led to the assignment of the cage symmetry to $D_{3h}(24109)$-C_{78} and suggested an almost linear arrangement of the internal Ti_2S cluster, with a formal electron transfer of six electrons from the inner cluster to the carbon framework. This work has been done in collaboration with Prof. Echegoyen's group at the University of Texas at El Paso.

5.1. Introduction

Sulfide clusterfullerenes are the most recently developed cluster fullerene family and only a few, such as $M_2S@C_{82}$ (M= Sc, Y, Lu, Dy) and $Sc_2S@C_{2n}$ (n = 35, 36, 41), have been isolated and reported.[1-4] These new fullerenes have yet to be fully explored. Much is still to be discovered by using other metals in the SCFs synthesis.

All of those reported clusterfullerenes contain encapsulated rare earth metals *i.e.* group-III (Sc, Y, and lanthanides), and there are very few reports of clusterfullerenes with a non-rare earth metal trapped inside the carbon cage. In 1992, encaging of only non-rare earth metals inside a carbon cage was reported, $Ti@C_{28}$, which was only observed by mass spectrometry.[5] In 2001, a titanium carbide cluster fullerene, Ti_2C_{80},[6] whose structure was later determined to be $Ti_2C_2@D_{3h}$-C_{78},[7] and $Ti_2@C_{84}$ were isolated and identified.[8] In 2009, Yang and co-workers attempted to synthesize Ti-only nitride cluster fullerenes using pure TiO_2, however, no Ti-containing NCFs were detected in the extract. Subsequently, they modified the method using a TiO_2/Sc_2O_3 mixture instead of pure TiO_2 and achieved the first mixed metallic nitride cluster fullerene encapsulating Ti, $TiSc_2N@I_h$-C_{80}.[9] Following the same synthetic procedure using a TiO_2/Y_2O_3 mixture, $TiY_2N@I_h$-C_{80} was synthesized.[10] On the basis of these results, the synthesis of Ti only NCFs seems impractical using just TiO_2, it must be accompanied by rare earth metals such as Sc and Y, and only one Ti atom seems to be encaged. An alternative way to encage a Ti-only cluster could involve the use of a sulfide instead of nitride in this work, thus we used SO_2 instead of N_2 as a gas source.

Here we report the first sulfide clusterfullerene with no rare-earth metals inside the cage, $Ti_2S@C_{78}$. Combining an extensive DFT study with the experimental data recorded, we have been able to elucidate the structure of the EMF, which has a $D_{3h}(24109)$-C_{78} symmetry and the Ti_2S cluster is almost linear.

5.2. Everything starts with the experimental detection

$Ti_2S@C_{78}$ was synthesized, by members of the research group of Prof. Echegoyen at UTEP, in a conventional Krätschmer-Huffman reactor using a TiO_2-graphite mixture in a weight ratio of 1:4 in a mixture of helium and SO_2 atmosphere. The procedures are very similar to those already described for the synthesis of scandium sulfide cluster fullerenes.[11] The obtained soot was extracted with ether and further extracted with CS_2 and analyzed by HPLC and MALDI-TOF-MS. Figure 5.1 shows the initial HPLC of the extract. As it can be seen in the mentioned figure, the $Ti_2S@C_{78}$ fraction is overlapped with those of C_{88}, C_{90}, C_{92} and $Ti_2@C_{84}$. Multistage HPLC methods were used to isolate and purify the $Ti_2S@C_{78}$ fraction.

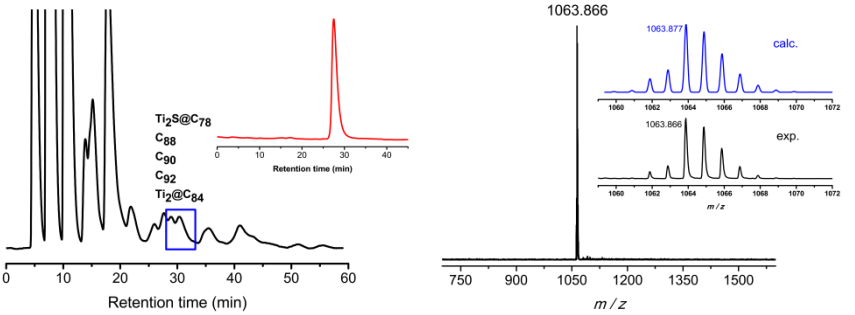

Figure 5.1 (Left) HPLC chromatogram from the initial extract. The inset (red line) corresponds to the HPLC chromatogram from the isolated and purified fraction. (Right) MALDI-TOF mass spectrum of the HPLC-purified $Ti_2S@C_{78}$. The simulated (blue) and experimental (black) isotopic distributions are shown (inset).

The purified $Ti_2S@C_{78}$ was initially characterized by mass spectrometry. The MALDI-TOF mass spectrum shows a single peak with m/z 1063.866, corresponding to the mass of $Ti_2S@C_{78}$. The experimental isotopic distribution shows an excellent agreement with the theoretical one, further corroboration of the composition of $Ti_2S@C_{78}$. It is worth mentioning that in this case, non other members of the Ti_2S clusterfullerene family were observed as it happened for Sc_2S were a broad range of sizes were reported (2n=35-50). This indicates the difficulties of trapping transition metals inside the carbon cages.

5.3. Computational Elucidation of the $Ti_2S@C_{78}$ structure

After the experimental detection, isolation and characterization by mass spectrometry, it is turn for the computational studies to make a step forward. The amount of product obtained in the synthesis is usually very small. Therefore, the possibility of growing crystals for the X-Ray data analysis to determine the structure is usually very difficult. For this reason, the tools provided by the Computational Chemistry become very useful to elucidate which is the isolated isomer or isomers among the thousands of them that can be obtained.

5.3.1. Computations on the anions

For the C_{78} family, there are a total of 24109 cages that can be constructed following the spiral algorithm. Among them, we considered all the structures that (i) satisfy the isolated pentagon rule (IPR, 5 isomers); (ii) show one adjacent pentagon pair (APP1, 18 isomers); and (iii) show two adjacent pentagon pairs (APP2, 228 isomers). This selection is based on the energetic properties of the fullerenes. It is widely accepted that IPR isomers are more stable than other structures showing adjacent pentagon pairs in the carbon framework. That is because of the absence of fused pentagons and the corresponding lower strain energy No structures with three or more APPs were considered because they are found at much higher energies and there are only two metal ions inside the cage (the two Ti ions in the cluster) able to interact with up to two pentalene units. These fused pentagons are seen to interact with the metal ions of the cluster, thus providing an extra stabilization to the system by means of both ionic and covalent contributions.

Experimental evidences, more concretely, the spectroscopic data obtained from the UV-vis-NIR analysis, strongly suggest that there is a formal transfer of six electrons from the trapped Ti_2S unit to the carbon cage. We built up our computational strategy on this fact. Thus, the selected set of structures was computed at first as C_{78}^{6-} at AM1 level. Taking into account the relatively large set of isomers, it is very useful to start computing them

at this cheap level of computation. The lowest energy structures were recomputed at DFT level afterwards.

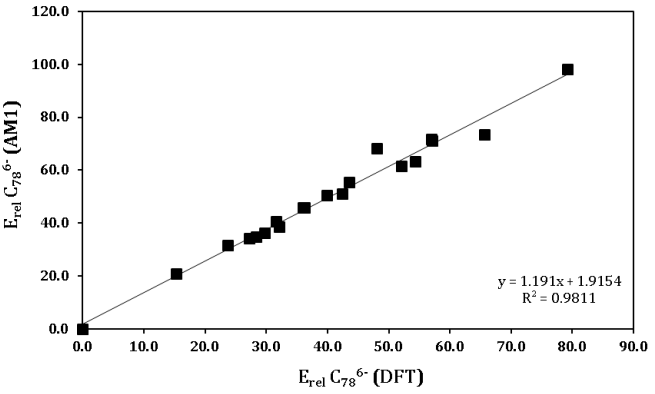

Figure 5.2 AM1 versus DFT relative energies (in kcal mol^{-1}) for the C_{78}^{6-} lowest-energy anions. Very good linear correlation was found.

Figure 4.2 shows the correlation between the energies obtained at AM1 level with respect to the energies obtained at DFT level for the lowest-energy hexaanions. A very good correlation and a slope close to 1 (1.19) were found. Therefore, we can ensure that this first step of the strategy is valid, and the selected structures using the AM1 correspond to the lowest-energy ones also when computed at a higher level. Once we have reduced the initial set of structures, the next step is to compute all the lowest-energy hexaanions isomers as endohedrals at DFT level in order to find the candidate structure for which we will compute all the properties with the aim of determining which one is the detected in the experiments.

5.3.2. Looking for the endohedral fullerene

This is the most complex and resource-demanding part of the strategy due to the large number of different conformations that the cluster can have inside the cage. We have to explore a broad part of the potential energy surface for each system in order to find the lowest-energy position of the Ti_2S into the carbon framework. It is relatively simple when the cage shows adjacent pentagon pairs in the structure. Due to the strong

interaction between the pentalene units and the metal ions, in all the systems studied so far, in the lowest-energy conformations the metal ions are pointing toward the fused pentagon motifs (see figure 5.3). Therefore, the number of different positions that the cluster can adopt is dramatically reduced for the non-IPR isomers. The energies of the most stable conformations for the lowest-energy endohedral systems are collected in table 5.1. The D_{3h}(24109)-C_{78} cage was found to be, by large difference, the one with the lowest energy when computed as hexaanion and with the Ti_2S cluster trapped inside the cage. This indicates that the cage has the best electronic structure to accept the six electron transfer from the inner moiety, and that the distribution, interaction and space available for the cluster inside the carbon framework are also optimal. This IPR cage shows the maximal separation between pentagons, the smaller IPSI index, in good agreement with the Maximum Pentagon Separation Rule. All the other considered isomers were found to have more than 15 kcal mol^{-1} higher energies. It is worth mentioning that the relative energies of the endohedral species with respect to the $Ti_2S@D_{3h}$(24109)-C_{78} were larger than those computed for the hexaanions. This indicates that there is an extra stabilization of the system due to the favorable interaction between the Ti_2S cluster and the D_{3h}(24109)-C_{78} cage, for which the Ti-S and Ti···C are optimal. We also wanted to rationalize why the almost linear arrangement of the Ti_2S is the lowest-energy orientation of the cluster inside the D_{3h}(24109)-C_{78}. To do so, we analyzed the angles and distances for all the different computed orientations of the cluster inside that IPR cage.

Table 5.1 Relative energies (in kcal mol^{-1}) for several isomers of C_{78} in the hexaanionic and endohedral forms. [a,b]

Isomer	Symmetry	APP	C_{78}^{6-}	$Ti_2S@C_{78}$	IPSI
21828	C_1	2	43.6	68.1	12.985
21975	C_1	2	29.8	44.0	12.978
21981	C_1	2	31.7	49.9	12.979
21982	C_1	2	36.3	54.6	12.981
21983	C_1	2	54.4	42.0	12.984
22010	C_2	2	15.4	29.2	12.972
22033	C_1	2	57.2	72.8	12.991
22096	C_1	2	52.2	59.6	12.992
22135	C_1	2	36.1	50.5	12.983
22590	C_1	2	42.5	51.5	12.988
22646	C_1	2	27.3	41.5	12.981
23298	C_2	2	39.9	60.1	12.981
23349	C_1	1	32.2	38.7	12.864
24088	C_{2v}	2	28.4	23.6	12.969
24101	C_s	2	65.8	49.5	12.864
24105	D_3	0	48.1	78.5	12.771
24106	C_{2v}	0	57.0	63.0	12.767
24107	C_{2v}	0	23.7	31.6	12.744
24108	D_{3h}	0	79.3	104.0	12.738
24109	D_{3h}	0	0.0	0.0	12.729

[a] Isomer number according to the spiral algorithm of Fowler and Manolopoulos. [b] APP stands for adjacent pentagon pairs.

As a result of the analysis of the data obtained from these computations, differences up to 30 kcal mol^{-1} were found being the most favorable one the structure showing a Ti-S-Ti angle of 172 degrees. Not only the angle but also the distances between the Ti ions were found to be crucial. As it can be seen in table 5.2, the lowest-energy structure is found to be the one with larger distances between the Ti ions. For all the clusterfullerenes possessing a non-IPR cage, the lowest-energy structures are those where the metal atoms are pointing toward the pentalene units, as found so far for all the non-IPR systems studied. Therefore, for a given cage, the structure of the Ti_2S cluster adapts in order to (i) optimize the interaction with the fullerene cage, for example the Ti atoms pointing toward the

pentalene units in the non-IPR cages; and (ii) minimize the repulsion between the formal Ti^{4+} cations, i.e. assuming a linear Ti-S-Ti arrangement and increasing the Ti-S distances as much as possible. As a result of the combination of all these different factors, the cage D_{3h}(24109)-C_{78} satisfies the three principal required conditions to host the Ti_2S cluster: (i) it has the most suitable electronic structure to accommodate the six electrons formally transferred; (ii) it shows optimal Ti···C interactions; and (iii) it allows the internal cluster to be in an almost linear arrangement with maximally separated Ti^{4+} ions.

Table 5.2 Relative energies for all the computed orientations of Ti_2S in $Ti_2S@D_{3h}$(24109)-C_{78}. Ti-Ti distances, in Å, and Ti-S-Ti angles in degrees.

Orientation	E (kcal mol^{-1})	Ti - Ti	Ti - S - Ti
1	27.5	3.99	121.3
2	18.1	3.63	104.6
3	33.9	3.69	107.6
4	29.9	3.14	86.6
5	13.9	3.80	111.9
6	30.8	3.93	118.7
7	15.4	4.00	121.8
8	30.4	3.97	120.8
9	18.2	3.63	104.9
10	18.2	3.62	104.1
11	30.7	3.94	118.9
12	34.0	3.69	107.5
13	14.0	3.80	111.7
14	19.2	3.84	114.8
15	18.4	4.20	131.9
16	19.2	3.84	114.9
17	15.2	4.00	121.9
18	0.0	4.69	171.7
19	18.22	3.64	105.1

The next step, after the selection of our candidate, is to compute all the properties of this structure in order to compare the computational and

experimental data obtained. This comparison will be the definitive test to confirm or discard if the selected isomer is, in fact, the one isolated in the experiments.

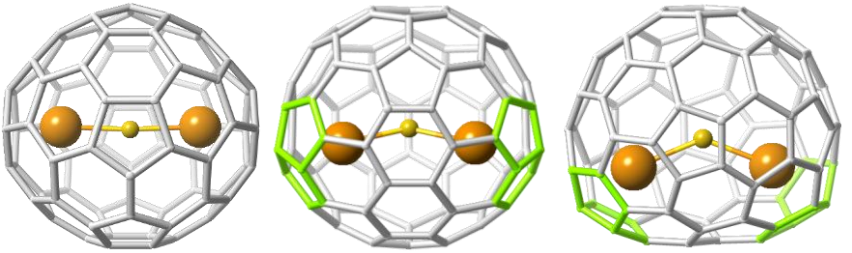

$Ti_2S@D_{3h}(24109)$-C_{78} $Ti_2S@C_s(24088)$-C_{78} $Ti_2S@C_2(22010)$-C_{78}

Figure 5.3 DFT-optimized structures for the lowest-energy IPR and APP2 isomers of the $Ti_2S@C_{78}$ clusterfullerene.

5.4. Comparing computed properties and experimental data for the selected candidate

In this section, we present all the computations we carried out in order to predict properties of the selected cage candidate and compare them with the experimental data to confirm or discard the proposed isomer.

5.4.1. Confirming the formal electron transfer

To confirm the electron transfer suggested by the experiments and, used as the basis to carry out the computations on the first stages of out computational strategy, we analyzed the molecular orbital interaction diagram for the $Ti_2S@D_{3h}(24109)$-C_{78}. In this diagram (figure 5.4), the interaction between the molecular orbitals of the empty cage and the cluster are shown. The six electrons from the three highest-occupied molecular orbitals (HOMO) of the Ti_2S unit are formally transferred to the three lowest-energy unoccupied molecular orbitals (LUMO) of the carbon cage.

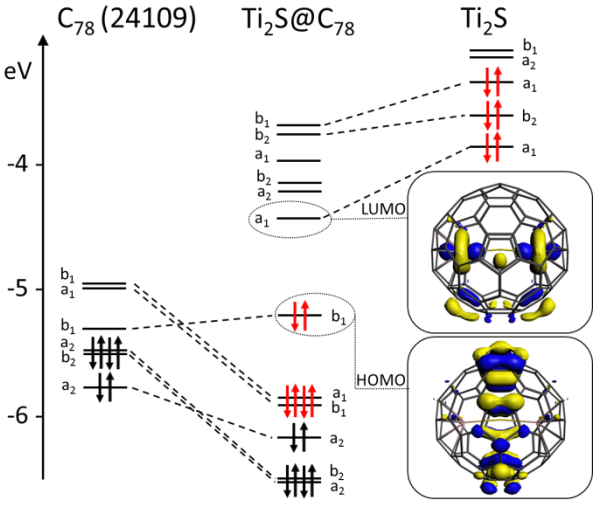

Figure 5.4 Orbital interaction diagram for $Ti_2S@D_{3h}(24109)$-C_{78}. The fragments, Ti_2S and $D_{3h}(24109)$-C_{78}, were calculated with the same geometry that they have in the clusterfullerene. Six electrons from the neutral Ti_2S cluster (highlighted in red) are formally transferred to cage orbitals.

The orbital interaction diagram for the lowest-energy clusterfullerene $Ti_2S@D_{3h}(24109)$-C_{78} verifies that there is a formal transfer of six electrons from the cluster to the cage, as also seen for nitride $Sc_3N@D_{3h}(24109)$-C_{78} and carbide $Ti_2C_2@D_{3h}(24109)$-C_{78}. The HOMO is mainly localized on the carbon framework. The LUMO, however, has predominant contributions from the Ti_2S cluster; in particular, from the bonding combination of the dz^2-like atomic orbitals of the two Ti ions. The computed HOMO-LUMO gap is 0.66 eV, significantly smaller than the gap for the hexaanionic cage, 1.22 eV. This reduction of the gap is due to the presence of the cluster molecular orbital (LUMO of the clusterfullerene) between those molecular orbitals of the carbon cage. Taking into account the six electron transfer, the oxidation state of the titanium is Ti^{4+}, not Ti^{3+}, as is the case for $TiSc_2N@C_{80}$ and $TiY_2N@C_{80}$. Thus according to the ionic model, $Ti_2S@C_{78}$ can be formally considered to be $(Ti_2S)^{6+}@(C_{78})^{6-}$.

5.4.2. Electrochemical study

The cyclic voltammetry of $Ti_2S@C_{78}$ recorded in a *o*-dichlorobenzene (*o*-DCB) solution containing 0.05M tetra-*n*-butylammonium hexafluorophosphate (*n*-Bu_4NPF_6) as the supporting electrolyte is represented in figure 5.5. $Ti_2S@C_{78}$ exhibits three reversible reductions with half wave potentials at -0.92, -1.53, and -1.80 V, respectively versus Fc/Fc^+, and two additional irreversible reductions with peak potentials at -2.29 and -2.41 V, respectively. In the anodic scan, two reversible oxidation steps with half wave potentials at +0.23 and +0.65 V are observed along with one quasi-reversible oxidation at +1.03 V versus Fc/Fc^+.

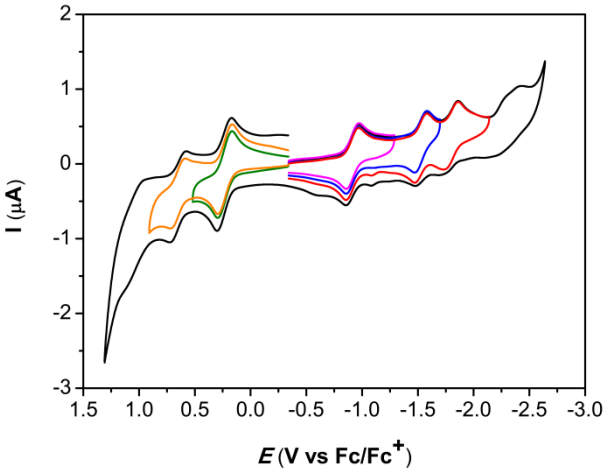

Figure 5.5 Cyclic voltammogram of $Ti_2S@C_{78}$ recorded in a 0.05M *o*-DCB/*n*-Bu_4NPF_6 solution at a scan rate of 100 mVs^{-1}. Ferrocene was added as the internal standard.

The electrochemically reversible behavior of $Ti_2S@C_{78}$ is dramatically different from most metallic clusterfullerenes which usually display irreversible reductions under the same conditions. $TiSc_2N@C_{80}$, $Sc_2S@C_{72}$ and $Sc_4O_2@C_{80}$ are some of the very few clusterfullerenes that exhibit reversible reductions. Although $Sc_3N@D_{3h}$-C_{78} possesses the same cage isomer as $Ti_2S@D_{3h}$-C_{78}, the CV of the scandium nitride endohedral

fullerene shows irreversible reduction steps, which indicates that the encaged clusters have a significant influence on the electrochemical behavior. Moreover, the first reduction and the first oxidation potentials of $Ti_2S@D_{3h}$-C_{78} are anodically shifted by 620 mV and 110mV respectively compared to those of $Sc_3N@D_{3h}$-C_{78} (see table 5.3). Hence, the titanium sulfide clusterfullerene is much easier to reduce and somewhat harder to oxidize than the scandium nitride endohedral. The electrochemical gap (EG) of $Ti_2S@D_{3h}$-C_{78}, 1.15 V, is 0.51 V smaller than that of $Sc_3N@D_{3h}$-C_{78} and is comparable to that of $TiSc_2N@I_h$-C_{80}, 1.10 V, which is 0.75 less than that of $Sc_3N@I_h$-C_{80}, 1.85 V. Similarly, $TiY_2N@I_h$-C_{80} has an electrochemical gap of 1.11 V, which is 0.94 V smaller than that of the corresponding $Y_3N@I_h$-C_{80}, 2.05 V. The EG of $Ti_2S@D_{3h}$-C_{78} is also 0.22-0.63 V less than those of the reported scandium sulfides clusterfullerenes. These results confirm that Ti-containing clusterfullerenes possess smaller electrochemical gaps than the corresponding rare earth metallic clusterfullerenes.

Table 5.3 Redox potentials (V vs. Fc/Fc^+) of $Ti_2S@D_{3h}$-C_{78} along with other related clusterfullerenes.

	$E^{+/2+}$	$E^{0/+}$	$E^{0/-}$	$E^{-/2-}$	$E^{2-/3-}$	$E^{3-/4-}$	$E^{4-/5-}$	$\Delta E_{gap,ec}$
$Ti_2S@D_{3h}$-C_{78}	+0.65[a]	+0.23[a]	-0.92[a]	-1.53[a]	-1.80[a]	-2.29[b]	-2.41[b]	1.15
$Sc_3N@D_{3h}$-C_{78}		+0.12[a]	-1.54[b]					1.66
$TiSc_2N@I_h$-C_{80}		+0.16[a]	-0.94[a]	-1.58[a]	-2.21[a]			1.10
$TiY_2N@I_h$-C_{80}		+0.00[a]	-1.11[a]	-1.79[b]				1.11

[a] Half-wave potential (reversible redox process).[b] Peak potential (irreversible redox process).

Given the topology of the frontier molecular orbitals, the oxidation of the clusterfullerene is predicted to take place in the carbon cage. The reduction, however, is predicted to happen *in cavea*, *i. e.* in the internal cluster, as in $M_2@C_{80}$ (M=La, Ce) or $TiM_2N@C_{80}$ (M=Sc, Y). Since the formal oxidation state of the Ti is 4+ in $Ti_2S@C_{78}$, the oxidation process of the endohedral cannot be based on the Ti centers, so the Ti atoms control only the reduction processes in this case, in contrast with the redox results reported by Popov and Dunsch for $TiSc_2N@C_{80}$, where the Ti^{3+} atoms are responsible for both the reductive and oxidative electrochemical behavior.

Computed oxidation and reduction potentials agree reasonably well with the experimental values measured by CV (see Table5.4). The first anodic potential, corresponding to the first oxidation process, is predicted at +0.08 V, in rather good agreement with the measured half-wave potential (+0.23 V). The predicted first cathodic potential, corresponding to the first reduction process, is predicted at -1.02, also very close to the experimental value with a difference of only 100 mV. We were also able to compute the second oxidation potential, +0.56 V, which is within less than 100 mV from the experimental value. The computed value for the EG is also listed in table 5.4 and is in very good agreement with the experimental value.

Table 5.4 Experimental and computed oxidation and reduction potentials (in V versus Fc/Fc^+), as well as the computed HOMO-LUMO gap (in eV) for $Ti_2S@D_{3h}$-C_{78}.

	$E^{+/2+}$	$E^{0/+}$	$E^{0/-}$	EG	H-L gap
Experimental	+0.65	+0.23	-0.92	1.15	
Computed	+0.56	+0.08	-1.02	1.10	0.66

It is worth remarking here that the computation of the spin density for the singly reduced $Ti_2S@D_{3h}$-C_{78}^- confirms that the first reduction takes place in the internal cluster as shown in figure 5.6.

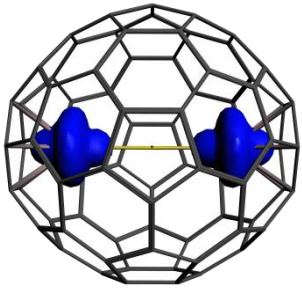

Figure 5.6 Spin density representation for the monoreduced $Ti_2S@D_{3h}$-C_{78}.

5.4.3. UV-vis-NIR spectrum

The data obtained using the UV-vis-NIR spectroscopy can also be used to confirm the selection of the isomer obtained. Figure 5.7 shows the experimental absorption spectrum of $Ti_2S@C_{78}$ in toluene, along with the computed one using TDDFT.

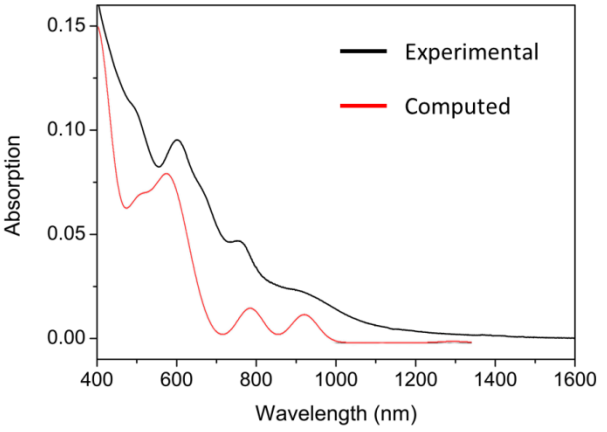

Figure 5.7 Experimental (black) and predicted (red) UV-vis-NIR spectra.

In the experiment, absorptions at 498, 602, 657, 757 and 896 nm were observed with an onset around 1470nm. The value of the onset indicates that this titanium sulfide clusterfullerene has a small HOMO-LUMO gap, in good agreement with the previously discussed data obtained from the molecular interaction diagram and from the electrochemical studies. The optical band-gap is estimated to be 0.84 eV based on the absorption spectral onset which is smaller than that reported for $Ti_2C_2@C_{78}$. The feature-rich absorptions of $Ti_2S@C_{78}$ resemble those of $Ti_2C_2@D_{3h}(24109)$-C_{78} and $Sc_3N@D_{3h}(24109)$-C_{78} and are dramatically different from those of $M_3N@C_2$-C_{78} (M=Gd, Sc, Tm, Dy). Taking into account that the absorption spectra of fullerenes in the visible and NIR regions are dominated by the π-π* transitions of the carbon cages, the spectra are very sensitive to the carbon cage symmetries which indicates that in this case, the Ti_2S must be also trapped in the $D_{3h}(24109)$-C_{78}.

We carried out calculations using time-dependent (TD) DFT in the Vis-NIR region, for wavelengths larger than 450 nm. Despite the systematic underestimation of excitation energies by TDDFT, this methodology provides reasonably agreement with experimental results for the family of sulfide clusterfullerenes. The lowest-energy transitions, which are fingerprints of $Ti_2S@D_{3h}(24109)$-C_{78} due to the titanium-based character of the LUMO orbitals, are predicted at rather large wavelengths, in good agreement with the large spectral onset obtained from the experiments (1470 nm). The feature-rich absorption region of $Ti_2S@C_{78}$ that resembles that of $Ti_2C_2@D_{3h}(24109)$-C_{78} and $Sc_3N@D_{3h}(24109)$-C_{78} and is due to cage-to-cage transitions, is rather well reproduced at the TD-DFT level, both the position of the peaks as well as their relative intensities (see table 5.5).

Table 5.5 Time-Dependent DFT predictions for the most intense lowest-energy excitations in the absorptions spectrum of $Ti_2S@D_{3h}(24109)$-C_{78}.

E (eV)	λ (nm)	[a] f	[b] Leading configurations (%)
1.1685	1061	0.00420	HOMO → LUMO+3 (98)
1.3204	938	0.00553	HOMO → LUMO+4 (96)
1.5036	825	0.00259	HOMO-3 → LUMO+1 (97)
1.5731	788	0.01134	HOMO-3 → LUMO+2 (93)
			HOMO-2 → LUMO+1 (36)
1.6536	750	0.01823	HOMO-1 → LUMO+5 (28)
			HOMO-1 → LUMO+2 (23)
1.7243	719	0.00355	HOMO-5 → LUMO (92)

[a] Only excitations with f (oscillator strength) > 0.001 are listed. [b] Contributions less than 10% are omitted.

As in the case of the electrochemical data, all these observations lead us to the assignment of the $D_{3h}(24109)$ cage .

5.4.4. Thermal effects

The effects of temperature could play an important role and have to be taken into account as it has been demonstrated previously for other endohedral metallofullerenes. The molar fractions of the lowest-energy

$Ti_2S@C_{78}$ isomers as a function of the temperature were computed using the rigid harmonic oscillator (RRHO) and the free encapsulating model (FEM) as proposed by Slanina. The two approximations provide the same prediction in this case. The $Ti_2S@D_{3h}(24109)$-C_{78} is the most abundant isomer for the whole temperature range up to 4000 K (see figure 5.8).

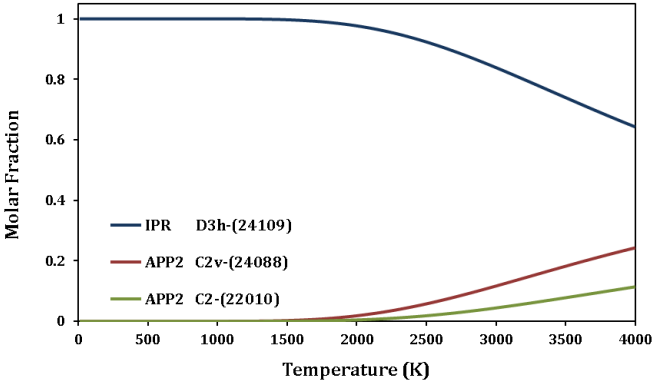

Figure 5.8 Predicted molar fractions within the FEM approximation as a function of the temperature for three different isomers of $Ti_2S@C_{78}$.

5.5. Conclusions

In summary, a sulfide cluster metallofullerene containing only transition metals inside the cage has been successfully synthesized using SO_2 as a source in a Krätschmer-Huffman DC-arc reactor. The new clusterfullerene was characterized by mass spectrometry, UV-vis-NIR absorption spectrometry, cyclic voltammetry, and DFT calculations.

Based on the comparison of the data obtained in the experiments and the results obtained from the calculations, we concluded that (i) the symmetry of the isolated cage is assigned to the $D_{3h}(24109)$-C_{78} isomer, which is the lowest-energy structure as hexaanion and as endohedral; (ii) there is a formal transfer of six electrons from the Ti_2S cluster to the

carbon cage; (iii) the cluster has an almost linear disposition inside the cage in order to minimize the electrostatic repulsion between the two Ti cations; (iv) this isomer exhibits a surprising electrochemical behavior with both reversible anodic and cathodic processes, and a small electrochemical gap which are remarkably different from those of the corresponding rare earth metallic clusterfullerenes. The computational results obtained are in good agreement with the experimental data; (v) the UV-vis-NIR spectra is also predicted in good agreement with the experimental recorded data; and (vi) the selected isomer from the computations is also predicted to be the one with larger molar fractions when the effects of the temperature are taken into account.

5.6. References

1. L. Dunsch, S. Yang, L. Zhang, A. Svitova, S. Oswald and A. A. Popov, *J. Am. Chem. Soc.*, 2010, **132**, 5413-5421.
2. B. Q. Mercado, N. Chen, A. Rodríguez-Fortea, M. A. Mackey, S. Stevenson, L. Echegoyen, J. M. Poblet, M. M. Olmstead and A. L. Balch, *J. Am. Chem. Soc.*, 2011, **133**, 6752-6760.
3. N. Chen, C. M. Beavers, M. Mulet-Gas, A. Rodríguez-Fortea, E. J. Munoz, Y.-Y. Li, M. M. Olmstead, A. L. Balch, J. M. Poblet and L. Echegoyen, *J. Am. Chem. Soc.*, 2012, **134**, 7851-7860.
4. N. Chen, M. Mulet-Gas, Y.-Y. Li, R. E. Stene, C. W. Atherton, A. Rodriguez-Fortea, J. M. Poblet and L. Echegoyen, *Chem. Sci.*, 2013, **4**, 180-186.
5. T. Guo, M. Diener, Y. Chai, M. Alford, R. Haufler, S. McClure, T. Ohno, J. Weaver, G. Scuseria and R. Smalley, *Science* 1992, **257**, 1661-1664.
6. B. Cao, M. Hasegawa, K. Okada, T. Tomiyama, T. Okazaki, K. Suenaga and H. Shinohara, *J. Am. Chem. Soc.*, 2001, **123**, 9679-9680.
7. T. Yumura, Y. Sato, K. Suenaga and S. Iijima, *J. Phys. Chem. B*, 2005, **109**, 20251-20255.
8. B. Cao, K. Suenaga, T. Okazaki and H. Shinohara, *The Journal of Physical Chemistry B*, 2002, **106**, 9295-9298.
9. S. Yang, C. Chen, A. A. Popov, W. Zhang, F. Liu and L. Dunsch, *Chem. Commun.* , 2009, 6391-6393.
10. C. Chen, F. Liu, S. Li, N. Wang, A. A. Popov, M. Jiao, T. Wei, Q. Li, L. Dunsch and S. Yang, *Inorg. Chem.*, 2012, **51**, 3039-3045.
11. N. Chen, M. N. Chaur, C. Moore, J. R. Pinzon, R. Valencia, A. Rodriguez-Fortea, J. M. Poblet and L. Echegoyen, *Chem. Commun.* , 2010, **46**, 4818-4820.

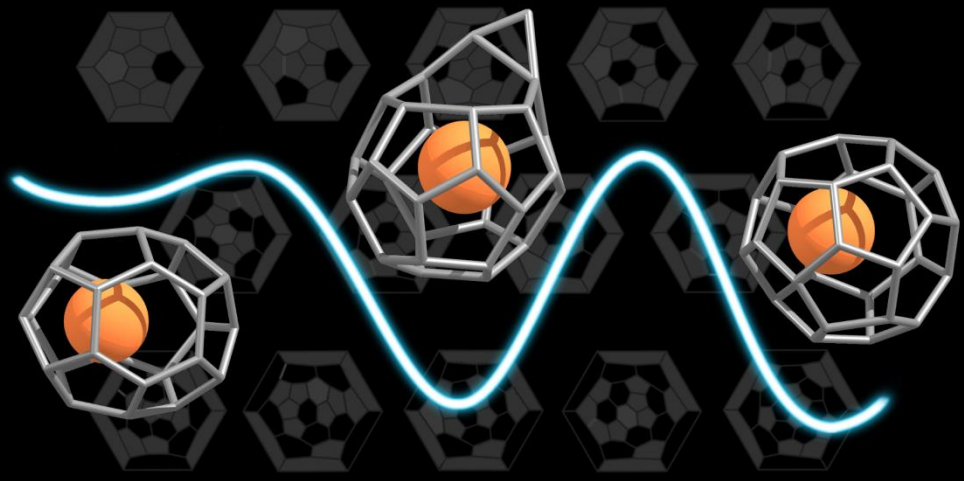

Chapter 6 // *Small Endohedral Metallofullerenes: Structures, Growth and Abundances*

Related Publications:

Bottom-Up Formation of Endohedral Metallofullerenes is Directed by Charge Transfer and Ionic Radius

P. W. Dunk, M. Mulet-Gas, Y. Nakanishi, N. K. Kaiser, A. Rodríguez-Fortea, H. Shinohara, J. M. Poblet, A. G. Marshall and H. W. Kroto. *Nature Communications*, **2014** (accepted)

Small Endohedral Metallofullerenes: Exploration of the Structure and Growth Mechanism in the Ti@C_{2n} (2n=26-50) Family

M. Mulet-Gas, L. Abella, P. W. Dunk, A. Rodríguez-Fortea, H. W. Kroto and J. M. Poblet. *Chemical Science*, **2014** (accepted)

The Smallest Stable Fullerene, M@C_{28} (M=Ti, Zr, U): Stabilization and Growth from Carbon Vapor

P. W. Dunk, M. Mulet-Gas, N. K. Kaiser, A. Rodríguez-Fortea, J. M. Poblet, H. Shinohara, C. L. Hendrickson, A. G. Marshall and H. W. Kroto. *Journal of the American Chemical Society*, **2012**, 134, 9380-9389.

Chapter 6

Small Endohedral Metallofullerenes: Study of the Structures, Growth and Abundances

This chapter contains the work we have done in an intensive collaboration with the group of Prof. Harold W. Kroto, at Florida State University, and Prof. Alan G. Marshall's group, at the National High Magnetic Field Laboratory. Using the state-of-the-art Fourier Transform Ion Cyclotron Resonance (FT-ICR) mass spectrometry, a new family of fullerenes, $Ti@C_{2n}$, was detected. Combining the experimental results and an extensive DFT-based computational study we have theoretically characterized the lowest-energy isomers, rationalized their electronic structure and properties, and studied the possible growth path. Moreover, the computational study of the $Ca@C_{2n}$ is also reported along with the rationalization of the experimental abundances.

6.1. Introduction

The smallest fullerene to form in condensing vapor has received considerable interest since the discovery of Buckminsterfullerene, C_{60}.[1] Smaller fullerenes remain a largely unexplored class of all-carbon molecules that are predicted to exhibit fascinating properties due to the large degree of curvature and resulting highly pyramidalized carbon atoms in their structures.[2-4] However, the curvature also renders the smallest fullerenes highly reactive, making them difficult to detect experimentally. Gas-phase attempts to investigate the smallest fullerenes by stabilization through cage encapsulation of a metal have been hindered by the complexity of mass spectra that result from vaporization experiments which include non-fullerene clusters, empty cages and metallofullerenes. The developing of the high resolution Fourier Transform Ion Cyclotron Resonance (FT-ICR) mass spectrometry has become the key factor to overcome that problem and investigate the formation of the smallest fullerene and the entire families of, up to now, missed endohedral fullerenes.[5-7]

Understanding how small fullerenes form is essential to uncovering mysteries of endohedral metallofullerene formation. In this chapter, by use of comprehensive quantum chemical investigations, we study the stabilization of the smallest fullerenes by encapsulation of Ti atoms. In particular, we studied all the possible structures in order to find the lowest-energy isomer for each C_{2n} family (2n=26-50) after the successful synthesis and detection of these structures. We also verified the validity of our computational strategy for the small fullerenes and checked the possible growth process by single C_2 insertion following the Closed Network Growth (CNG) mechanism.[8, 9]

6.2. Detection of the $Ti@C_{2n}$ (2n=26-50) family

It is likely that any small, highly strained fullerenes will coalesce in the solid state or react upon exposure to solvent and air. Therefore, the molecular beam technique that has been used in this work is most suitable for exploration of the smallest fullerenes because the species remain in the gas phase in a vacuum. The experimental configuration is particularly powerful for such an investigation because the present 9.4 T FT-ICR mass spectrometer gives the highest resolution yet for the analysis of cluster experiments. Gas-phase investigations probing the synthesis of the smallest endohedral metallofullerenes have been hindered by the complexity of the mass spectra that result from non-fullerene clusters, empty cages, and endohedral fullerenes which all form spontaneously in carbon vapor.

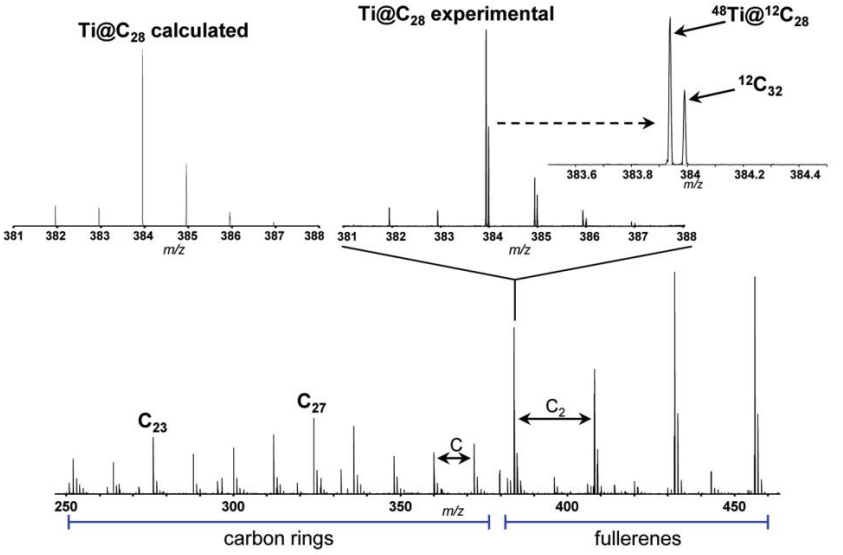

Figure 6.1 FT-ICR mass spectrum (positive ions) resulting from the laser vaporization of a titanium-doped graphite target under conditions that probe the ring-to-fullerene transition. $Ti@C_{28}$ forms as the smallest fullerene. The 52 mDa difference between the smallest empty cage, C_{32}, and $Ti@C_{28}$ is clearly resolved.

That restriction is clearly illustrated in the case of titanium, an attractive tetravalent candidate for C_{28} stabilization by encapsulation. The major

isotope, ^{48}Ti, differs in mass by only 52 mDa from C_4. Therefore, $Ti@C_{28}$ would not be resolved from empty cage C_{32} with conventional mass spectrometers.

The experimental results show that only a few tetravalent metals sufficiently stabilize the C_{28} fullerene, and in particular, $Ti@C_{28}$ form as a highly favored member of the $M@C_{28}$ (M= group IV metal) fullerenes. Figure 6.1 shows the cluster cations formed from the laser vaporization of a titanium-doped (0.8% Ti) graphite target rod under conditions that prove the "ring-to-fullerene" structure transition region. Carbon rings appear to be dominantly observed in the C_{22} to C_{30} region as expected. A cluster corresponding to $Ti@C_{28}$ is revealed to be the most abundant molecular ion in the ring-to fullerene transition region. Even-numbered fullerene species, C_{2n} and $Ti@C_{2n}$, dominate for larger clusters in the spectrum.

Figure 6.2 shows that the $Ti@C_{28}$ metallofullerene becomes even more abundant under cluster source conditions (higher He pressure) that most efficiently generate fullerenes. In fact, the $Ti@C_{28}$ cluster has more than 3 times the relative abundance of the smallest empty cage, the C_{32}. Under these conditions, the cyclic species are not observed, and fullerenes are exclusively detected. The distribution of $Ti@C_{2n}$ shows that only a $Ti@C_{44}$ forms also in high relative abundance. Empty-cage fullerenes are also formed and exhibit a typical distribution in which C_{60} is the most abundant fullerene (not showed in the spectrum). However, $Ti@C_{60}$ is weakly formed, and most Ti abundant metallofullerenes are small fullerenes. Titanium encapsulation appears to be an efficient method to produce the smallest fullerenes that do not form in abundance as pristine cages.

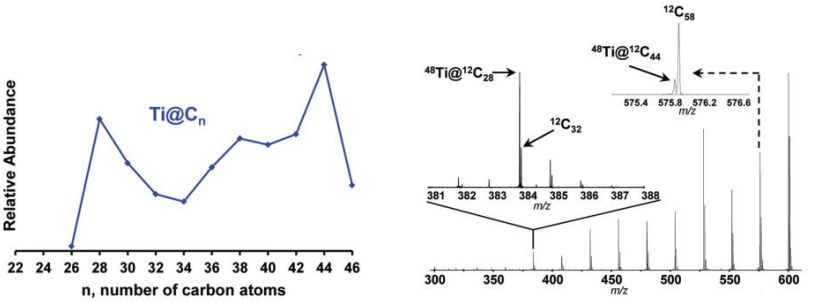

Figure 6.2 Cluster cations generated from vaporization of a Ti-doped graphite target under conditions that most efficiently generate fullerenes. Ti@C_{28} and Ti@$_{44}$ are found to be formed in higher abundances. Note that empty C_{28} is not formed.

Collision-induced dissociation (CID) experiments were performed to confirm that the metal is located within the fullerene cage. The fragmentation pattern of a fullerene is unique among various structural forms of carbon clusters because, when excited to high internal energy, loss of neutral C_2 units occurs with retention of the internal metal atom.

Ti@C_{28} was isolated by the application of a Stored-Waveform Inverse Fourier Transform (SWIFT)[7] event that ejects all species except for Ti@C_{28} (and C_{32}) from the ICR cell. The isolated molecular ions are subsequently excited to higher kinetic energy by applying an off-resonant radiofrequency. The ions then undergo many collisions with the carrier gas (helium or argon) to achieve high internal energies above the threshold energy for dissociation, and all resulting products ions are detected. As it is shown in figure 6.3, Ti@C_{28} remains completely intact without loss of Ti after many collisions with He or Ar at kinetic energies of several kiloelectronvolts, and the cluster does not fragment by C_3 or C_2. Thus the metal is not bond to the outside of the cage, and the molecular structure is neither linear nor cyclic. It is also clear that Ti@C_{28} does not fragment to any smaller fullerene, which further demonstrates the high stability of this system.

Larger species were also studied using the same technique in order to check whether they were endohedrals or not. In figure 6.3, the

fragmentation of $Ti@C_{38}$ is also represented. In this case, $Ti@C_{38}$ was isolated along with the empty cage C_{42}. After the excitation and fragmentation, the detection of the ionic products shows several losses of C_2 units without any loss of Ti. Demonstrating that the $Ti@C_{38}$ is an endohedral fullerene and that for these systems, the C_2 loss is the path followed during the fragmentation process. The abundance of $Ti@C_{28}$ formed by fragmentation of larger metallofullerenes is low, suggesting that it is not formed as a result of the fragmentation during the growth process.

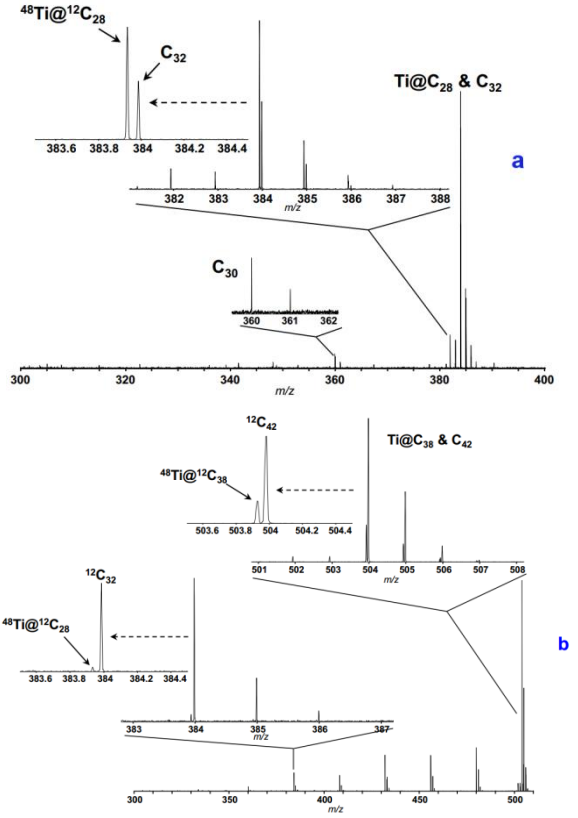

Figure 6.3 (top) Fragmentation pattern of the SWIFT-isolated $Ti@C_{28}$ along with the C_{32}. $Ti@C_{28}$ does not fragment to a smaller endohedral and no C or C_2 losses are observed. The empty cage C_{30} results from fragmentation via C_2 loss of C_{32}. (bottom) Fragmentation patterns of the SWIFT-isolated $Ti@C_{38}$ and C_{42}. The metallofullerene exhibits C_2 loss, with $Ti@C_{28}$ as the smallest fragmentation product. C_{42} cluster fragments by C_2 loss to a minimum size of C_{30}.

6.3. Computational study of the Ti@C_{2n} family

The experimental detection of the new family of endohedral metallofullerenes Ti@C_{2n} (2n = 26-46) is the starting point of this work. Common structural characterization techniques, which are key toward understanding EMF formation, are generally not applicable in gas-phase studies. Therefore, the first step of the investigation was to compute all the possible isomers for each of the Ti@C_{2n} detected. To do so, we designed the computational strategy taking into account all the factors involved in the stabilization of the EMFs: (i) the electronic structure of the empty cages; (ii) the formal charge transferred from the trapped metal atom to the carbon cage; and (iii) the interaction and position of the metal inside the carbon framework.

6.3.1. Structure and stabilization of Ti@C_{28}

Having established that Ti@C_{28}, along with all the other Ti@C_{2n} species detected, is an endohedral fullerene, we turn our attention to its cage structure and how the encapsulated metal may stabilize such a small and highly strained fullerene. We focused our first studies on Ti@C_{28} not only because it is one of the most abundant Ti@C_{2n}, but also because there are only two possible isomers (D_2 and T_d symmetry) for the C_{28} cage. We have carried out theoretical investigations to discern the molecular structure and elucidate the factors that govern the stabilization of Ti@C_{28}. This endohedral metallofullerene exhibits high relative abundance, but empty cage C_{28} is not observed in the experiments, indicating that encapsulation of titanium significantly stabilizes the C_{28} fullerene cage.

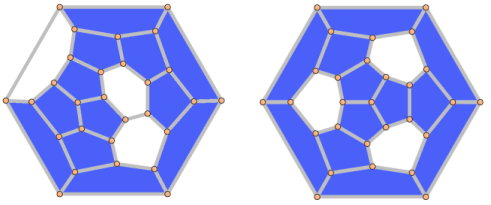

Figure 6.4 Schlegel representations for $D_2(1)$-C_{28} and $T_d(2)$-C_{28}. The five-membered rings are highlighted in blue.

The $T_d(2)$-C_{28} isomer possesses four units of directly fused triple pentagons in the structure, whereas $D_2(1)$-C_{28} contains a much more highly strained pentagon configuration with four directly abutting pentagons (figure 6.4). The ground state of the neutral T_d isomer is a quintuplet; while in contrast, the ground state of the neutral D_2 is a singlet. The electronic structure and the frontier orbitals involved are shown in figure 6.5. We found that the presence of the four energetically deep quasi-degenerate singly occupied molecular orbitals for the T_d isomer which receive the four electrons formally transferred from the Ti atom to the cage, results in much stronger stabilization than for the D_2 isomer. Accordingly, the HOMO for the Ti@$T_d(2)$-C_{28} shows much lower energy than the HOMO for Ti@ $D_2(1)$-C_{28}. Therefore, the encapsulation of a Ti atom renders the T_d isomer much more stable than the D_2 isomer. Indeed, the energy difference between the neutral empty-cage species is about 17 kcal mol^{-1}, but this difference increases for the tetraanion and Ti@C_{28} endohedral species to 61 and 55 kcal mol^{-1}, as shown in table 6.1.

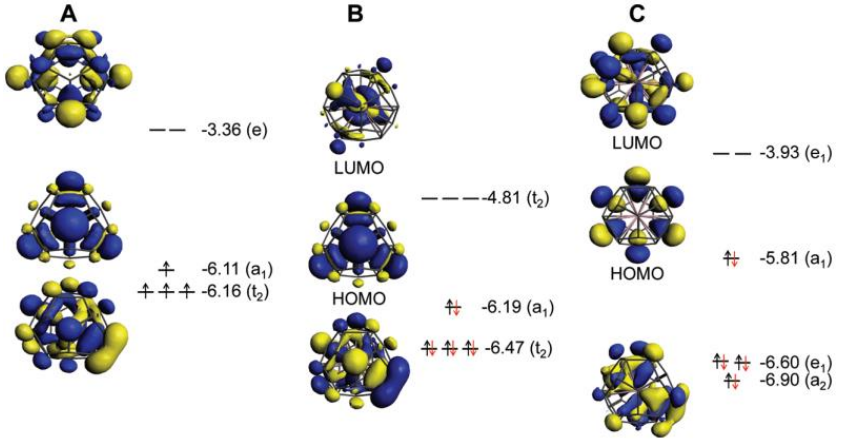

Figure 6.5 Frontier orbitals computed from DFT calculations for the $T_d(2)$-C_{28} (A), and the corresponding endohedral Ti@$T_d(2)$-C_{28} with the Ti centered within the cage (B) and Ti occupying and off-center position (C). Electrons formally transferred from the Ti atom to the carbon cage are highlighted in red.

Previous studies found that the transferred charge from the trapped atom to a fullerene cage is preferentially located at the most strained bonds, corresponding to the most pyramidalized atoms. In $T_d(2)$-C_{28}, those

carbon atoms are located at the directly fused triple pentagon junctions. Transferred charge is found to reside at the [5,5] bonds of these triple fused pentagons, as shown in figure 6.6.[10] The $T_d(2)$-C_{28} isomer has an optimal structure to accommodate the four electrons that minimized the Coulomb repulsion.

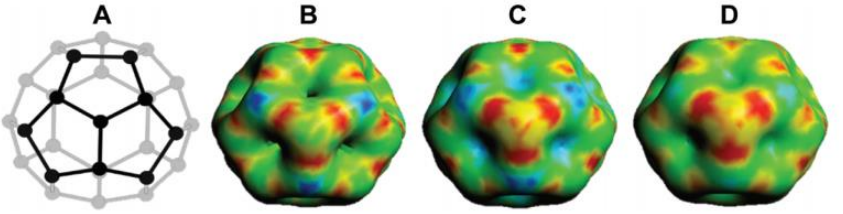

Figure 6.6 Representation of the strucuture of the $T_d(2)$-C_{28} cage (A) and the molecular electrostatic potentials (MEP) for the neutral $T_d(2)$-C_{28} (B), tetraanionic $T_d(2)$-C_{28}^{4-} (C), and endohedral Ti@$T_d(2)$-C_{28} (D) systems. The charge transferred from the encapsulated Ti atom to the carbon framework is localized at the four most pyramidalized carbon atoms in the $T_d(2)$-C_{28} fullerene. The molecular structure is optimal to accommodate four electrons.

The Ti trapped in the cage, formally Ti^{4+}, prefers nucleophilic regions of the fullerene. We found a significant interaction with the cage resulting in additional stabilization. A large energy difference between the endohedral metallofullerene with the Ti atom in the center of the cage and that with a shifted position off the center is found. Ti@$T_d(2)$-C_{28} with the Ti atom shifted is about 37 kcal mol^{-1} lower in energy than the structure with the atom residing in the center. The displacement of the Ti atom toward the nucleophilic region from the center of the molecule is 0.535 Å. (figure 6.7)

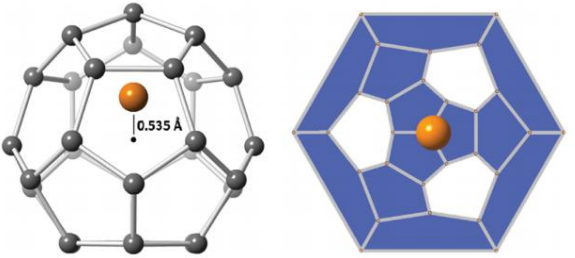

Figure 6.7 Bond and stick 3D representation (left) and Schlegel diagram (right) for Ti@$T_d(2)$-C_{28}. The internally located Ti atom is shifted off-center, yielding additional stabilization.

All those features that we have found and rationalized for Ti@C_{28}, are going to be the basis for the study and better-understanding of the whole Ti@C_{2n} family.

6.3.2. Smallest Ti@C_{2n} systems (2n=28-34): validation of the ionic model for small EMFs

The number of isomers that we can construct rapidly increases from 1 single isomer for C_{26} to 271 for C_{50}.[11] For this reason, we decided to divide the whole family into two sets of structures, from C_{28} to C_{34} and from C_{36} to C_{50}. We used the first set of isomers to determine if the ionic model, widely accepted for middle and large sized fullerenes, is also valid for these smaller systems.[12, 13]

This first set of systems includes a total of 17 isomers: 2 for C_{28}, 3 for C_{30}, 6 for C_{32} and 6 for C_{34} (Table 1). All isomers were constructed and labeled following the spiral algorithm. The relative energies of the anions are essentially maintained for the endohedrals (table 6.1), showing the validity of the ionic model for such small EMFs as well. As we have already shown in a previous section for Ti@C_{28}, the $T_d(2)$-C_{28} is the most stable isomer for the neutral, tetraanionic, and endohedral species. As we have mentioned previously, the energy difference between the two C_{28} isomers increases from 17.5 kcal·mol^{-1} for the neutral cages to more than 50 kcal·mol^{-1} for tetraanions and EMFs. The $T_d(2)$-C_{28} cage has an optimal electronic structure to accommodate the 4 electrons formally transferred from the Ti atom to the carbon cage (figure 6.5). For the next larger cage formed by C_{28}+C_2, $C_{2v}(3)$-C_{30} is by far the lowest-energy isomer, around 17 and 20 kcal·mol^{-1} for the anion and endohedral systems, respectively. Upon further increasing cage size by sequential additions of C_2, the resulting C_{32} and C_{34} families show two isomers within a rather small range of energies. The lowest-energy Ti@C_{32} isomer is $D_3(6)$-C_{32} with $C_2(4)$-C_{32} only 4 kcal·mol^{-1} higher in energy. For C_{34}, the most stable system is $C_2(5)$-C_{34} with $C_s(2)$-C_{34} at almost 6 kcal·mol^{-1}.

Calculated molar fractions at different temperatures, within both (i) the rigid rotor and harmonic oscillator approximation (RRHO) and (ii) the free encapsulation model (FEM), applicable when the internal metal atoms are able to rotate freely inside the carbon cage, predict Ti@D_3(6)-C_{32} and Ti@C_2(5)-C_{34} to be the most abundant isomers for the whole range of temperatures.[14, 15] The most stable isomers at 0 K for Ti@C_{28} and Ti@C_{30} were also found to be the most abundant ones at any temperature.

Table 6.1 Relative energies, in kcal mol^{-1}, of the C_{2n} isomers (2n=28-34) for neutral, tetraanions and endohedral fullerenes. The lowest-energy EMFs are highlighted in bold. N_p: number of fused pentagons or [5,5] bonds.

Cage	Isomer	C_{2n}	C_{2n}^{4-}	Ti@C_{2n}	N_p[b)]
C_{28}	D_2 (1)	17.5	61.6	54.9	20
	T_d (2)	**0.0**	**0.0**	**0.0**	**18**
C_{30}	D_{5h} (1)	49.7	58.6	62.9	20
	C_{2v} (2)	2.6	17.6	20.1	18
	C_{2v} (3)	**0.0**	**0.0**	**0.0**	**17**
C_{32}	C_2 (1)	51.6	16.3	15.5	17
	D_2 (2)	62.5	39.4	35.1	18
	D_{3d} (3)	66.1	29.1	31.0	18
	C_2 (4)	24.5	1.8	4.0	16
	D_{3h} (5)	77.8	58.6	69.0	18
	D_3 (6)	**0.0**	**0.0**	**0.0**	**15**
C_{34}	C_2 (1)	73.9	51.5	51.7	17
	C_s (2)	25.4	4.6	5.9	15
	C_s (3)	30.8	25.6	28.6	15
	C_2 (4)	15.3	7.9	8.0	15
	C_2 (5)	**0.0**	**0.0**	**0.0**	**14**
	C_{3v} (6)	31.4	14.7	18.2	15

Small non-IPR EMFs behave differently than middle-size and large systems. Larger EMFs that host a metal ion or cluster typically exhibit a different isomer than when the cage is empty. However, for the small

Ti@C_{2n} systems, the hosting cage and the empty cage match. The so-called strain energy is the main factor that controls the relative stability in these systems. For this reason, those isomers with less structural tension, i.e. with less pentagon adjacencies, are the ones with the lowest energies. It is important to note that the formally transferred charge from the Ti atom to the carbon cage is preferentially located at the most strained regions, namely the [5,5] bonds and [5,5,5] junctions. Consequently, when encapsulated, the Ti ion prefers the most nucleophilic regions of the carbon cage, resulting in an off-center shift to maximize the interaction with these regions (figure 6.8). The energy difference between the Ti-centered and the Ti-shifted systems is not negligible: about 37 kcal·mol^{-1} for Ti@T_d(2)-C_{28}, 67 kcal mol^{-1} for Ti@C_{2v}(3)-C_{30}, 50 kcal mol^{-1} for Ti@D_3(6)-C_{32} and 60 kcal mol^{-1} for Ti@C_2(5)-C_{34}.

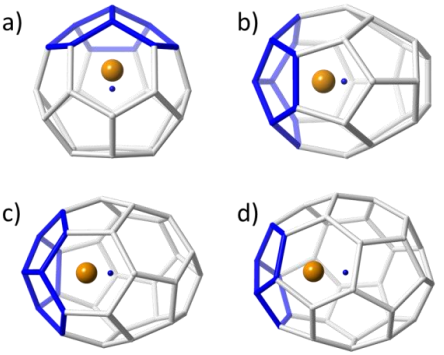

Figure 6.8 Ball and stick representations showing the displacement of the Ti atom form the center of the cage for (a) Ti@T_d(2)-C_{28}, (b) Ti@C_2(3)-C_{30}, (c) Ti@D_2(6)-C_{32} and, (d) Ti@C_2(5)-C_{34}. The nearest pentagons to the Ti atom are highlighted in blue.

6.3.3. Larger systems: Ti@C_{2n} (2n=36-50)

The results obtained for the C_{28}-C_{34} series clearly confirm the validity of the ionic model for small EMFs, as previously demonstrated for fullerenes with more than 60 atoms. When the number of carbon atoms increases, the number of isomers rapidly grows. For this second set of structures, the number of possible isomers is rather large (792), but still affordable to be computed at DFT BP86/TZP level.

For the lowest-energy tetraanions in a range of 30 kcal·mol^{-1}, an accurate exploration of the different possible positions of the Ti inside the cage was carried out to obtain the lowest-energy endohedral structures (table 6.2). Compared to the C_{28}-C_{34} series, this second set of structures is found to exhibit a larger number of isomers in a smaller range of energies. Different trends were found to correlate with increasing EMF size. For example, two isomers, $D_{2d}(14)$ and $D_{6h}(15)$, were found degenerate in energy for C_{36} as neutral and tetraanionic species. However, isomer $D_{2d}(14)$ was somewhat more favored when the Ti atom was encapsulated inside the cage (figure 6.9). For C_{38}, although the $C_2(17)$ empty neutral cage was by far the lowest-energy isomer, $C_2(13)$ was the most stable cage computed as tetraanion. For Ti@C_{38}, cages $C_2(10)$ and $C_2(17)$ became competitive in terms of energy. Analogous results were observed for C_{40}.

Table 6.2 Relative energies, in kcal mol^{-1}, of the C_{2n} isomers (2n=36-50) for neutral, tetraanions and endohedral fullerenes. The lowest-energy EMFs are highlighted in bold. N_p: number of fused pentagons or [5,5] bonds.

Cage	Isomer	C_{2n}	C_{2n}^{4-}	Ti@C_{2n}	N_p[b]
C_{36}	C_s (8)	23.0	13.6	2.0	14
	C_{2v} (9)	9.1	6.0	8.0	13
	C_2 (11)	12.8	10.2	5.3	13
	C_{2v} (12)	7.8	7.2	4.4	13
	D_{2d} (14)	**0.6**	**0.0**	**0.0**	**12**
	D_{6h} (15)[c]	0.0	0.0	4.3	12
C_{38}	**C_2 (10)**	**23.3**	**5.4**	**0.0**	**12**
	C_2 (13)	17.6	0.0	5.6	12
	C_1 (14)	24.3	7.4	6.7	12
	C_2 (17)	0.0	4.0	0.5	11
C_{40}	**C_s (24)**	**23.9**	**3.4**	**0.0**	**11**
	C_s (29)	16.7	5.4	6.0	11
	C_s (31)	14.6	3.5	3.0	11
	D_2 (38) [c]	0.0	0.0	11.2	10
	D_{5d} (39)	9.2	8.9	12.0	10
	T_d (40)	37.8	1.1	7.5	12
C_{42}	C_1 (32)	20.4	2.8	8.1	10
	C_1 (33)	**19.6**	**0.0**	**0.0**	**10**

	C_s (35)	23.3	6.9	4.5	10
	C_1 (39)	21.8	7.8	12.9	10
	D_3 (45)[c]	0.0	1.3	3.3	9
C_{44}	D_2 (75)	0.0	7.2	5.0	8
	D_2 (89)	**1.8**	**0.0**	**0.0**	**8**
C_{46}	C_3 (94)	27.5	9.9	5.5	9
	C_2 (109)	0.0	9.3	14.9	8
	C_1 (114)[c]	1.9	0.0	7.9	8
	C_3 (115)	22.9	9.9	12.0	9
	C_2 (116)	**2.5**	**0.9**	**0.0**	**8**
C_{48}	C_2 (171)	0.0	7.7	10.7	7
	C_1 (196)[c]	2.0	1.3	5.4	7
	C_s (197)	**6.2**	**3.6**	**0.0**	**7**
	C_2 (199)[c]	0.8	0.0	4.2	7
C_{50}	C_2 (260)	24.0	4.6	8.0	6
	C_2 (263)	10.5	7.2	11.7	6
	C_s (266)	**7.3**	**1.6**	**0.0**	**6**
	D_3 (270)	0.0	5.2	7.9	6
	D_{5h} (271)	2.1	0.0	5.5	5

[c]Isomers that become the most abundant at higher temperatures.

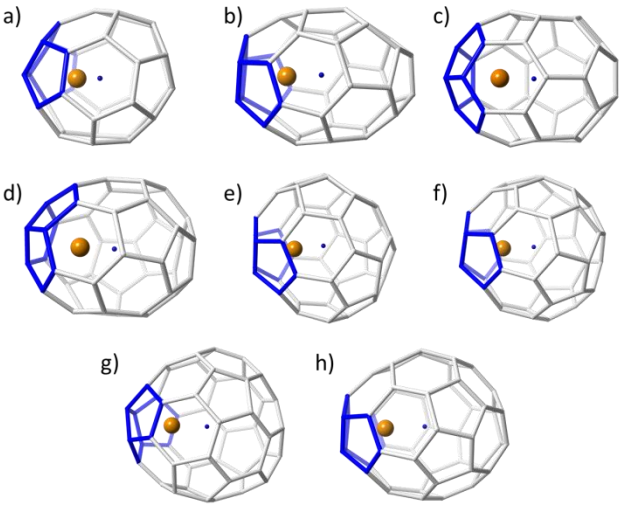

Figure 6.9 Ball and stick representations for the lowest-energy Ti@C_{2n} (2n=36-50): (a) D_{2d}(14)-C_{36}, (b) C_2(10)-C_{38}, (c) C_s(24)-C_{40}, (d) C_1(33)-C_{42}, (e) D_2(89)-C_{44}, (f) C_2(116)-C_{46}, (g) C_s(197)-C_{48}, and (h) C_s(266)-C_{50}.

The D_{5d}(39) cage was found to be the lowest-energy isomer, both in neutral and tetraanion states. The most stable endohedral in this family was, however, Ti@C_s(24)-C_{40}. Several isomers in a small range of energies were found as well for C_{42}. The D_3(45) neutral empty cage was clearly the lowest-energy isomer. However, for C_{42}^{4-} and Ti@C_{42} the cage C_1(33) was the most stabilized one. A different trend is observed in the case of C_{44}, where only two isomers are found to be candidates within a large range of relative energies. The two cages, D_2(75) and D_2(89), showed small relative energy differences as neutrals, tetraanions and EMFs. Isomer D_2(75) was the lowest-energy cage when the fullerene was computed as neutral, but isomer D_2(89) became the most favorable when computed as tetraanion and Ti@C_{44}. For C_{46}, we found again several isomers in a small range of relative energies. The neutral empty cages C_2(109), C_1(114) and C_2(116) showed similar energies. Two of them, C_1(114) and C_2(116), were almost degenerate as tetraanions, the latter leading to the lowest-energy Ti@C_{46}. Similar results were obtained for C_{48} and C_{50}. Isomers C_2(171)-C_{48} and C_2(199)-C_{48} were the lowest-energy empty cages, C_2(199) being favored in the tetraanionic state and C_s(197) as Ti@C_{48}. Finally, for C_{50}, there was again a change in the relative stability depending on the charge state of the system. The lowest-energy isomers were D_3(270) for neutral cages, D_{5h}(271) for tetraanions and C_s(266) for Ti@C_{50}.

To explain these changes in the relative stabilities between the neutral cages, the tetraanions and the endohedrals, different factors have to be considered. The strain energy, which is a trend-setting factor for the smallest systems, is not as important when the size of the cage increases.[2] Therefore, when the relative energies between isomers are small, the formal charge transfer and the interaction between the Ti atom and the carbon framework can reverse the relative stabilities of some isomers as occurs for larger metallofullerenes.

Because the relative energy between the endohedrals is rather small in many cases and they are synthesized at high temperatures, we have evaluated whether the effect of the temperature can reverse the stability of some isomers using the RRHO approximation and also the FEM model.

The Ti atom in Ti@C_{2n} systems is seen to move appreciably, but not freely inside the fullerene.[9] Therefore, the real behavior of these systems should be at any point in between the two RRHO and FEM approximations. Figure 6.10 shows the molar fractions (RRHO) of the most stable isomers for each Ti@C_{2n} family (2n = 36, 40, 42, 46, 48) in the temperature range up to 4000 K. Inversions in the isomer populations were found at around 1000 K or even below for cages C_{36}, C_{40}, C_{42} and C_{48}. For the rest of the cages, there were no inversions in the molar fractions, that is, the lowest-energy isomers at 0 K were predicted to be the most abundant species in the whole range of temperatures. Similar results were obtained when computing the molar fractions using the FEM model; the two most abundant isomers at T > 2000 K are predicted to be the same for almost all the families.

To sum up, whereas for smaller systems (2n < 36) the empty C_{2n} and endohedral Ti@C_{2n} match, when the number of carbon atoms increases, several isomers have similar stabilities and the most abundant EMFs are usually different from those predicted for the empty cages, as happens for fullerenes with more than 60 carbon atoms. The effect of the temperature was found relevant to predict the most abundant isomer for several Ti@C_{2n} families.

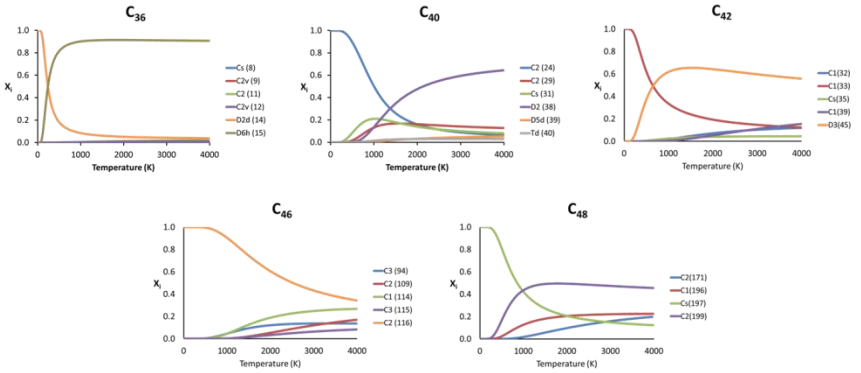

Figure 6.10 Representation of the molar fraction (x_i) for the competitive isomers of C_{36}, C_{40}, C_{42}, C_{46} and C_{48} families using the RRHO approximation.

6.3.4. Closed Network Growth mechanism (CNG)

The CNG mechanism is based on the insertion of a C_2 unit to one hexagonal ring to form two fused pentagonal rings, in line with that proposed by Endo and Kroto in the early nineties.[16] One consequence of this mechanism would be that the new fullerene does not obey the isolated pentagon rule, but fullerenes smaller than C_{60}, as analyzed in this work, cannot obey this rule. In addition, the number of fused pentagons is progressively reduced as small fullerenes grow by C_2 insertion (see last column in tables 61. and 6.2). According to the CNG formation of fullerenes, we propose a general mechanism for the growth of the cages from Ti@C_{26} to Ti@C_{48} based on successive C_2 ingestions, in analogy to that recently proposed by Zhao and Nagase for empty C_{2n} fullerenes,[17] based on the ideas of Fowler and Manolopoulos.[11] The growth mechanism, represented in figure 6.11, relates the most abundant isomers for each Ti@C_{2n} family from 2n = 26 to 2n=48 through simple C_2 insertions and, in some cases (only two), Stone-Wales (SW) rearrangements.

The first step, shown in figure 6.11, relates cages D_{3h}(1)-C_{26} and T_d(2)-C_{28}. Once the C_2 is ingested into the hexagon, two fused pentagons are formed (the new bond is remarked in red in figure 6.11). Next, insertion of an additional C_2 unit into the T_d(2)-C_{28} cage leads to the formation of C_{2v}(3)-C_{30}. Further growth proceeds by inserting C_2 molecules successively to give D_3(6)-C_{32}, C_2(5)-C_{34} and D_{2d}(14)-C_{36}, as for the hollow cages. This latter isomer is the second most abundant Ti@C_{36} after D_{6h}(15)-C_{36}. These two cages are intimately related by a single SW rearrangement (the bond that rotates is marked in green in figure 6.11). Although SW transformations show rather large free energy barriers, 111 kcal mol^{-1} (4.8 eV) in the present case, they might be easily overcome at T > 1000 K. Moreover, previous theoretical and experimental reports find for hollow C_{60} that such rearrangements could be carbon-catalyzed leading to atom exchange.[5, 18, 19] For Ti@C_{36}, the free energy barrier for the carbon-catalyzed transformation between cages D_{2d}(14)-C_{36} and D_{6h}(15)-C_{36} drops significantly to only 36 kcal mol^{-1} (1.6 eV). Thus, carbon-catalyzed

bond rearrangements could be a process involved in metallofullerene formation. It is important to remark here that the two cages D_{2d}(14)-C_{36} and D_{6h}(15)-C_{36} yield, after C_2 insertion, the most abundant Ti@C_2(17)-C_{38} isomer. Ti@D_2(38)-C_{40} is then obtained and would evolve to Ti@D_3(45)-C_{42}, the most abundant Ti@C_{42} isomer, after successive C_2 ingestions. That specie then grows to Ti@D_2(75)-C_{44}, which is the second most stable Ti@C_{44} isomer, but with almost zero molar fraction for the full range of temperatures compared to the most abundant Ti@D_2-C_{44}(89). An alternative formation path to reach Ti@D_2-C_{44}(89) is through the Ti@C_1-C_{42}(33) precursor, formed by SW rearrangement of the initially formed Ti@D_3-C_{42}(45) species. C_2 insertions into Ti@D_2-C_{44}(89) and Ti@D_2-C_{44}(75) lead to Ti@C_1-C_{46}(114) and Ti@C_2-C_{46}(109), respectively, which are among the most abundant Ti@C_{46} isomers at high temperatures, and are also related by a SW transformation. Additionally, Ti@C_1-C_{46}(114) is related to the most abundant Ti@C_2-C_{46}(116) isomer by a single SW rearrangement. Finally, the two most abundant Ti@C_{48} isomers, Ti@C_1-C_{48}(196) and Ti@C_2-C_{48}(199), are formed by direct C_2 insertion into these Ti@C_{46} isomers. Therefore, the present mechanistic proposal relates the most abundant isomers of the Ti@C_{2n} series (2n = 26-48) by successive C_2 insertions and a few number of SW rearrangements, in line with the CNG mechanism. It is worth remarking that the energy barriers for the different steps of the CNG mechanism were found to be accessible at temperatures of fullerene formation.[9]

Figure 6.11 Schlegel diagrams connecting the most abundant isomers of each Ti@C_{2n} family. The hexagons where C2 inserts are highlighted in yellow, the formed C-C bonds are highlighted in red, and the bonds that rearrange (Stone-Wales) are in green.

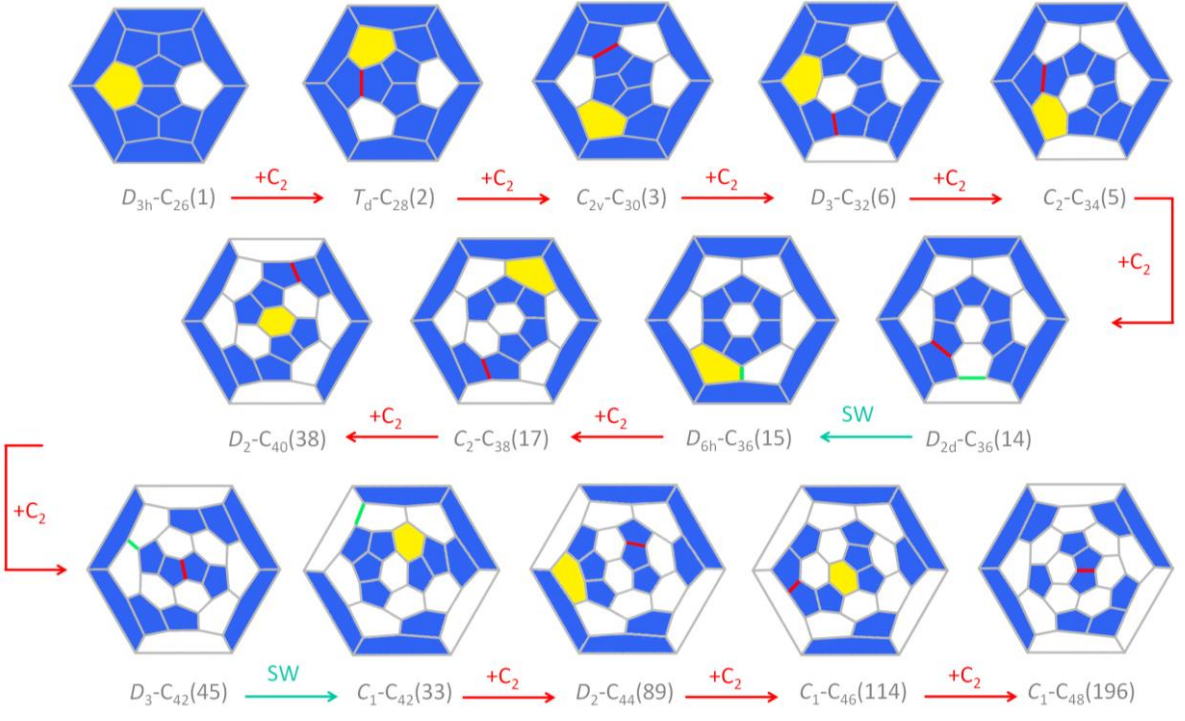

6.4. Study of the growth for other M@C_{2n}

After the extensive study of the Ti@C_{2n} family, further experiments with other metals were performed in order to give more insight into the metallofullerene formation mechanism and the factors that govern the formation and stabilization of these species. Using the same experimental techniques and set up that were established before for the successful synthesis and detection of the titanium endohedral fullerenes, a large number of elements of the periodic table were studied.[20]

All group I-IV metals, lanthanides and actinides are found to form M@C_{2n} from evaporated metal-doped graphite, except for Li, Be, and Mg under the present conditions. It is worth noting that the formation of $Li^+@C_{60}^-$ by the ion implantation in the pre-existing carbon cage has been reported very recently.[21] All other transition metals do not form EMFs from graphite in detectable abundance under the present conditions. Surprisingly, Ga and In are observed to be encapsulated in carbon cages.

If we observe the experimental detected species summarized in figure 6.12, we can clearly recognize a different behavior depending on the metal group. When metals from the group I are trapped, transferring one electron to the cage, the formation of M@C_{60} and M@C_{70} is favored. For the divalent species trapped in carbon cages, metals of group II and divalent lanthanides, the most abundant metallofullerenes are found to be M@C_{50} and M@C_{60}. The encapsulation of species that formally transfer three electrons to the carbon cages, group III metals and trivalent lanthanides, is found to favor the formation of M@C_{44} and M@C_{50} and, as we have already shown for the Ti@C_{2n}, when four electrons are transferred, the most abundant metallofullerenes detected are M@C_{28} and M@C_{44}. Therefore, as more negative charge is progressively transferred to the carbon cage ($M^+@C_{2n}^-$, $M^{2+}@C_{2n}^{2-}$, $M^{3+}@C_{2n}^{3-}$ and $M^{4+}@C_{2n}^{4-}$), smaller cages become highly stabilized. The main reason is that the negative charge is preferentially located at the pentagons, [5,5] bonds and [5,5,5] junctions (in directly triple-fused pentagons).[10] Consequently, charge

transfer stabilizes highly pyramidalized C atoms induced by pentagon adjacencies in cages that do not obey the IPR rule. In other words, larger charge transfers are needed to stabilize the energy penalty and the strain induced by the pentagon adjacencies for the smaller species. Thus, the charge transfer is found to be the driven force in the stabilization of larger or smaller species in the synthesis of monometallofullerenes.

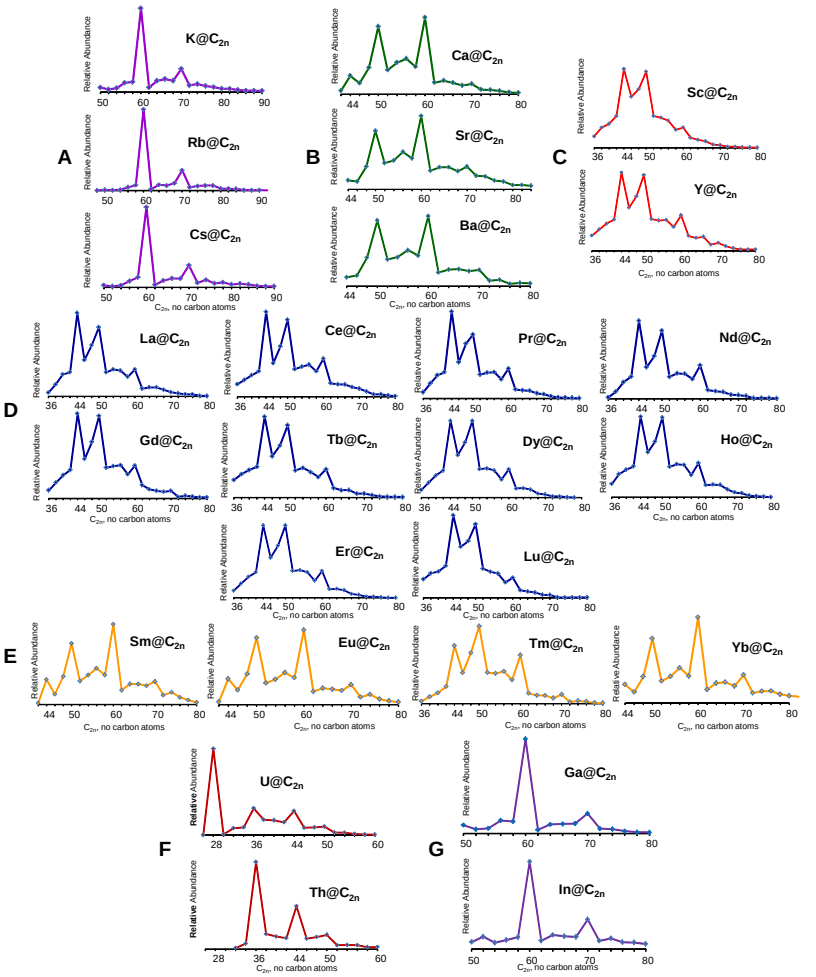

Figure 6.12 M@C2n formation trends for group I (a), group II (b), group III (c), trivalent lanthanides (d), divalent lanthanides (e), actinides (f), Ga and In (g).

Curious formation behavior is observed for actinide-containing EMFs. Uranium is known to form U@T_d(2)-C_{28}, the same structure studied for Ti@C_{28}, which is stabilized by transfer of four electrons to the cage.[8, 22] Accordingly, it was predicted that thorium should exhibit similar behavior because its primary oxidation state is Th^{4+}. Interestingly, Th@C_{28} is not observed; however, Th@C_{36} is the most abundant isomer for this family detected (figure 6.12). That observation is likely due to the larger ionic radius of Th^{4+} relative to U^{4+}. The smallest cage that the Th^{4+} can effectively nucleate must be greater that C_{28} and in this case is C_{36}. The distribution of the Th@C_{2n} mimics U@C_{2n} formation beyond C_{36}, which can be explained by a decrease in the effect of the radii when the size of the cage increases. These results indicate that the ionic radius is also an important factor for the smallest cages and when the same amount of charge is transferred to the cage.

On the other hand, very similar ionic radii exist for encapsulated elements such as Na^+ (1.02 Å), Ca^{2+} (1.00 Å), and Ce^{3+} (1.01 Å). In these cases, although the metals show similar radii, the favored cages are different due to the different amount of charge transferred.

Therefore, the charge transfer is found to be the determinant driven force for the stabilization of different-sized endohedral metallofullerenes, and the ionic radii would only be determinant for the smallest cages.

6.4.1. Computational study: the Ca@C_{2n} family

In order to identify the lowest-energy isomers and to understand the formation distribution of the divalent metallofullerenes, all possible isomers for dianions, C_{2n}^{2-}, and Ca@C_{2n} endohedral fullerenes were computed from C_{42} to C_{60}, as done before for the tetravalent systems, Ti@C_{2n}. Among all the different metals that have been reported to be trapped forming metallofullerenes, carbon cages that encapsulate such divalent cations are advantageous for computational analysis because of the closed shell nature of their ground states. The relative energies of the lowest-energy isomers are listed in table 6.3. We found that the relative

energies of the empty cage dianions and the $Ca@C_{2n}$ follow the same trends, and therefore, the ionic model is also applicable to Ca-encapsulated EMFs.

Table 6.3 Relative energies of the C_{2n} isomers (2n=42-58) for neutral, dianions and endohedral metallofullerenes computed at BP86/TZP level of theory.[a]

Cage		C_{2n}	C_{2n}^{2-}	$Ca@C_{2n}$	Cage		C_{2n}	C_{2n}^{2-}	$Ca@C_{2n}$
C_{42}	32	20.4	15.6	18.7	C_{50}	264	18.4	19.1	16.8
	33	19.6	14.5	15.6		266	7.3	16.4	13.1
	35	23.3	7.9	6.7		270	0.0	17.9	26.8
	39	21.8	15.5	18.3		**271**	**2.1**	**0.0**	**0.0**
	45	**0.0**	**0.0**	**0.0**	C_{52}	421	20.8	18.3	18.2
C_{44}	55	12.2	21.9	21.0		**422**	**0.0**	**0.0**	**0.0**
	69	16.7	15.0	14.1		436	10.1	15.6	15.7
	72	5.2	17.2	26.4	C_{54}	537	11.1	19.4	23.0
	75	0.0	0.0	0.0		**540**	**0.0**	**0.0**	**0.0**
	89	1.8	1.0	0.3		541	12.0	17.6	16.8
	55	**12.2**	**21.9**	**21.0**	C_{56}	836	24.6	15.0	19.5
C_{46}	99	3.6	17.9	19.3		843	3.4	2.0	6.0
	103	1.8	7.8	8.9		864	0.0	6.2	7.3
	108	**2.1**	**2.8**	**0.0**		**913**	**3.1**	**0.5**	**0.0**
	109	0.0	0.0	4.4		916	1.0	0.0	4.1
	114	1.9	7.3	8.3		919	28.4	11.6	19.8
	116	2.5	6.4	8.8		920	25.2	17.0	23.5
C_{48}	138	10.2	23.4	25.7	C_{58}	1195	18.9	18.3	20.6
	171	0.0	14.2	13.4		1196	17.3	19.0	18.5
	196	2.0	5.6	5.4		1198	16.5	22.3	20.7
	197	6.2	23.0	20.9		**1205**	**0.0**	**0.0**	**0.0**
	199	**0.8**	**0.0**	**0.0**					

[a]Relative energies in kcal mol^{-1}. Isomers labeled following the spiral algorithm of Fowler and Manolopoulos.

It is worth mentioning that, as we found in the case of the tetravalent $Ti@C_{2n}$, the metal atoms are found to be shifted off center, leading to an extra stabilization due to the interaction with the nucleophilic regions of the cages. Moreover, the most stable $Ca@C_{2n}$ and C_{2n}^{2-} match the least-strained, lowest-energy empty cages an thus, although smaller EMF systems are described by charge transfer from the metal to cage, strain is playing an important role in establishing the relative stability of isomers for a particular cage size.

6.4.2 New elements trapped in carbon cages

Gallium and Indium are new elements discovered to incorporate in cages. Based on observed formation distributions (figure 6.13), they are predicted to be uncommon Ga^+ and In^+, instead of exhibiting the common 3+ oxidation state.

This prediction is based on the close similarity of the experimental distribution for the Ga and In with respect to those from the group I elements. We corroborated the oxidation state of the Ga in $Ga@C_{60}$ by means of DFT calculations. As it is shown in the molecular orbital interaction diagram (figure 6.13), one single electron form the 4p atomic orbital of the Ga is transferred to the LUMO of the carbon cage. Thus, in future cases the oxidation states of the metal atoms can be predicted from the experimental distributions.

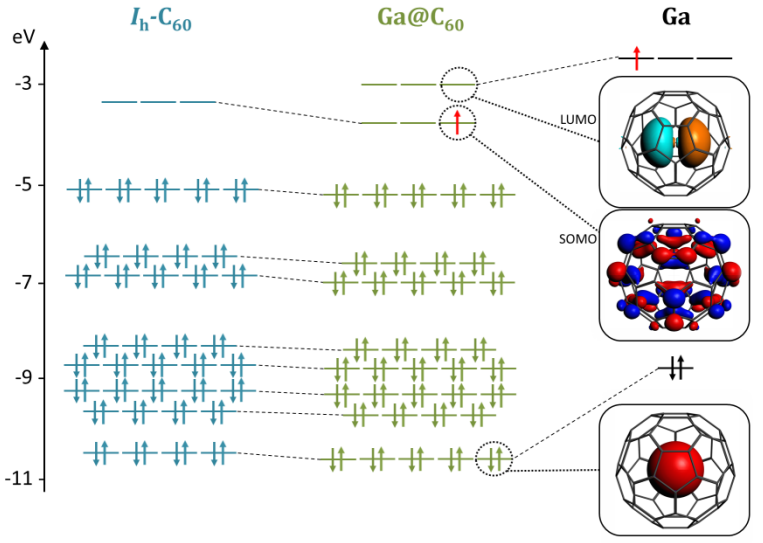

Figure 6.13 Orbital interactions for $Ga@C_{60}$ (green), empty C_{60} (blue), and Ga (black). One electron is formally transferred from the 4p orbital of Ga to a molecular orbital localized on the carbon framework of the $Ga@C_{60}$ endohedral. Orbital labels are omitted for clarity.

6.5. Predicting the experimental relative abundances

At this point, we have already studied and proposed our candidates for each of those families. After this part of the work, we wanted to explain the relative abundances showed in the experimental mass spectrum.

As done previously by Popov and co-workers to explain the relative abundances of the $M_3N@C_{2n}$ (2n=68-98) systems, to compare the energies of the fullerenes of different sizes, the absolute energies were normalized to the number of atoms in the given fullerene. Figure 6.14 plots the normalized energies of the most stable C_{2n}^{4-} isomers versus the number of atoms. The smooth decay observed can be perfectly fitted by an exponential decay. This trend is due to the decrease of the curvature of the cage with the increase of the size, and the decrease of the Coulomb repulsion as the cage size increases. As it is shown in the figure 6.14, cages T_d-C_{28}(2) and D_2-C_{44}(89) showed deviations of -24.3 and -17.3 kcal·mol^{-1}, respectively, with respect to the general behavior, i.e. fitted line in figure 6.14, confirming the enhanced stability of these two isomers. The same behavior was observed for the endohedral metallofullerenes. In this case, deviations of -15.8 and -11.5 kcal·mol^{-1} were found for Ti@T_d-C_{28}(2) and Ti@D_2-C_{44}(89) respectively.

On the other hand we followed the same procedure in order to rationalize the relative abundance in the mass spectra for the $Ca@C_{2n}$ family. In this particular case, cages D_{5h}(271)-C_{50} and I_h(1812)-C_{60} showed deviations of -15.2 and -21.6 kcal·mol^{-1}, respectively, for the dianions confirming the special stability of this two structures among all cage sizes. The same trend was observed for the Ca endohedral metallofullerenes, which showed deviations of -11.2 and -14.8 kcal·mol^{-1}, respectively.

These results plenty agree with the experimental FT-ICR mass spectrum obtained by Kroto and co-workers where the highest intensities for the $Ti@C_{2n}$ corresponded to $Ti@C_{28}$ and $Ti@C_{44}$ and for the $Ca@C_{2n}$ corresponded to $Ca@C_{50}$ and $Ca@C_{60}$.

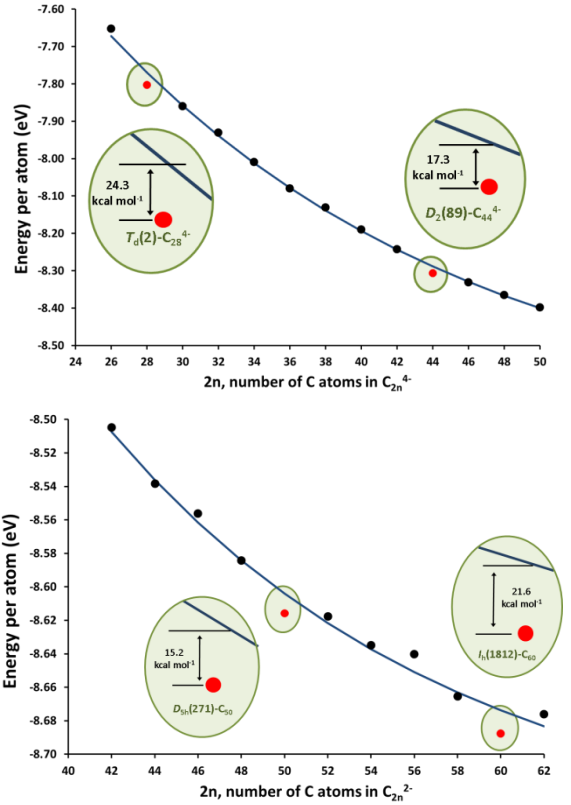

Figure 6.14 (top) Energy per atom, in eV, of the lowest-energy C_{2n}^{4-} structures (2n=26-50), black dots; and their fit to an exponential decay function, blue line. The energies for the $T_d(2)$-C_{28} and $D_2(89)$-C_{44} tetraanions are shown as red dots. The insets show the extra stability of these two isomers. (bottom) Energy per atom, in eV, of the lowest-energy C_{2n}^{2-} structures (2n=42-62), black dots; and their fit to an exponential decay function, blue line. The energies for the $D_{5h}(271)$-C_{50} and $I_h(1812)$-C_{60} tetraanions are shown as red dots. The insets show the extra stability of these two isomers.

Finally, we also wanted to understand if the signals reported from the detection of the corresponding species were purely due to their abundances or if the ionization potentials are biasing the results. This could be an important issue considering the ionization process that takes place in the mass spectrometry. We have computed the ionization potentials (IPs) for all the endohedral species in the Ca@C_{2n} (2n=42-60)

and Ti@C_{2n} (2n=26-50) families to check whether the intensities in the mass spectra might be biased by the IPs.

As shown in figure 6.15, the IPs are not found to be correlated to the signal intensities. The most abundant fullerenes, depicted as red points in figure 6.15, do not show the smallest IPs for any of the two Ca@C_{2n} (2n=42-60) or Ti@C_{2n} (2n=26-50) families. Only Ca@C_{60} shows a small IP, which can be easy rationalized taking into account that the orbitals where the oxidation takes place are rather high in energy (the LUMO in the neutral C_{60}). However, in the experiments, Ca@C_{50} and Ca@C_{60} show comparable intensities, and contrarily they have very different IPs. Therefore, these results support that abundances/intensities are not (significantly) biased by IPs.

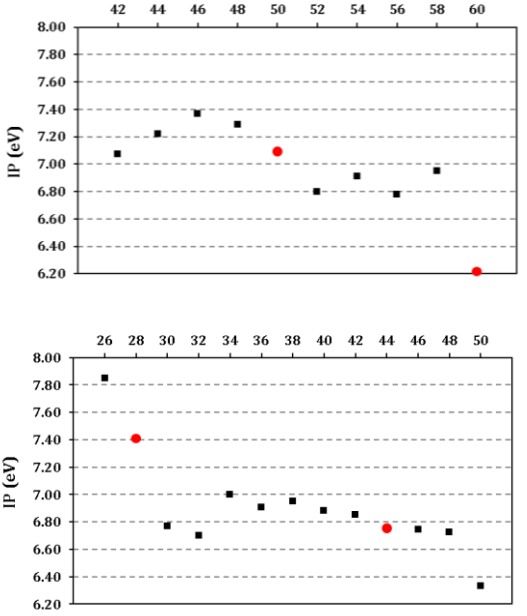

Figure 6.15 Computed ionization potentials, in eV, for the lowest-energy isomers of the Ca@C_{2n} (2n=42-60) (top) and Ti@C_{2n} (2n=26-50) families (bottom). Red points correspond to the endohedrals that show the most intense signals in the mass spectra. No correlation between the IPs and the signal intensities (abundances) is found.

6.6. Conclusions

After the comprehensive exploration of the most favorable isomers and the combination of the experimental evidences along with the computational results, we can conclude that (i) the ionic model, widely accepted for larger fullerenes, is also valid for these smaller and more strained systems; (ii) in contrast to larger EMFs (2n>60), in which the empty cage is different from the optimal metallofullerene cage, non-IPR small endohedral fullerenes encapsulating a tetravalent ion often exhibit the same cage as empty fullerenes. Small metallofullerenes are well described by the ionic model, in these systems, the strain energy should dominate over electronic repulsion, in contrast to larger, less strained EMFs; (iii) the most abundant Ti@C_{2n} isomers are formally linked by direct C_2 insertions, and only in two cases by additional Stone-Wales transformations; (iv) endohedral Ti@C_{28} forms in carbon vapor as the smallest stable endohedral metallofullerene. The endohedral structure of the whole family was confirmed by means of collision-induced dissociation (CID) experiments; (v) the transferred negative charge is found to be located at the pentalene bonds and the [5,5,5] junctions; (vi) Ti atom is found to be shifted off the center of the cage, in order to interact with the nucleophilic regions of the cage, giving an extra stabilization; and (vii) the higher relative abundance of Ti@C_{28} and Ti@C_{44} can be explained by the special electronic properties of these cages and their higher relative stabilities with respect to the other systems.

Further studies including a large number of the elements of the periodic table was carried out leading to important conclusions: (i) charge transfer from the metal to the cages is found to be a driven force in the stabilization of metallofullerenes; (ii) the more charge is transferred, the smaller the fullerene favored, this is due to the localization of the charge on the most pyramidalized atoms, which favors the stabilization of more strained and smaller cages; (iii) ionic radii is important for the smallest cages as shown in the case of the encapsulation of tetravalent metals; (iv) Ga and In were reported to form endofullerenes for the first time, this

metals show uncommon Ga^+ and In^+ when encapsulated, which was corroborated by comparison with the group I metals distributions and by means of DFT calculations; (vi) from the computational study of both families, $Ti@C_{2n}$ and $Ca@C_{2n}$, the special stability of $Ti@C_{28}$, $Ti@C_{44}$ and $Ca@C_{50}$ and $Ca@C_{60}$ was rationalized; and (vii) the computed ionization potentials of these species show that the abundances are not directed by the IPs.

6.7. References

1. H. W. Kroto, J. R. Heath, S. C. Obrien, R. F. Curl and R. E. Smalley, *Nature*, 1985, **318**, 162-163.
2. H. W. Kroto, *Nature*, 1987, **329**, 529-531.
3. T. Krenke, M. Acet, E. F. Wassermann, X. Moya, L. Mañosa and A. Planes, *Phys. Rev. B*, 2005, **72**, 014412.
4. T. Stauber, N. M. R. Peres and F. Guinea, *Phys. Rev. B*, 2007, **76**, 205423.
5. P. W. Dunk, N. K. Kaiser, C. L. Hendrickson, J. P. Quinn, C. P. Ewels, Y. Nakanishi, Y. Sasaki, H. Shinohara, A. G. Marshall and H. W. Kroto, *Nat. Commun.*, 2012, **3**, 855-863.
6. I. J. Amster, *J. Mass Spectrom.*, 1996, **31**, 1325-1337.
7. A. G. Marshall, C. L. Hendrickson and G. S. Jackson, *Mass Spectrom. Rev.*, 1998, **17**, 1-35.
8. P. Dunk, N. Kaiser, M. Mulet-Gas, A. Rodríguez-Fortea, J. Poblet, H. Shinohara, C. Hendrickson, A. Marshall and H. Kroto, *J. Am. Chem. Soc.*, 2012, **134**, 9380-9389.
9. M. Mulet-Gas, L. Abella, P. W. Dunk, A. Rodríguez-Fortea, H. W. Kroto and J. M. Poblet, *Chem. Sci.*, 2014, (Accepted).
10. A. Rodriguez-Fortea, N. Alegret, A. L. Balch and J. M. Poblet, *Nature Chem.*, 2010, **2**, 955-961.
11. P. W. Fowler and D. E. Manolopoulos, *An Atlas of Fullerenes*, Oxford University Press, Oxford, 1995.
12. J. M. Campanera, C. Bo and J. M. Poblet, *Angew. Chem. Int. Ed*, 2005, **44**, 7230-7233.
13. A. A. Popov and L. Dunsch, *J. Am. Chem. Soc.*, 2007, **129**, 11835-11849.
14. Z. Slanina and S. Nagase, *ChemPhysChem*, 2005, **6**, 2060-2063.
15. X. Zhao, Z. Slanina, H. Goto and E. Osawa, *J. Chem. Phys.*, 2003, **118**, 10534.
16. M. Endo and H. W. Kroto, *J. Phys. Chem.*, 1992, **96**, 6941-6944.
17. J.-S. Dang, W.-W. Wang, J.-J. Zheng, X. Zhao, E. Ōsawa and S. Nagase, *J. Phys. Chem. C*, 2012, **116**, 16233-16239.
18. B. R. Eggen, M. I. Heggie, G. Jungnickel, C. D. Latham, R. Jones and P. R. Briddon, *Science*, 1996, **272**, 87.
19. C. P. Ewels, M. I. Heggie and P. R. Briddon, *Chem. Phys. Lett.*, 2002, **351**, 178-182.
20. P. W. Dunk, M. Mulet-Gas, Y. Nakanishi, N. K. Kaiser, A. Rodríguez-Fortea, H. Shinohara, J. M. Poblet, A. G. Marshall and H. W. Kroto, *Nat. Commun.*, 2014, (Accepted).
21. S. Aoyagi, E. Nishibori, H. Sawa, K. Sugimoto, M. Takata, Y. Miyata, R. Kitaura, H. Shinohara, H. Okada, T. Sakai, Y. Ono, K. Kawachi, K.

Yokoo, S. Ono, K. Omote, Y. Kasama, S. Ishikawa, T. Komuro and H. Tobita, *Nat Chem*, 2010, **2**, 678-683.

22. T. Guo, M. Diener, Y. Chai, M. Alford, R. Haufler, S. McClure, T. Ohno, J. Weaver, G. Scuseria and R. Smalley, *Science* 1992, **257**, 1661-1664.

UNIVERSITAT ROVIRA I VIRGILI
COMPUTATIONS ON ENDOHEDRAL METALLOFULLERENES: CHARACTERIZATION, PROPERTIES AND GROWTH.
Marc Mulet Gas
Dipòsit Legal: T 1604-2015

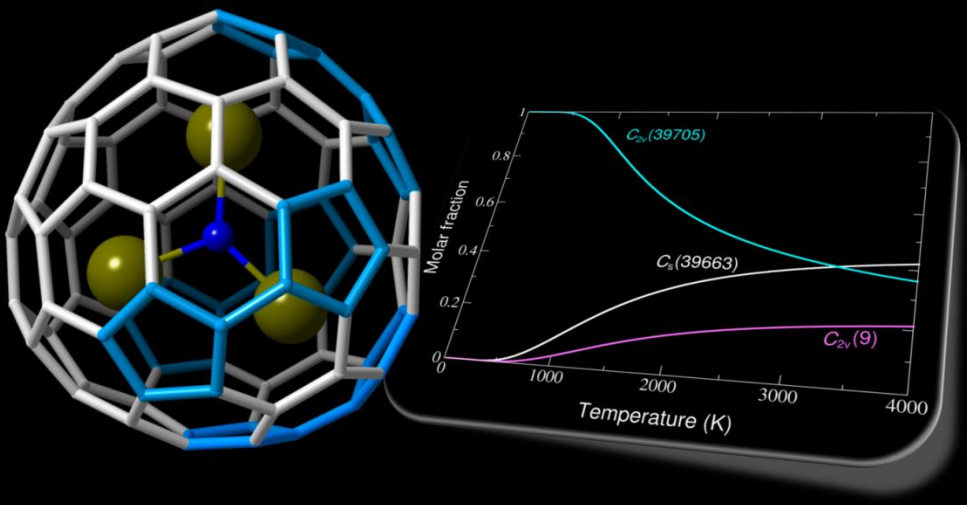

Chapter 7 // ***Relevance of Thermal Effects in the Formation of Metallofullerenes: the Case of $Gd_3N@C_s(39663)$-C_{82} and Other Related Structures***

Related Publications:

Relevance of Thermal Effects in the Formation of Endohedral Metallofullerenes: the Case of $Gd_3N@C_s(39663)$-C_{82} and Other Related Systems

M. Mulet-Gas, A. Rodríguez-Fortea, L. Echegoyen and J. M. Poblet. *Inorganic Chemistry*, **2013**, 52, 1954-1959.

Chapter 7

Relevance of Thermal Effects in the Formation of Metallofullerenes: the Case of $Gd_3N@C_s(39663)$-C_{82} and Other Related Systems

In this chapter we show that thermal contributions to the free energy have to be taken into account to rationalize the formation of $Gd_3N@C_s(39663)$-C_{82}, a nitride endohedral metallofullerene that possesses a carbon cage with two fused pentagons, which is not predicted to have the lowest electronic energy among the C_{82} isomers.

7.1. Introduction

The simple rules derived from the ionic model and the topological properties of the cages are able to explain the relative stabilities and abundances of a large number of endohedral metallofullerenes.[1, 2] However, the electronic energies at 0 K cannot justify the experimental results for other EMFs. Slanina and co-workers demonstrated that the Gibbs energy has to be taken into account to incorporate the effect of the high temperatures that are reached in the reactor during the synthesis of fullerenes.[3, 4] Recently, our group showed that the oxide EMF $Sc_2O@C_s(6)$-C_{82} is the first example in which the relevance of the thermal and entropic contributions to the stability of the fullerene isomer has been confirmed through the characterization of the X-ray structure.[5] The other scandium oxide cluster fullerene, $Sc_2O@C_{3v}(8)$-C_{82}, is predicted to be the most abundant product at low temperatures, but $Sc_2O@C_s(6)$-C_{82} is more favored when thermal effects are taken into account and becomes the most abundant species at higher temperatures (above 1200 K). Analogous studies with the $C_s(6)$, $C_{3v}(8)$ and $C_{2v}(9)$ isomers of $Sc_2S@C_{82}$ confirmed the fact that both $C_s(6)$ and $C_{3v}(8)$ cages are observed.[6]

Similar results are also predicted for empty fullerenes. For instance, Slanina found that while the lowest-energy IPR isomer for C_{80} is $D_{5d}(1)$, at synthetic conditions the $D_2(2)$ isomer is the most abundant one, as confirmed later by NMR experiments.

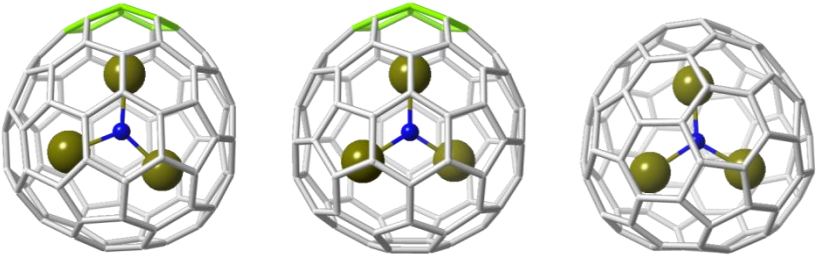

$Gd_3N@C_s(39663)$-C_{82} $Gd_3N@C_{2v}(39705)$-C_{82} $Gd_3N@C_{2v}(9)$-C_{82}

Figure 7.1 Structures of the three isomers of $Gd_3N@C_{82}$, with the non-IPR $C_s(39663)$-C_{82} (a), the non-IPR $C_{2v}(39705)$-C_{82} (b) and the IPR $C_{2v}(9)$-C_{82} (c) cages. The pentalene unit in the two non-IPR structures is highlighted in black.

Recently, X-ray diffraction experiments have unambiguously shown that the carbon cage in $Gd_3N@C_{82}$ is the egg-shaped non-IPR C_s(39663)-C_{82} isomer (figure 7.1),[7] which is neither the lowest-energy hexaanion nor gives the most stable nitride EMF for M = Sc and Y, as shown by the computations of Popov and Dunsch.[2] We herein study the different isomers of $Gd_3N@C_{82}$ to assess the relevance of thermal contributions to their relative stabilities to understand why $Gd_3N@C_s$(39663)-C_{82} is the cage experimentally observed. We also analyze the relationship between C_s(39663)-C_{82} and other IPR and non-IPR cages that encapsulate metal clusters of the C_{80}, C_{82} and C_{84} families.

7.2. Results and discussion

We have computed the free energies using the rigid rotor and harmonic oscillator approximation (RRHO) at different temperatures as well as their molar fractions derived from the free-energy calculations as done by Slanina and co-workers.[8] We have analyzed three isomers of $Gd_3N@C_{82}$, the non-IPR C_s(39663)-C_{82} and C_{2v}(39705)-C_{82}, and the IPR C_{2v}(9)-C_{82} cages, which are the three lowest-energy structures predicted by Popov and Dunsch for $Y_3N@C_{82}$,[2] a system that has been shown to be a good model for $Gd_3N@C_{82}$.[9] Isomer $Gd_3N@C_{2v}$(39705)-C_{82} has the lowest energy at 0 K, with a difference of 6.2 and 8.0 kcal mol^{-1} (BP86/TZP) compared to $Gd_3N@C_s$(39663)-C_{82} and $Gd_3N@C_{2v}$(9)-C_{82}, respectively. The contribution of the zero-point energy vibrational correction to the relative stabilities is not very important (table 7.1, second row). The C_{2v}(39705)-C_{82} isomer is the most stable EMF even when the thermal and entropic effects are taken into account within the RRHO approximation. A modified treatment based on the idea that the encapsulated cluster can exercise large amplitude motions, especially at high temperatures, was also used. Within this approximation, called the free, fluctuating or floating encapsulated model (FEM),[5, 6, 10] which better reproduces the experimental results, the stability of the $Gd_3N@C_s$(39663)-C_{82} isomer increases at high

temperatures, becoming the most abundant isomer at around 3400 K (see table 7.1 and figure 7.2). Although the predicted crossing temperature for the predominance of $Gd_3N@C_s(39663)$-C_{82} is somewhat high, the important result is that the experimentally observed $Gd_3N@C_s(39663)$-C_{82} is the favored isomer at high temperatures. The use of other density functionals, for instance those that include the exact exchange or additional dispersion corrections, to optimize the geometries and/or to compute the frequencies may provide lower crossing temperatures, in better agreement with experiments than the BP86/TZP results, but probably with the same qualitative information predicted here, i.e. the inclusion of thermal effects are compulsory to understand the formation of $Gd_3N@C_s(39663)$-C_{82}, which is the favored isomer at high temperatures.

Table 7.1 Relative stabilities, in kcal mol^{-1}, for the three isomers of $Gd_3N@C_{82}$. The FEM model is considered to compute the free energies.

	$C_s(39663)$	$C_{2v}(39705)$	$C_{2v}(9)$
ΔE (0 K)	6.2	0.0	8.0
ΔH (0 K)	6.1	0.0	7.3
ΔG (1000 K)	4.4	0.0	7.1
ΔG (2000 K)	2.6	0.0	6.4
ΔG (3000 K)	0.8	0.0	5.6
ΔG (4000 K)	−1.0	0.0	4.9

We have also estimated the relative energies at 0 K, ΔE (0K), between the two lowest-energy isomers using other density functionals (table 7.2). The revPBE functional,[11] also of the GGA type, leads to the same energy difference as BP86. The energy difference is somewhat larger (6.9 kcal mol^{-1}) when the hybrid B3LYP functional is used.[12] However, when including the dispersion corrections to the BP86 functional according to the D3 method by Grimme, the difference is slightly reduced to 6.0 kcal·mol^{-1}.[13] Moreover, we have computed the frequencies at the B3LYP level for the model compounds $Y_3N@C_s(39663)$-C_{82} and $Y_3N@C_{2v}(39705)$-C_{82}.

Table 7.2 Relative energies, in kcal mol^{-1}, of $Gd_3N@C_s(39663)$-C_{82} with respect to $C_{2v}(39705)$-C_{82} at 0 K computed using different density functionals.

	$C_s(39663)$	$C_{2v}(39705)$
BP86	6.2	0.0
revPBE	6.2	0.0
B3LYP [a]	6.9	0.0
BP86-D3	6.0	0.0

[a] Single-point energy calculation on the BP86/TZP geometry.

We have made this approximation due to the difficulties, in terms of convergence and computational cost, to obtain the frequencies at this level for the Gd endohedral fullerenes. Although one could argue that Gd (157.25) is much heavier than Y (88.91) and hence vibrational frequencies of $Gd_3N@C_{82}$ involving metal atoms must be lower than those in $Y_3N@C_{82}$, we have checked that this approximation is totally valid. The main reason is that most of the normal modes of vibration that involve metal atoms, which show the lowest frequencies, are not taken into consideration within the FEM approximation. Moreover, the stretching M−N frequencies, with larger values, are almost identical in the two isomers, $Y_3N@C_s(39663)$-C_{82} and $Y_3N@C_{2v}(39705)$-C_{82}, so their contributions to the corresponding partition functions is identical and they cancel out in the computation of the predicted molar fraction as a function of temperature. Furthermore, we have checked the validity of our approximation computing the vibrational frequencies for the $Gd_3N@C_{82}$ systems from the hessian computed for $Y_3N@C_{82}$ and correcting the mass of Y (88.91) with the mass of Gd (157.25). The crossing point for the molar fractions of the two isomers is essentially the same (0.3% difference), as expected.

The predictions for the molar fractions of $Gd_3N@C_s(39663)$-C_{82} and $Gd_3N@C_{2v}(39705)$-C_{82} using the frequencies computed for the Y models at the abovementioned computational level combined with the energy difference obtained with BP86/TZP (6.2 kcal mol^{-1}) and with BP86-D3/TZP (6.0 kcal mol^{-1}) decreases the crossing temperature to 3090 and 2990 K, respectively.

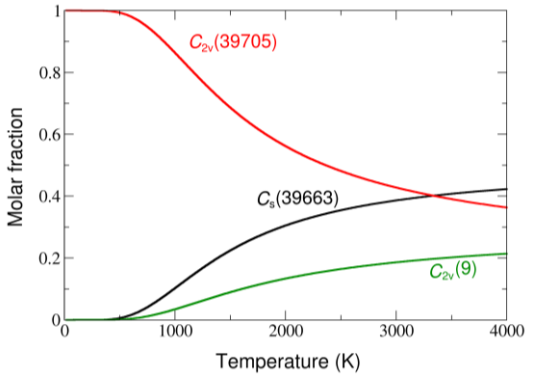

Figure 7.2 Plot of the computed molar fractions within the FEM model for $Gd_3N@C_s(39663)$-C_{82}, $Gd_3N@C_{2v}(39705)$-C_{82} and $Gd_3N@C_{2v}(9)$-C_{82} isomers.

At this point, it is worth remarking the structural resemblance that the two lowest-energy non-IPR $C_s(39663)$-C_{82} and $C_{2v}(39705)$-C_{82} cages show. The two structures are related by a 36-degree rotation of a pentagonal motif, as can be seen in figure 7.3. This small structural change, however, does not mean that the conversion between the two structures is energetically feasible. High-energy barriers would have to be surmounted to break the C–C bonds to allow this rotation.

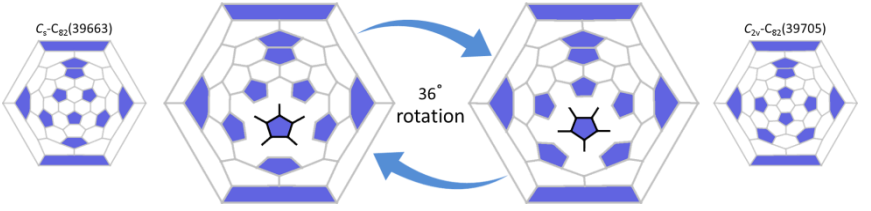

Figure 7.3 Schematic two-dimensional (Schlegel) representations of the $C_s(39663)$-C_{82} and $C_{2v}(39705)$-C_{82} cages showing the close similarities between them. The 36-degree rotation of the highlighted in black C_{10} pentagonal motif can be also seen as the 36-degree rotation of the C_{40} fragment (C_{10} + 30 C around it) that contains the central pentagon and five other pentagons surrounding it. It is the same relationship that exists between $I_h(7)$-C_{80} and $D_{5h}(6)$-C_{80}.

Figure 7.4 shows that each of these non-IPR EMFs is also intimately related with one of the two observed isomers of $M_3N@C_{80}$, $I_h(7)$-C_{80} and

D_{5h}(6)-C_{80}. In fact, $Gd_3N@C_{2v}$(39705)-C_{82} can be obtained from a single C_2 insertion to one hexagon of the prototypical $Gd_3N@I_h$-C_{80}, as pointed out by other authors;[2] analogously, $Gd_3N@C_s$(39663)-C_{82} can be obtained from $Gd_3N@D_{5h}$-C_{80}. Therefore, it is possible that these C_{82}-based EMFs form from the C_{80} cages by C_2 insertion through the recently proposed closed network growth (CNG) mechanism.[14-16]

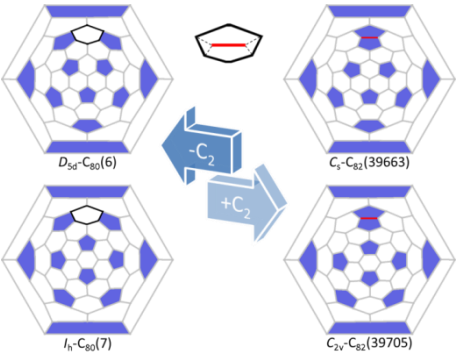

Figure 7.4 Schematic two-dimensional representations of the relation between the non-IPR C_s(39663)-C_{82} and C_{2v}(39705)-C_{82} with the IPR D_{5h}(6)-C_{80} and I_h(7)-C_{80} cages, respectively.

The close similarities between the topologies of the lowest-energy $Gd_3N@C_{80}$ and $Gd_3N@C_{82}$ EMFs help to understand the effect of temperature on the predicted relative abundances of the isomers. We have computed the molar fractions and the free energy differences between the two hexaanionic I_h(7)-C_{80}^{6-} and D_{5h}(6)-C_{80}^{6-} cages for the range of temperatures between 0 and 4000 K. The predicted molar fractions are analogous (see figure 7.5) to those found by Slanina for the two isomers of $Sc_3N@C_{80}$,[10] i.e. the relative abundance of D_{5h}(6)-C_{80}^{6-} with respect to I_h(7)-C_{80}^{6-} increases with temperature resulting in a 0.15/0.85 ratio at 2500 K.

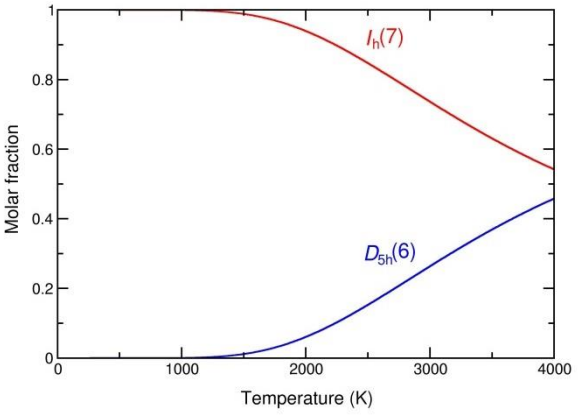

Figure 7.5 Predicted molar fractions as a function of temperature for the two $I_h(7)$-C_{80}^{6-} and $D_{5h}(6)$-C_{80}^{6-} isomers.

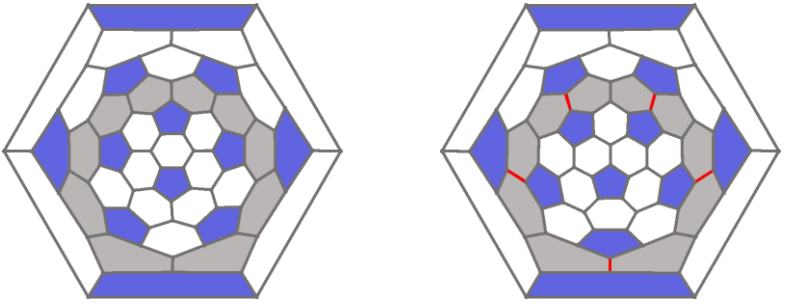

$I_h(7)$-C_{80} $D_{5h}(6)$-C_{80}

Figure 7.6 Comparison of the Schlegel diagrams for the two $I_h(7)$-C_{80} and $D_{5h}(6)$-C_{80} isomers. The only difference is found in the region connecting the two C_{40} caps, which is highlighted in grey with the pyracylene motifs in $D_{5h}(6)$-C_{80} in red.

These two isomers, which are also related by a 36-degree rotation of a pentagonal motif, show the same C_{40} caps and they only differ in the region connecting the two caps (see figure 7.6), with $I_h(7)$-C_{80} showing no pyracylene motifs and $D_{5h}(6)$-C_{80} showing five of them. From these results, therefore, one could infer that those cages with higher number of pyracylenes are favored at higher temperatures. The free energy difference between these two isomers as a function of temperature is plotted in figure 7.7 (blue line).

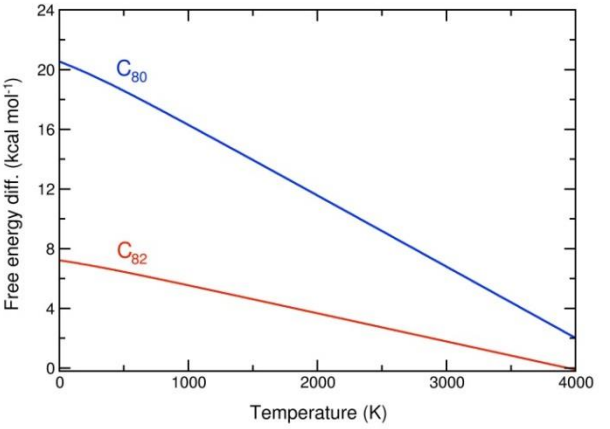

Figure 7.7 Free energy difference (in kcal mol^{-1}) as a function of temperature for C_s(39663)-C_{82}^{6-} and C_{2v}(39705)-C_{82}^{6-} (red line) and D_{5h}(6)-C_{80}^{6-} and I_h(7)-C_{80}^{6-} (blue line).

The difference at 0 K of around 20 kcal mol^{-1} is reduced to only 2 at 4000 K (approximate slope of −4.50 cal mol^{-1} K^{-1}). The two related C_{82} cages, C_{2v}(39705)-C_{82} and C_s(39663)-C_{82}, show instead two and four pyracylene motifs, respectively. The difference at 0 K, around 7 kcal mol^{-1}, becomes negative, i.e. inversion of relative abundance, at a temperature near 4000 K (approximate slope of −1.75 cal mol^{-1} K). Remarkably, the slope per pyracylene unit is around 0.9 cal mol^{-1} K^{-1} for the two free energy differences plotted in figure 7.7. However, a more detailed analysis of the contributions to the free energy differences for these C_{80} and C_{82} isomers shows that both the rotational and the vibrational parts contribute significantly. On one hand, those isomers with lower symmetries are favored at higher temperatures, as can be easily understood from an inspection of the rotational partition function. The rotational contribution to the free energy difference is mainly a consequence of the different symmetry of the isomers. On the other hand, we also observe that there is a correlation between the vibrational contribution to the free energy difference and the number of pyracylene units. Those isomers with larger number of pyracylenes are more favored at higher temperatures (see table 7.3). An inspection of the normal modes of vibration for the different

isomers, which are largely delocalized on the whole cage, does not allow a simple explanation in terms of characteristic topological patterns though.

Table 7.3 Slopes of the rotational (rot) and vibrational (vib) contributions to the free energy differences with respect to I_h(7)-C_{80}^{6-} for the IPR C_{80}^{6-} isomers (1-6) as a function of temperature, along with the symmetry index (σ), the number of pyracylene units (pyra) and the point group for each isomer (sym).[a,b]

Iso	Sym	σ	Pyra	Rot[a]	Vib[a]
1	D_{5d}	10	20	3.57	13.20
2	D_2	4	18	5.38	5.31
3	C_{2v}	2	13	6.75	4.44
4	D_3	6	15	4.57	4.42
5	C_{2v}	2	9	6.75	2.91
6	D_{5h}	10	5	3.55	1.08
7	I_h	60	0	0.00	0.00

[a] Units for the slopes are cal·mol^{-1}·K^{-1}. [b] The absolute values of the slopes of the plots in Fig. S5 and S6 are shown.

Besides the relationships already mentioned between the IPR D_{5h}(6)-C_{80} and I_h(7)-C_{80} and the non-IPR C_s(39663)-C_{82} and C_{2v}(39705)-C_{82} structures, these four cages are also related to other C_{80}, C_{82} and C_{84} isomers that encapsulate a wide variety of metal atoms or metal clusters as schematically depicted in figure 7.8. Cages C_s(39663)-C_{82} and C_{2v}(39705)-C_{82} convert to C_s(6)-C_{82} and C_{3v}(8)-C_{82}, respectively, after a single Stone-Wales (SW) transformation in one pyracylene motif near the pentalene. Moreover, the latter two cages can be interconverted by means of two SW isomerizations. The non-IPR C_s(51365)-C_{84} can be obtained from C_s(39663)-C_{82} after a C_2 insertion and two SW transformations. The structures shown in figure 7.8 represent an important fraction of all the EMFs characterized so far. These apparently different structures share a common fragment with the I_h(7)-C_{80} cage, which ensures maximum separation between pentagons, and only rather small modifications of this prototypical structure lead to other stable EMFs.

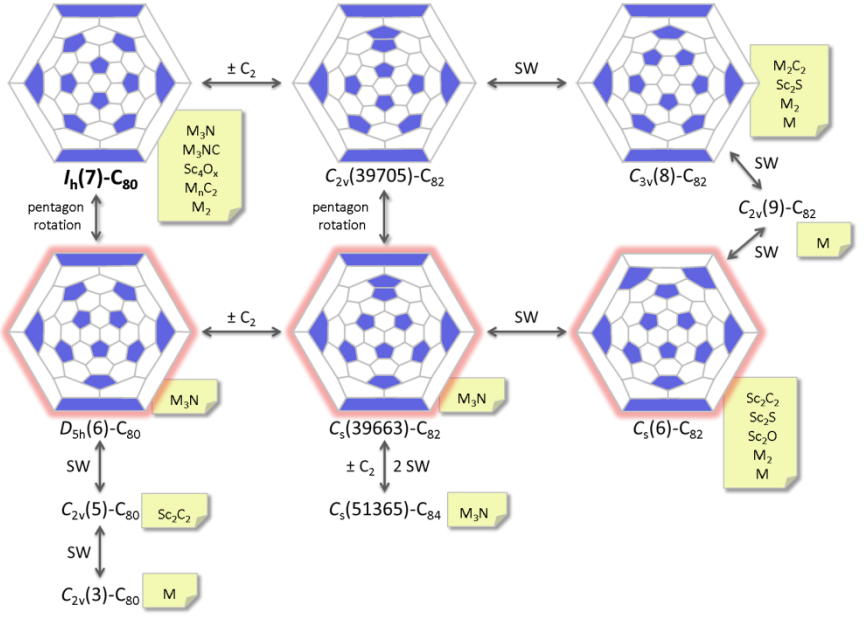

Figure 7.8 Schematic representation showing the connections between the different IPR and non-IPR structures of the C_{80}, C_{82} and C_{84} families that are seen to encapsulate metal atoms or metal clusters. SW stands for Stone-Wales isomerization. The clusters that are seen encapsulated within each of these structures are also shown. The EMFs derived from these structures represent an important fraction of all the EMFs reported so far. The prototypical $I_h(7)$-C_{80} cage, which shares an important part of the structure with the other cages thus ensuring maximum separation of pentagons, is shown at the left top part of the figure. The cages in the central part of the figure, with the contour highlighted in red, $D_{5h}(6)$-C_{80}, $C_s(39663)$-C_{82} and $C_s(6)$-C_{82}, are those favored at high temperatures compared to the cages at the top part.

7.3. Conclusions

The incorporation of thermal contributions in the computations is necessary to explain the formation of $Gd_3N@C_s(39663)$-C_{82} at high temperatures, a non-IPR nitride EMF that was characterized by X-ray crystallography. Therefore, the formation of this EMF is also thermodynamically controlled as for other nitride, carbide, oxide and sulfide EMFs. These results also show that $Gd_3N@C_{2v}(39705)$-C_{82} could be also detected in future experiments. Furthermore, close similarities exist between the cages of the lowest-energy $Gd_3N@C_{80}$ and $Gd_3N@C_{82}$ EMFs, which are related by insertion/extrusion of a single C_2 fragment. In fact, several C_{80}, C_{82} and C_{84} isomers that encapsulate a wide variety of metal clusters and share common motifs with the prototypical $I_h(7)$-C_{80} are related by C_2 insertions/extrusions and Stone-Wales transformations. We also find that both rotational (different symmetries) and vibrational contributions (different topologies) are significant to explain the free energy differences between the isomers within the same C_{2n} family of EMFs.

7.4. References

1. J. M. Campanera, C. Bo and J. M. Poblet, *Angew. Chem. Int. Ed*, 2005, **44**, 7230-7233.
2. A. A. Popov and L. Dunsch, *J. Am. Chem. Soc.*, 2007, **129**, 11835-11849.
3. X. Zhao, Z. Slanina, H. Goto and E. Osawa, *J. Chem. Phys.*, 2003, **118**, 10534.
4. Z. Slanina, S. L. Lee, L. Adamowicz, F. Uhlik and S. Nagase, *Int. J. Quantum Chem.*, 2005, **104**, 272-277.
5. B. Q. Mercado, M. A. Stuart, M. A. Mackey, J. E. Pickens, B. S. Confait, S. Stevenson, M. L. Easterling, R. Valencia, A. Rodríguez-Fortea, J. M. Poblet, M. M. Olmstead and A. L. Balch, *J. Am. Chem. Soc.*, 2010, **132**, 12098-12105.
6. B. Q. Mercado, N. Chen, A. Rodríguez-Fortea, M. A. Mackey, S. Stevenson, L. Echegoyen, J. M. Poblet, M. M. Olmstead and A. L. Balch, *J. Am. Chem. Soc.*, 2011, **133**, 6752-6760.
7. B. Q. Mercado, C. M. Beavers, M. M. Olmstead, M. N. Chaur, K. Walker, B. C. Holloway, L. Echegoyen and A. L. Balch, *J. Am. Chem. Soc.*, 2008, **130**, 7854-7855.
8. Z. Slanina, S.-L. Lee, F. Uhlík, L. Adamowicz and S. Nagase, *Theor. Chem. Acc.*, 2007, **117**, 315-322.
9. R. Valencia, A. Rodríguez-Fortea, A. Clotet, C. de Graaf, M. Chaur, L. Echegoyen and J. M. Poblet, *Chem. Eur. J.*, 2009, **15**, 10997-11009.
10. Z. Slanina and S. Nagase, *ChemPhysChem*, 2005, **6**, 2060-2063.
11. Y. Zhang and W. Yang, *Phys. Rev. Lett.*, 1998, **80**, 890.
12. A. D. Becke, *J. Chem. Phys.*, 1993, **98**, 5648.
13. S. Grimme, J. Antony, S. Ehrlich and H. Krieg, *J. Chem. Phys.*, 2010, **132**, 154104.
14. P. W. Dunk, N. K. Kaiser, C. L. Hendrickson, J. P. Quinn, C. P. Ewels, Y. Nakanishi, Y. Sasaki, H. Shinohara, A. G. Marshall and H. W. Kroto, *Nat. Commun.*, 2012, **3**, 855-863.
15. P. Dunk, N. Kaiser, M. Mulet-Gas, A. Rodríguez-Fortea, J. Poblet, H. Shinohara, C. Hendrickson, A. Marshall and H. Kroto, *J. Am. Chem. Soc.*, 2012, **134**, 9380-9389.
16. M. Mulet-Gas, L. Abella, P. W. Dunk, A. Rodríguez-Fortea, H. W. Kroto and J. M. Poblet, *Chem. Sci.*, 2014, (Accepted).

UNIVERSITAT ROVIRA I VIRGILI
COMPUTATIONS ON ENDOHEDRAL METALLOFULLERENES: CHARACTERIZATION, PROPERTIES AND GROWTH.
Marc Mulet Gas
Dipòsit Legal: T 1604-2015

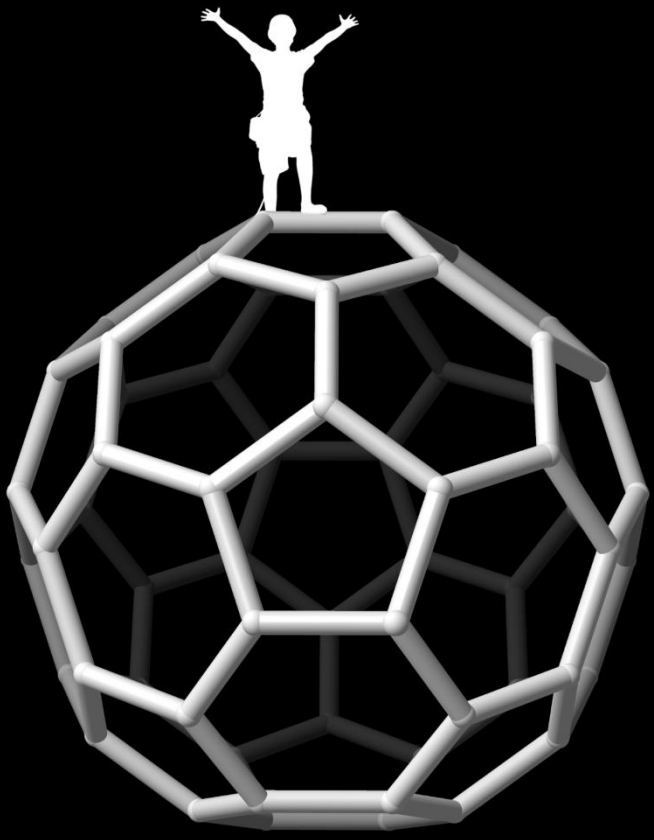

Chapter 8 // *Concluding Remarks*

Chapter 8

Concluding Remarks

In this last chapter, we want to summarize the most important achievements presented in this thesis. Most of the goals of this thesis have been reached and some others will be reached in the future. I would like to remark that, sometimes we strictly focus on the project conclusions, for me they are as important as the personal skills I got or/and improved during the development of this work. Next pages contain a brief chapter-by-chapter summary of the concluding remarks for each project.

Chapter 3 | *Computational Methods and Modeling*

In this chapter we have analyzed all the most important factors that govern the stabilization of endohedral metallofullerenes in order to design an effective and efficient computational strategy. The most important conclusions that arise from this work were:

- The ionic model can be used as a tool for predicting the energies of the endohedral species. We have shown that this is valid for semiempirical AM1 level and BP86/TZP level.
- The computational protocol developed taking into account all the key factors that govern the stabilization of endohedral fullerenes is a step-by-step too to solve the structural characterization of new EMFs.
- The comparison of the experimental data and the computed properties of the EMFs is a very valuable tool for either confirm or discard the cage candidates selected.

Chapter 4 | *Identifying the First Two Scandium Sulfide Endohedral Fullerenes with non-IPR Cages*

In this chapter we described the extensive computational study we carried out in collaboration with the group of Prof. Echegoyen at UTEP for the purpose of characterizing the two new EMFs that they synthesized and isolated. We followed a very similar strategy for both systems and concluded that:

- Four electrons are formally transferred from the Sc_2S to the carbon cages.
- The strong interaction between the metal atoms and the pentalene motifs is determinant for the cluster geometry inside the cages and for the system stabilization.

- The prediction of the absorption spectra by means of TDDFT gives reasonably good results and helped to confirm the candidates proposed form the endohedral calculations.
- The combination of the experimental and computational data led to the identification of the $Sc_2S@C_2(7892)$-C_{70} and the $Sc_2S@C_s(10528)$-C_{72}.
- The structural analysis showed that those two cages are related by a single addition/extrusion of a C_2 unit. This suggests that this system could grow via the closed network growth mechanism.

Chapter 5 | *$Ti_2S@D_{3h}(24109)$-C_{78}: a Sulfide Cluster Fullerene Containing Only Transition Metal Atoms*

As a result of another extensive collaboration with the UTEP group, we were able to characterize combining experiments and theory a new endohedral sulfide cluster fullerene. The main conclusions after this work are:

- The charge transfer from the Ti_2S to the carbon cage is of six electrons; therefore, in this EMF the titanium is formally Ti^{4+}.
- The geometry of the cluster is more important than the interaction of itself with the carbon cage for IPR isomers.
- As predicted by the shape of the frontier orbitals, the reduction is found to happen *in cavea*, and the spin density of the monoreduced system confirms that the reduction takes place on the titanium atoms.
- The cluster is found to have an almost linear arrangement in order to maximally reduce the electrostatic repulsion between the two Ti^{4+}.
- The work led us to the unambiguous assignment of $Ti_2S@D_{5h}(5)$-C_{78} as thee isomer obtained in the experimetns, showing a similar structure to the $Ti_2C_2@D_{5h}(5)$-C_{78}.

Chapter 6 | *Small Endohedral Metallofullerenes: Exploration of the Structure, Growth and Abundances*

The experimental detection of new families of metallofullerenes, $M@C_{2n}$, achieved by means of the state-of-the-art Fourier Transform Ion Cyclotron Resonance (FT-ICR) mass spectrometry in combination with the computational studies led us to the following conclusions:

- The ionic model, widely accepted for larger fullerenes, is also valid for these smaller and more strained systems.
- In contrast to larger EMFs, in which the empty cage is different form the optimal metallofullerene cages, non-IPR small endohedral fullerenes encapsulating tetravalent metals often exhibit the same cage as empty fullerenes.
- The most abundant $Ti@C_{2n}$ are formally linked by direct C_2 insertions, and only in two cases a SW isomerization is needed.
- $Ti@C_{28}$ forms in carbon vapor as the smallest stable endohedral fullerene. The endohedral structure of the whole family was confirmed by means of collision induced dissociation (CID) experiments.
- The transferred negative charge is located at the pentalene bonds and [5,5,5] junctions.
- Ti atoms are found to be shifted off the center of the cage, in order to interact with the nucleophilic regions, giving an extra stabilization.
- Charge transfer is found to be the driven force in the stabilization of metallofullerenes.
- The more charge is transferred the smaller the fullerene favored.
- Ionic radii is important for the smallest cages as shown in the case of the encapsulation of tetravalent metals
- Ga and In were found to form EMFs for the first time showing uncommon Ga^+ and In^+ oxidation states.
- From the computational study of both families, $Ti@C_{2n}$ and $Ca@C_{2n}$, the special stability of $Ti@C_{28}$, $Ti@C_{44}$ and $Ca@C_{50}$ and $Ca@C_{50}$ was rationalized.

- The computed ionization potentials of these species show that the abundances are not directed by the IPs.

Chapter 7 | *Relevance of Thermal Effects in the Formation of Metallofullerenes: the Case of $Gd_3N@C_s(39663)$-C_{82} and Other Related Systems*

The main conclusions that arise from the study of the thermal effects on the formation of the metallofullerenes included in this study are:

- The incorporation of thermal contributions in the computations is necessary to explain the formation of $Gd_3N@C_s(39663)$-C_{82} at high temperatures, a non-IPR nitride EMF that was characterized by X-ray crystallography.
- The formation of $Gd_3N@C_s(39663)$-C_{82} is thermodynamically controlled as for other nitride, carbide, oxide and sulfide EMFs. These results also show that $Gd_3N@C_{2v}(39705)$-C_{82} could be also detected in future experiments.
- Close similarities exist between the cages of the lowest-energy $Gd_3N@C_{80}$ and $Gd_3N@C_{82}$ EMFs, which are related by insertion/extrusion of a single C_2 fragment.
- Rotational (different symmetries) and vibrational contributions (different topologies) are significant to explain the free energy differences between the isomers within the same C_{2n} family of EMFs.

UNIVERSITAT ROVIRA I VIRGILI
COMPUTATIONS ON ENDOHEDRAL METALLOFULLERENES: CHARACTERIZATION, PROPERTIES AND GROWTH.
Marc Mulet Gas
Dipòsit Legal: T 1604-2015

List of publications

[1] **Bottom-Up Formation of Endohedral Metallofullerenes is Directed by Charge Transfer and Ionic Radius**

P. W. Dunk, M. Mulet-Gas, Y. Nakanishi, N. K. Kaiser, A. Rodríguez-Fortea, H. Shinohara, J. M. Poblet, A. G. Marshall and H. W. Kroto. *Nature Communications*, **2014** (accepted)

[2] **Small Endohedral Metallofullerenes: Exploration of the Structure and Growth Mechanism in the Ti@C_{2n} (2n=26-50) Family**

M. Mulet-Gas, L. Abella, P. W. Dunk, A. Rodríguez-Fortea, H. W. Kroto and J. M. Poblet. *Chemical Science*, **2014** (accepted)

[3] **Relevance of Thermal Effects in the Formation of Endohedral Metallofullerenes: the Case of $Gd_3N@C_s$(39663)-C_{82} and Other Related Systems**

M. Mulet-Gas, A. Rodríguez-Fortea, L. Echegoyen and J. M. Poblet. *Inorganic Chemistry*, **2013**, 52, 1954-1959.

[4] **$Ti_2S@D_{3h}$(24109)-C_{78}: a Sulfide Cluster Metallofullerene Containing Only Transition Metals Inside the Cage**

F-F. Li, M. Mulet-Gas, N. Chen, V. Triana, J. Murillo, A. Rodríguez-Fortea, J. M. Poblet and L. Echegoyen. *Chemical Science*, **2013**, 4, 3404-3410.

[5] **$Sc_2S@C_2$(7892)-C_{70}: a Metallic Sulfide Cluster Inside a non-IPR C_{70} Cage**

N. Chen, M. Mulet-Gas, Y.-Y. Li, R. E. Stene, C. W. Atherton, A. Rodríguez-Fortea, J. M. Poblet and L. Echegoyen. *Chemical Science*, **2013**, 4, 180-186.

[6] **The Smallest Stable Fullerene, M@C_{28} (M=Ti, Zr, U): Stabilization and Growth from Carbon Vapor**

P. W. Dunk, M. Mulet-Gas, N. K. Kaiser, A. Rodríguez-Fortea, J. M. Poblet, H. Shinohara, C. L. Hendrickson, A. G. Marshall and H. W. Kroto. *Journal of the American Chemical Society*, **2012**, 134, 9380-9389.

[7] **$Sc_2S@C_s$(10528)-C_{72}: a Dimetallic Endohedral Fullerene with a non-IPR Cage**

N. Chen, M. Mulet-Gas, C. M. Beavers, A. Rodríguez-Fortea, E. J. Muñoz, Y.-Y. Li, M. M. Olmstead, A. L. Balch, J. M. Poblet and L. Echegoyen. *Journal of the American Chemical Society*, **2012**, 134, 7851-7860.

[8] **Electronic Structure of IPR and non-IPR Endohedral Metallofullerenes: Connecting Orbital and Topological Rules**

N. Alegret, M. Mulet-Gas, X. Aparicio-Anglès, A. Rodríguez-Fortea and J. M. Poblet. *Comptes Rendus Chimie*, **2012**, 15, 152-158.

UNIVERSITAT ROVIRA I VIRGILI
COMPUTATIONS ON ENDOHEDRAL METALLOFULLERENES: CHARACTERIZATION, PROPERTIES AND GROWTH.
Marc Mulet Gas
Dipòsit Legal: T 1604-2015

Posters and Oral Presentations

Electronic Structure and Stabilization of non-IPR Sulfide Cluster Fullerenes
XI Girona Seminar: on Carbon, Metal and Carbon-Metal Clusters
Girona (Spain) | July 2014
Poster presentation

Metal·loful·lerens Endoèdrics no-IPR: Estructura Electrònica, Estabilització, Propietats i Connectivitat
VIII Trobada de Joves Investigadors dels Països Catalans
Andorra La Vella (Andorra) | November 2013
Oral presentation

Electronic Structure and Properties of non-IPR Sulfide Endofullerenes
IX European Conference on Computational Chemistry EUCO-CC9
Sopron (Hungary) | September 2013
Poster presentation

Computational Chemistry Applied to Endohedral Fullerenes
Jornada d'Investigadors Predoctorals Interdisciplinària
Barcelona (Spain) | January 2013
Oral presentation

Electronic Structure and Stabilization of non-IPR Endohedral Fullerenes
XVI International Symposium on Small Particles and Inorganic Clusters
Leuven (Belgium) | July 2012
Poster presentation

Estructura Electrònica i Estabilització de Metal·loful·lerens no-IPR
XXVIII Reunió de la Xarxa de Referència en Química Teòrica i Computacional
Barcelona (Spain) | June 2012
Oral presentation

Electronic Structure of IPR and non-IPR Metallofullerenes: Connecting Orbital and Topological Rules
IX Triennial Congress of the World Association of Theoretical and Computational Chemists (WATOC)
Santiago de Compostela (Spain) | July 2011
Poster presentation

UNIVERSITAT ROVIRA I VIRGILI
COMPUTATIONS ON ENDOHEDRAL METALLOFULLERENES: CHARACTERIZATION, PROPERTIES AND GROWTH.
Marc Mulet Gas
Dipòsit Legal: T 1604-2015

Merits & Distinctions

Metal·loful·lerens Endoèdrics no-IPR: Estructura Electrònica, Estabilització, Propietats i Connectivitat
VIII Trobada de Joves Investigadors dels Països Catalans
Andorra La Vella (Andorra) | November 2013
Awarded the best oral communication

Electronic Structure and Properties of non-IPR Sulfide Endofullerenes
IX European Conference on Computational Chemistry EUCO-CC9
Sopron (Hungary) | September 2013
Awarded the best poster presentation

Chemical Science

Front Cover

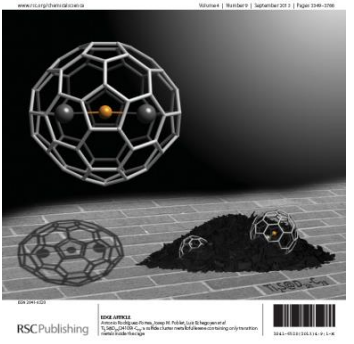

$Ti_2S@D_{3h}(24109)$-C_{78}: a Sulfide Cluster Metallofullerene Containing Only Transition Metals Inside the Cage
F-F. Li, M. Mulet-Gas, N. Chen, V. Triana, J. Murillo, A. Rodríguez-Fortea, J. M. Poblet and L. Echegoyen. *Chemical Science*, **2013**, 4, 3404-3410.

UNIVERSITAT ROVIRA I VIRGILI
COMPUTATIONS ON ENDOHEDRAL METALLOFULLERENES: CHARACTERIZATION, PROPERTIES AND GROWTH.
Marc Mulet Gas
Dipòsit Legal: T 1604-2015

Collaborations

University of Texas at El Paso

Prof. Luis Echegoyen

Florida State University

Prof. Sir Harold W. Kroto

Research Abroad

Project	Experimental and theoretical study of the formation and growth of endohedral metallofullerenes
Supervisor	Prof. Sir Harold W. Kroto
Center	Florida State University National High Magnetic Field Laboratory
Period	January – May 2014

UNIVERSITAT ROVIRA I VIRGILI
COMPUTATIONS ON ENDOHEDRAL METALLOFULLERENES: CHARACTERIZATION, PROPERTIES AND GROWTH.
Marc Mulet Gas
Dipòsit Legal: T 1604-2015

UNIVERSITAT ROVIRA I VIRGILI
COMPUTATIONS ON ENDOHEDRAL METALLOFULLERENES: CHARACTERIZATION, PROPERTIES AND GROWTH.
Marc Mulet Gas
Dipòsit Legal: T 1604-2015

Acknowledgments / Agraïments

In the last few pages of this book I would like to thank all the people that have contributed, helped and supported me during this adventure, formally called PhD thesis. Although I thought this would be an easy part to write, it is taking longer than I expected. It is really difficult for me to express my feelings in a few lines, but I tried to do my best.

Primer que tot, vull agrair als meus supervisors, Toni i Josep M., la seva paciència, motivació, consells i tota la seva ajuda i suport en cadascun dels diferents períodes, des d'aquella primera beca de col·laboració fins al final d'aquesta tesi doctoral. Espero que hagi valgut la pena. Vull que sabeu que sigui quin sigui el camí que em toqui seguir en el futur, mai oblidaré qui em va iniciar en tot això, i sempre us tindré present per haver estat uns grans 'companys' en els primers passos de la meva etapa científica. De tot cor, moltes gràcies.

I would also like to express my gratitude to Harry for giving me the opportunity of joining your team at Florida State University, for being really nice from the very beginning and for having always a smile in your face. It was a pleasure to build some fullerenes with the one who discovered them. I also thank Alan Marshall for the time I spent at the Mag Lab working in the ICR facilities. I really appreciate the opportunity I had to work in your lab. I want to extend my gratitude to Paul. You are the one who spent the time with me, who had the patience and perseverance to explain me everything, and for helping me with all the things I needed (and also for picking me up on the rainy days!). As I've already told you, that was one of the best experiences I've ever had. Let's see if the future allows us to form the fullerene team again!

Als membres sèniors del grup: Xavi, Jordi, Mar, Anna, Rosa i Coen, ha estat un plaer compartir xerrades, seminaris i discussions sobre el món en general a les pauses del cafè. L'ambient genial, tant científic, laboral, com personal, és conseqüència de l'aportació de cadascun de vosaltres. Menció especial, ben merescuda, als '*totpoderosos Deus*' encarregats de que sigui

possible tirar càlculs cada dia (excepte quan plou... jje), Jose, Elisenda i Moisés. Aquest grup, sense vosaltres seria molt difícil de tirar endavant. Moltes gràcies per solucionar gairebé de manera instantània totes les '*cagades*' que nosaltres cometem, i per fer-ho sempre amb un somriure.

Lluny queda ja la meva primera participació en aquest grup, aquella beca de col·laboració al 2009. Des de llavors fins ara, molta gent ha anat passant pel grup i un record de cadascun de vosaltres sempre quedarà amb mi. Agraeixo a tota aquesta primera generació de doctors, amb qui menys temps he compartit, però que hi van ser per acollir-me quan tot començava. Laia, Sonia, Ramón. Jhon, Mireia, Yanick, Àlex i Zahra. Crec que vosaltres vau ser els culpables de que aquest grup fos una petita família. Espero que ens veiem algun dia per aquest món. Alberto, de tu vaig heretar la taula i el PC, amb molta pressió (havies deixat el llistó molt alt). Gràcies pels teus consells als principi i gràcies per la visita a la UCL quan vaig parar per Londres, ens veiem aviat.

Als que em compartit gran part del camí en aquesta tesi, us vull donar les gràcies de tot cor. Pablo A. des del començament de tot menjant pizzes a l'office en diumenge fins ara, que tinguis molta sort. *Queen Maddie*, quins colors!! Espero que ho celebrem amb una bona esquiada. Sergi, ets un crack, mestre. Ja saps que et tinc un carinyo especial (sense mariconades). Menció especial per a la millor respostera del Delta! Per a quan un brownie Jess? Gràcies per tot. Pablo J. no se que hagués fet sense el meu únic suport blanc, espero veure't aviat. Ximo, si la barba ho permet, ens segui veient, ets un tio com Déu mana. Diego, he modificat això a ultima hora per tu, quan vulguis ens peguem... xD. Gerard, ets un dels primers que vaig conèixer allà pel 2005 quan tot va començar, espero que almenys per això tingui un VIP quan siguis una 'rockstar'. Als membre vitalicis del 204, gràcies per tot. A la Núria per ensenyar-me mil coses de tots els programes que puc recordar. Al Xavi, per les risses i el gran WATOC que vam compartir. I a la Laura, pubilla dels ful·lerens, que tinguis molta sort, gràcies per suportar-me com a parella de pàdel. A ti Gian, muchas gracias por todas las veces que me dejaste un rincón de tu casa para pasar la noche, suerte en Londres, y cuidate los pezones. A la resta, Pedro,

Mariano, Juan Carlos i Josep, espero que tot us vagi molt bé, us ho mereixeu.

Menció especial a la família del Màster de Química Teòrica i Computacional. Va ser una etapa dura, però tot i això, vam tenir molt bons moments que val la pena recordar. Melchor, con tus bolas y muelles, has sido un gran compañero, espero que tengas mucha suerte en el futuro. Jordi, feies por amb la *katana*, però es veu de lluny que ets molt bona persona i això ens va arribar a tots. Laia, perdona per haver hagut d'aguantar-nos a tots, vas jugar molt bé el teu paper de única noia del màster. Gràcies per cuidar-nos. Carlos, sempre recordarem el teu 'química teòrica nena...' al bus de camí al campus a Girona jje. Oriol, sempre llest per a la *voll*, un tio com cal, sempre disposat a ajudar, escolta i fer el que calgui pels amics. Arnau, el tio més llest i social que conec, espero poder venir algun dia al teu poble a enfangar-nos!. Merci per tot, de veritat. Marc, amb tu es amb qui potser he compartit més temps. Ha estat un plaer coincidir en congressos, xerrades, seminaris, sopars i festes. Gràcies per acollir-me a Girona. Espero que em contractis en un futur jeje.

I also want to thank my little family in Tally. Everyone I met there was really kind to me and that's why a I had a really good time. To all the guys from the Tallahassee Rugby Football Club and the girls from the FSU Rugby, I miss you so much and I can't wait to see y'all soon, (fingers crossed). And of course, to the 'niners', including Austin lol. The Nine was literally my second home (maybe the first one...). Thank you guys for taking me everywhere, for considering me a friend from the very beginning and for helping me a lot with everything.

No em puc oblidar dels meus amics del poble, a qui durant aquest període, i sobretot durant els últims mesos, he vist menys del que hagués volgut, però que sempre han estat allà quan de veritat ha fet falta. Núria, Berna, Blanca, Manel, Sergi 'en extinció', Sergi A., Xus, Clara i Jaumet... Gràcies a tots. A veure si ara que això s'acaba tenim una mica més de temps per a fer-ne alguna de bona jje.

A la colla de la uni, com ja sabeu, m'encanta que 5 anys després d'acabar la carrera (per a alguns no tant.. jeje) encara estiguem tan units com al principi. Espero de veritat que ,malgrat la vida ens porti per camins diferents, sempre tinguem temps per fer les nostres trobades.

Finalment, la part més important de totes i els agraïments a qui més ho mereixen. A vosaltres *papa* i *mama*. Vosaltres meu donat tot i més, heu estat sempre al meu costat, i heu fet tots els sacrificis possibles per mi. Espero que us pugueu sentir orgullosos del vostre fill. Mai podré agrair-vos ni tornar-vos tot el que heu fet per mi, però ho intentaré. Segurament us ho dic menys del que us mereixeu, però us estimo molt.

Hi ha molta més gent a qui li hauria de agrair alguna cosa. Disculpeu-me si em deixo a algú. De veritat que em sento molt afortunat de tenir-vos a tots al meu voltant.

" It always seems impossible until it's done "

Nelson Mandela (1918-2013)